Human Gut Microbes Under Power - Development of a Bioelectrochemical System to Uncouple and Interrogate H_2-Syntrophic Partners in the Human Gut Microbiota

Dissertation

der Mathematisch-Naturwissenschaftlichen Fakultät
der Eberhard Karls Universität Tübingen
zur Erlangung des Grades eines
Doktors der Naturwissenschaften
(Dr. rer. nat.)

vorgelegt von
M.Sc. Ulrike Biehain
aus Görlitz

Tübingen
2024

Gedruckt mit Genehmigung der Mathematisch-Naturwissenschaftlichen Fakultät
der Eberhard Karls Universität Tübingen.

Tag der mündlichen Qualifikation:	06.06.2024
Dekan:	Prof. Dr. Thilo Stehle
1. Berichterstatter/-in:	Prof. Dr. Ir. Largus Angenent
2. Berichterstatter/-in:	Prof. Dr. Lisa Maier

Oh my gut. We are not alone in our bodies.

This dissertation aims to unveil a hidden world of syntrophic interactions within our gut microbiome, where microbial partnerships navigate a delicate balance of competition and cooperation. As we delve into the complex landscape of the human intestinal microbiome, challenges abound, demanding a nuanced understanding of metabolic potentials and interspecies relationships.

Motivated by the complexities posed by the microbiome's dynamic nature, this research strives to decode the metabolic dance between microorganisms, fostering a more profound understanding that paves the way for developing cultivation methods essential in shaping the future of gut microbiome studies.

Acknowledgments

First, I thank Prof. Lars Angenent, my supervisor, for accepting me as a Ph.D. student in bioelectrochemistry. His guidance, patience, and support for my scientific career have been invaluable. I am also grateful for the opportunity to have developed various reactor setups and engaged with non-scientific audiences at the Science and Innovation Days. Finally, I would like to thank him for his assistance in editing my dissertation and reviewing my conference materials.

Second, I especially thank Prof. Ruth Ley for her support, helpful advice, and expertise on the human microbiome. With her help, I could see my results from another perspective, and investing a considerable amount of time in my Ph.D. for reactor development turned out to be sustainable and prosperous for my future research.

Third, I would like to sincerely thank my other committee members sincerely, Prof. Daniel Huson and Prof. Lisa Meier. Special thanks go to Prof. Dr. Daniel Huson for guiding, together with Prof. Dr. Lars Angenent, the multidisciplinary CMFI project collaboration from the bioinformatics site. I am very grateful for his support for the project development from the beginning on, for participating in the monthly CMFI meetings and in my oral defense. Also, I am very grateful to Prof. Lisa Maier, who already participated in the committee of my Ph.D. proposal, for reviewing my Ph.D. dissertation and participating in the oral defense.

Next, I would like to thank all members of the Environmental Biotechnology Lab. I will always keep the welcoming and warm working atmosphere in mind and that people are always willing to help. I am thrilled to meet many friendly, motivated, creative, and inspiring great scientists who are simultaneously warm-hearted people. I want to thank Dr. Sebastian Beblawy and Dr. Richard Hegner for their scientific input in the field of bioelectrochemistry and microbiology, for sharing their skateboard skills during the lunch breaks in the parking lot of the institute, and for all the great time we had together outside the lab with lots of good friends. Furthermore, I would like to extend my gratitude to my former colleague at the office, Dr. Sarah Schulz, for the good vibes she brought into the lab

and all the good times we had together while climbing, gardening, or hiking. This great community gave me lots of support and was very essential for the success of my Ph.D.

Special thanks go also to Nils Rohbohm, with whom I shared an office and a lab bench over almost my entire Ph.D. time. I am very thankful that he introduced me to the field of bioelectrochemistry, and part of the success of my Ph.D. is also a credit to him. In addition, I am happy that I also had great office mates over the last years, such as Dr. Han Wang (Angelia), Patrick Schweizer, Lucas Mühling, Mohammed Balboul, and Jose Antonio Velazquez Gomes. Special thanks to Angelia for always smiling, even when everything went wrong in the lab, and for all the sweats she shared with us. Furthermore, thanks go to Antonio, who brought lots of lightness and brilliance into the lab, and I enjoyed a lot of good moments while eating “Friday fries”.

In addition, I would like to extend my gratitude to Timo Lucas for his pivotal role in the development of the MMonitor system, which has significantly advanced our CMFI project. I would also like to acknowledge the valuable contributions of Dr. James Marsh and Dr. Alexander Tyakht in the field of bioinformatics.

I also want to thank Steffen Erdle, Annika Duczmal, and Hanna Heinzmann, who assisted me as HIWI students in running the experiments. Without their help, the realization of many experiments would not have been possible. In addition, Karla Polen-Beer provided crucial support from the Psychosocial Counseling Center. Without all the helping hands and the valuable mental support, the project would never have developed into what it became in the end.

Tremendous thanks go to my family and friends, who always supported me and shared many things with me apart from the lab. I especially thank my parents, Ute and Reiner Biehain, for their frequent visits, deep conversations in life, and constant motivation. I thank all the people who became friends since I moved to Tübingen and all the good old friends from the times before, which spread all over Germany. I value these friendships deeply in my heart and would be delighted if they stayed with me for a lifetime. Last but not least, I would like to thank my boyfriend Max for his incredible support, for sharing precious moments as inspiration to reflect and enjoy life, and for traveling with me through different stages of life and to the most beautiful mountains.

Table of Contents

Table of Figures

List of Tables

Abbreviations

$+H_2$	hydrogen evolution
$-H_2$	hydrogen removal
16S	small subunit of the ribosomal RNA gene
5-HT	serotonin
Ag/AgCl	silver/silver chloride
ATP	adenosine triphosphate
BBB	blood-brain barrier
MCC	branched-chain carboxylic acids
BES	bioelectrochemical system
BHI	brain heart infusion broth
BMI	body mass index
butyryl-CoA	butyryl coenzyme A
CFU/g	colony forming units *per* gram
CH_3COO^-	acetate
CH_4	methane
CLI	command line interface
CNS	central nervous system
CO_2	carbon dioxide
cotonyl-CoA	crotonyl coenzyme A
DB	database
ddNTP	dideoxynucleotide
dNTP	deoxynucleotide
E_{ce}	counter electrode
E_{ref}	reference electrode
E_{we}	working electrode
Fd_{ox}	oxidized ferredoxin
Fe_{red}^-	reduced ferredoxin
FFAR2	free fatty acid receptors 2
FFAR3	free fatty acid receptors 3
GA	glutaraldehyde
GABA	gamma-aminobutyric acid
GAPDH	glyceraldehyde-3-phosphate dehydrogenase
GC	gas chromatography
GI tract	gut intestinal tract
GLP1	gamma-aminobutyric acid

GPCR	G protein-coupled receptors
GPR109a/HCAR2	hydrocarboxylic acid receptor
GPR41	G protein-coupled receptor 41
GPR43	G protein-coupled receptor 43
GUI	graphical user interface
H^+	proton
H_2	hydrogen
H_2S	hydrogen sulfide
HCl	hydrochloric acid
HMDS	hexamethyldisilazane
MAGs	metagenome-assembled genomes
MCT	monocarboxylate transporters
MCCs	medium-chain charboxylates
V	volt
N_2	nitrogen
NAD	oxidized nicotinamide adenine dinucleotide
NADH	reduced nicotinamide adenine dinucleotide
NADP	oxidized Nicotinamide adenine dinucleotide phosphate
NADPH	reduced Nicotinamide adenine dinucleotide phosphate
NaOH	sodium hydroxide
O_2	oxygen
ONT	Oxford Nanopore Technologies
PBS	phosphate-buffered saline
PEP	phosphoenolpyruvate
PSS	polyanethole sulfonic acid sodium salt
Pt	platinum
Pt/C	platinum-doped carbon
PYY	peptide YY
SCCs	short-chain carboxylates
SMCT	sodium-dependent monocarboxylate transporters
SMRT	single-molecule real-time sequencing
SMS	single-molecule sequencing
Treg	regulator T cell
UV RGD	UV reduction gas detector
w/o	without
WGS	whole-genome sequencing
ZMW	zero-mode waveguides

β–NAD	β-nicotinamideadenine-dinucleotide hydrate
$\Delta G_0´$	Gibbs free energy

Summary

The fermentation of carbohydrates is one of the primary functions of the gut microbiome, which results in the production of short-chain carboxylates (SCCs) and gasses such as hydrogen (H_2) and carbon dioxide (CO_2) [1]. Fermentative H_2 production and interspecies H_2 transfer predominantly drive colonic H_2 metabolism rather than respiration [2]. Accumulating H_2 disrupts the gut function, harms humans, and needs to be prevented. However, H_2 is an important energy source for gut microbes such as sulfate-reducing bacteria, acetogens, and methanogens [3]. Interspecies H_2 transfer is a form of microbial syntrophy that dominates in the gut, but its role in modulating overall metabolism and microbial community dynamics is poorly understood. First investigations showed that *Christensenellaceae* and the archaeal family *Methanobacteriaceae* cooccur in humans with a lean body mass index. *Christensenella minuta* is a highly prevalent, heritable, health-associated bacterium from the human gut that cross-feeds H_2 to the methanogen *Methanobrevibacter smithii* [4]. It was previously found that in continuous co-culture, *C. minuta* produces less *n*-butyrate when *M. smithii* is abundant.

For Objective 1, we tested if H_2-removal by *M. smithii* leads to the downregulation of *n*-butyrate production. Therefore, we developed a bioelectrochemical system (BES) that removes H_2 by oxidation at the electrode, mimicking a syntrophic microbial partner that takes up H_2. The unique design of the BES brings the microbe at a 1 mm distance close to the platinum-doped carbon electrode and provides a large surface area (~122 cm^2) to ensure an efficient H_2 removal. Thus, it provides an environment favored by H_2-producing, carbohydrate-degrading bacteria. For proof of concept, *C. minuta* was used as an H_2-producing microbe. With H_2 removal by the BES electrode, *C. minuta* shifts its metabolism towards more acetate and less *n*-butyrate production, analogously to when the methanogen is present. Our findings underscore the importance of thermodynamics and H_2 transfer in regulating the metabolic output of the microbiota in the human gut. Furthermore, for Objective 2, we wanted to answer the question: Can the H_2 removal by the BES compete with a syntrophic H_2 consumer? This experiment was designed into two parts. In the experiment, *C. minuta* was co-cultivated with *M. smithii* in the working chamber of the BES. There, we generated H_2 at the cathode in addition to the H_2 that

C. minuta generated to grow *M. smithii* without substrate limitations. Again, we detected a drop in the ratio of *n*-butyrate to acetate production of *C. minuta*. The second part of Objective 2 was not performed. There, we planned the co-cultivation of both microbes in the same BES but separated from each other in two chambers, where *C. minuta* would grow at the anode and *M. smithii* at the cathode. The idea of this experiment was that *C. minuta* grows at the anode and produces H_2, which was removed by oxidation. The resulting H^+ protons migrate through an ion exchange membrane, which separates the anode and cathode, and get reduced to H_2 at the cathode, where *M. smithii* grows. For Objective 3, we wanted to use the BES to enrich syntrophic H_2-producing microbes from the human gut that hide from current lab cultivation approaches. Therefore, we cultivated a human fresh stool sample in the BES under H_2 removal conditions and detected the major fermentation products of the human gut microbiota and an enormous amount of biofilm formation. Because we detected fluctuation in the production profile of the SCCs and gasses, such as H_2 and CO_2, we assume that microbial composition changed during the cultivation period. The microbial community's evaluation and statistical analysis were done using the software tool “MMonitor” from Timo Lucas[1] and the group of Prof. Daniel Huson[1]. Unfortunately, the final correlation between the composition of the microbiota and the detected metabolites in relation to H2 removal by the BES was not performed out until the end of my PhD.

Future applications of the BES include isolating fastidious species requiring an H_2 sink for growth. The outcomes of this study are essential to developing an isolation approach for gut microbes without requiring a microbial (syntrophic) partner. Culturing *C. minuta* and the entire human gut microbiota in the BES will help further technical BES development and support our ultimate goal of understanding human gut microbes better. Therefore, future applications of the BES include isolating particular strains requiring an H_2 sink for growth. This approach could be used to enrich those host microbes that are highly prevalent, heritable, and health-associated bacteria without the need for drug treatment or fecal transplantation to cure intestinal diseases.

[1] Research group Algorithms in Bioinformatics, University of Tübingen

Summary (German)

Die Fermentation von Kohlenhydraten ist eine der Hauptfunktionen des Darmmikrobioms und führt zur Produktion von kurzkettigen Carboxylaten und Gasen wie Wasserstoff (H_2) und Kohlendioxid (CO_2) [1]. Die fermentative H_2-Produktion und der syntrophische H_2-Transfer treiben hauptsächlich den H_2-Stoffwechsel im Dickdarm von Menschen an, anstatt die Atmung [2]. Kommt es jedoch zur Anreicherung von H_2 wird die Darmfunktion gestört und kann sich schädlich auf den Menschen auswirken. Allerdings ist H_2 auch eine wichtige Energiequelle für Darmmikroben wie sulfatreduzierende Bakterien, Acetogene und Methanogene [3]. Syntrophischer H_2-Transfer ist eine Form von mikrobieller Syntrophie, die im Darm vorherrscht, und deren Einfluss bei der Modulation des Gesamtstoffwechsels und auf Dynamik der mikrobiellen Gemeinschaft bisher unzureichend verstanden ist. *C. minuta* ist ein weit verbreitetes, vererbbares, gesundheitsförderndes Bakterium, das H_2 an *M. smithii*, welches H_2 als Substrat verstoffwechselt, weitergibt. Unter kontinuierlicher Kultivierung mit *M. smithii* verändert sich der fermentative Stoffwechsel von *C. minuta* und weniger *n*-Butyrat wird produziert.

Im ersten experimentellen Teil testeten wir, ob die Aufnahme von H_2 durch *M. smithii* die Produktion von *n*-Butyrat von *C. minuta* herunterreguliert. Dazu entwickelten wir ein bioelektrochemisches System (BES), das H_2 durch Oxidation am Elektroden entfernt, um so den syntrophischen und H_2-konsumierenden mikrobiellen Partner zu imitieren. Das spezielle Design des BES bringt die Mikroben in bis zu 1 mm Abstand zu einer platin-beschichteten Kohlenstoffanode und bietet zudem eine große Oberfläche (~122 cm^2), um eine effiziente H_2-Entfernung sicherzustellen. Für den Proof-of-Concept wurde *C. minuta* als H_2-produzierende Mikrobe verwendet. Die Entfernung von H_2 durch die BES-Elektrode zeigt sich in einem veränderten Primätstoffwechsel von *C. minuta*, in welchem mehr Acetat und weniger *n*-Butyrat produziert wird, analog zur Anwesenheit des Methanogens *M. smithii*. Unsere Ergebnisse verdeutlichen die Bedeutung der Thermodynamik und des H_2-Transfers bei der Regulation des mikrobiellen Stoffwechsels im Darm. Im zweiten experimentellen Teil wollten wir die Frage beantworten: Kann die Entfernung von H_2 durch das BES mit Mikroben konkurrieren, welche in einem syntrophischen Verhältnis zu einander stehen und H_2 als Substrat konsumieren? Dieses Experiment wurde in zwei Teile

unterteilt. Im ersten Teil wurden *C. minuta* mit *M. smithii* auf der Seite des Arbeitselektrode im BES kultiviert. Dort erzeugten wir H_2 an der Kathode zusätzlich zum von *C. minuta* erzeugten H_2, um *M. smithii* ohne Substratbeschränkungen wachsen zu lassen. Wir beobachteten erneut einen Veränderung der Produktion von *n*-Butyrat zu Acetat bei *C. minuta*, und einen Rückgang der Produktion von *n*-Butyrate. Der zweite Teil dieses Experiments wurde nicht durchgeführt. In diesem planten wir die gemeinsame Kultivierung beider Mikroben im voneinander getrennt im selben BES, wo *C. minuta* an der Anode und *M. smithii* an der Kathode wachsen würde. Dabei würde das gebildete H_2 von *C. minuta* an der Anode oxidiert werden, und die dabei entstandenen Protonen gelangen über eine Ionenaustauschmembran zur Kathode. Dort würden sie zu H_2 reduziert werden und stehen *M. smithii* als Substrat bereit.

Im dritten experimentellen Teil sollte das BES als Kultivierungsmethode zur Anreicherung syntropher, H_2-produzierender Mikroben aus dem menschlichen Darm getestet werden. Dabei lag der Fokus besonders auf den H_2-produzierenden Mikroben, welche sich aktuell nicht im Labor kultivieren lassen. Hierfür kultivierten wir im BES eine frische human Stuhlprobe an der Anode unter H_2 oxidierenden Bedingungen, um den mikrobiell gebildeten H_2 aus dem BES zu entfernen und somit den Mikroben einen Wachstumsvorteil zu verschaffen, welche nur bedingt zusammen mit H_2-konsumierenden Mikroben wachsen können. In diesem Experiment konnten wir die Hauptfermentationsprodukte des menschlichen Darmmikrobiota sowie eine enorme Biofilmbildung an der Anode nachweisen. Da wir Schwankungen im Profil der Produktion von kurzkettigen Carbonsäuren und der Gase H_2 und CO_2 feststellten, gehen wir davon aus, dass sich die mikrobielle Zusammensetzung während der Kultivierungszeit im BES geändert hat. Die Auswertung und statistische Analyse der mikrobiellen Gemeinschaft und ihrer Veränderungen wurden mit dem Software-Tool MMonitor von Timo Lucas[2] und der Arbeitsgruppe von Prof. Daniel Huson[2] durchgeführt. Die endgültigen Korrelationen zwischen der Zusammensetzung der Mikrobiota und den nachgewiesenen Metaboliten in Bezug auf die H_2-Entfernung durch das BES waren bis zum Ende meiner Doktorarbeit noch in Bearbeitung.

[2] Arbeitsgruppe Algorithmen der Bioinformatik, Universität Tübingen

Zukünftige Anwendungen des BES umfassen die Isolierung anspruchsvoller Stämme, die für ihr Wachstum einen H_2-Senke benötigen. Die Ergebnisse dieser Studie sind entscheidend für die Entwicklung eines Isolationsansatzes für Darmmikroben, ohne einen mikrobiellen (syntrophischen) Partner zu benötigen. Die Kultivierung von *C. minuta* und eines gesamten menschlichen Darmmikrobioms im BES wird dazu beitragen, die technische BES-Entwicklung weiter voranzutreiben und unser ultimatives Ziel, das Verständnis der menschlichen Darmmikroben zu verbessern, zu unterstützen. Daher könnten zukünftige Anwendungen des BES dazu dienen, bestimmte Stämme zu isolieren, die für ihr Wachstum eine H_2-Senke benötigen. Dieser Ansatz könnte verwendet werden, um diejenigen Wirtsmikroben anzureichern, die weit verbreitet, vererbbar und gesundheitsfördernde Bakterien sind, ohne auf medikamentöse Behandlung oder Stuhltransplantation angewiesen zu sein, um Darmerkrankungen zu heilen.

Chapter 1
Motivation and Ph.D. Objectives

1.1. Motivation

The human microbiome is linked to health and disease and includes trillions of microbes such as bacteria, archaea, fungi, viruses, and other life forms. Researchers are still working out what shapes the community of microbes with hundreds of distinct bacterial species – some are pathogenic, and some beneficial. There is still a considerable amount of so-called microbial dark matter. The microbial dark matter includes the entire microbial diversity that remains uncultured, reaching from the millions of biomes (niches) to the uncultured microbial species and their genomes [5]. In 2019, 1.952 uncultured bacterial species were identified from 92.143 metagenome-assembled human gut microbial genomes. Thus, sequencing efforts show us the potential of microbes that are not cultured with current cultivation approaches [6].

Besides the considerable knowledge about the interaction of gut microbes with the host, less is understood about the microbe-microbe interactions—especially in the human gut's H_2 economy. H_2 is one of the end products of carbohydrate fermentation and plays a central role in microbial metabolism. H_2 maintains metabolic homeostasis by acting as an electron sink. Furthermore, H_2 can be taken up as an energy source by other gut microbes. Therefore, interspecies H_2 transfer and microbial syntrophy have become increasingly important to fill one gap in understanding the entire human gut microbiome. We must fill this gap with knowledge about microbes that hide from standard lab cultivation. These specific microbes or microbial patterns carry the vast potential to help us better understand the human gut metabolism and their link to human health and disease. Thus, we need cultivation systems that mimic the human gut's natural environment and provide only specific, uncultured microbes a growth advantage over others. Cultivating and studying syntrophic microbes is challenging because they count on the metabolic activity of other microbes in their community.

In this dissertation, I address the central question of H_2 availability and how it affects microbes' metabolic output in the human gut. For proof of concept, we used *Christensenella minuta*, which is a prominent member of the *Christensenellaceae* family, and which are heritable members of the human gut and associated with human health [2]. In co-cultures with *Methanobrevibacter smithii*, *C. minuta* supports CH_4 formation, suggesting a microbial syntrophy based on H_2 consumption [4]. Understanding the underlying molecular mechanisms of H_2 transfer and the benefits of microbial syntrophy is central to this research.

To address this question, a bioelectrochemical system (BES) has been developed to mimic a syntrophic microbial partner that actively takes up H_2. The BES, featuring a platinum-doped carbon electrode (Pt/C) and a close microbe-electrode interaction site facilitating H_2 removal, creates an environment favorable for H_2-producing, carbohydrate-degrading microbes. The initial experiments with *C. minuta* in the BES successfully demonstrated its influence on the microbe's metabolism.

The next step involves investigating the BES's ability to compete with a microbial syntrophic partner from the human gut. Once validated, we will consolidate this knowledge to enrich and isolate syntrophic H_2 producers from the human gut, contributing to a comprehensive understanding of the H_2 economy within the human gut. Developing new cultivation strategies can circumvent *in-vivo* experiments (performed in mice, rats, and pigs), which have several drawbacks, such as different phylogeny, ethical commitment, costs, and low reproducibility. Therefore, greater attention was brought to *in-vitro* cultivation models that allow us to recreate, study, and understand the effects of the human microbiota between microbes and the host. New innovative cultivation techniques, including new technologies, materials, and screening approaches, brought gut microbiota cultivation into a new area [7].

1.2. Ph.D. Objectives

The aims of the PhD could be separated into three successive objectives (**Figure 1**). In Objective 1, we focussed on the BES development and proof of concept of H_2 removal with *C. minuta*. We used *C. minuta* as microbes for the proof of concept because it was shown by Ruaud and Esquivel-Elizondo *et al.* (2020) that *C. minuta* shifts its metabolism towards

more acetate and less *n*-butyrate production when a methanogen consumes H_2 simultaneously. In Objective 2, we wanted to answer whether the BES competes with a microbial syntrophic H_2 consumer regarding H_2 removal. In Objective 3, we wanted to test the BES as a tool for the enrichment of syntrophic H_2 producers from the human gut.

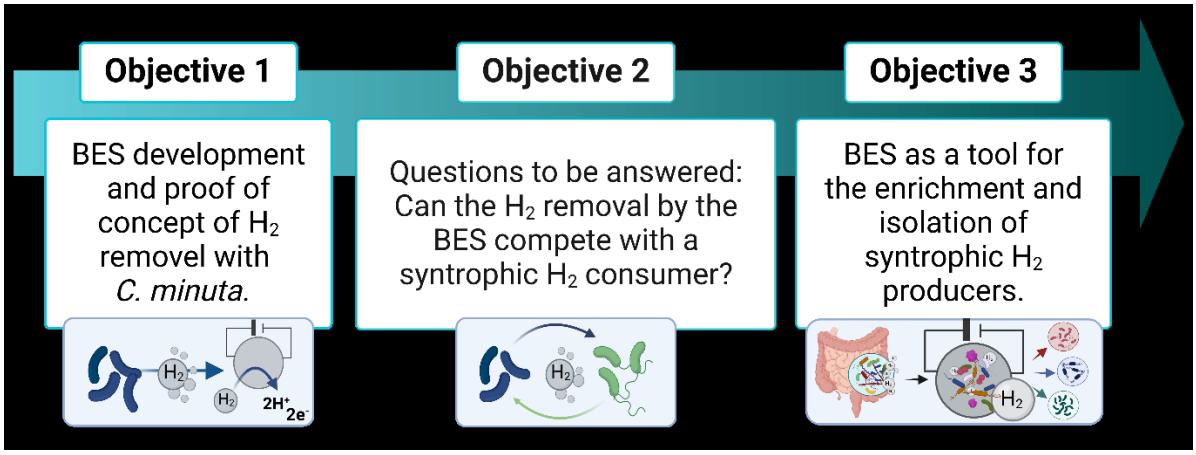

Figure 1: Overview of three Ph.D. objectives
The Ph.D. was split into three main objectives, from the initial BES development and proof of concept to the BES application as an enrichment tool for human gut microbes. The figure was created by BioRender.com.

Chapter 2
Introduction to Microbial Syntrophy of Human Gut Microbes, Interspecies H_2 Transfer, and the Potential Use of Bioelectrochemistry

2.1. Microbial Ecology – How a Microbial Syntrophic Relationship Leads to Colonic Homeostasis

2.1.1. Fermentation: an Introduction to the Anaerobic Breakdown of Substrates

Fermentation is an anaerobic and energy-yielding process that microbes use to generate energy for their metabolism. This process is defined by the production of adenosine triphosphate (ATP), which is the energy-yielding molecule, due to substrate-level phosphorylation that is associated with redox transformation between organic compounds [8]. Fermentation can occur in diverse anaerobic environments and is applied to many areas of human life such as the food industry, human health, wastewater and garbage disposal, environment, and soil management [9]. Furthermore, fermentation plays a central role and is economically feasible for the industrial production of bio-based products from renewable sources with less energy and waste. This bioprocessing approach also includes genetic and metabolic engineering techniques to produce new bio-based products, which have the potential to overcome the problem of environmental pollution and the global shortage of fossil fuels [10].

In recent years, the human gut flora and its influence on human health have received more attention. In the mammalian gut-intestinal system, digestion always follows the same route, starting from the mechanical digestion of food (carbohydrates, protein, and lipids) by chewing. Further down the digestion tract, hydrochloric acid, pepsin, and mucines of the stomach digest chemically dietary compounds and result, for example, in polypeptides. Dietary components that are not digested in the upper intestine of the human gut intestinal

tract reach the large intestine. Due to its high colonization of microbes, the large intestine becomes the most crucial region for fermentation in the human gut. Epithelial cells of the large intestine do not produce any digestive enzymes, such as bile acids, in the gut. Thus, microbial digestion of earlier degraded compounds from food is essential to degrade, for example, dietary fibers into short-chain carboxylates (SCCs) used as an energy source by intestinal cells to maintain growth and development. This process is the essence of microbial fermentation in the human gut.

2.1.2. Fermentation in the Human Gut Intestinal Tract

The human gut intestinal (GI) system represents the route of digestion, and it consists of the oral cavity, esophagus, stomach, and small and large intestine. The GI tract's overall surface area is 150 – 200 m^2 and is colonized by 10^{14} bacteria [11, 12]. Due to chemically (pH, redox potential) and physically diverse microhabitats caused by stomach, large intestine, and small intestine, the composition of the microbiome changes throughout the GI tract (**Figure 2**). For example, the pH changes from the large intestine to the small intestine from acidic to neutral pH. In parallel, the composition of microbes changes from a high concentration of *Actinobacteria*, *Bacteroidetes*, *Proteobacteria*, and *Ascomycota* in the large intestine to *Bacteroides*, *Clostridium*, and *Streptococcus* in the small intestine. Different microbes generally prefer different intestinal environments and favor specific niches in the GI tract [11, 13-15].

The large intestine is one compartment of the GI tract. It is composed of the caecum, colon (including the ascending colon, transverse colon, descending colon, and sigmoid colon), rectum, and anal tract. The colon possesses the highest biodiversity (10^{10}-10^{11} bacteria *per* g of intestinal content) of the whole GI tract. Its major characteristics regarding microbial colonization are its low cell turnover rate, low redox potential, and long transit time. The cell turnover rate is defined by cell production, cell death, and cell mean lifespan and varies by cell type and tissue. Gut epithelial cells have a turnover rate of 3-5 days [16]. Talking about redox potential refers to the tendency of a chemical species to acquire electrons (reduction) from or lose electrons (oxidation) to an electrode. In redox reactions, one compound's oxidation is coupled to another compound's reduction. Oxidants, as well as reductants, are essential for all living organisms and need to be present in a particular

range. Here, redox potentials are given either in volts (V) or millivolts (mV). Facultative anaerobic microbes require a redox potential between +300 mV and −100 mV, and anaerobes between +100 mV and less than −250 mV [17].

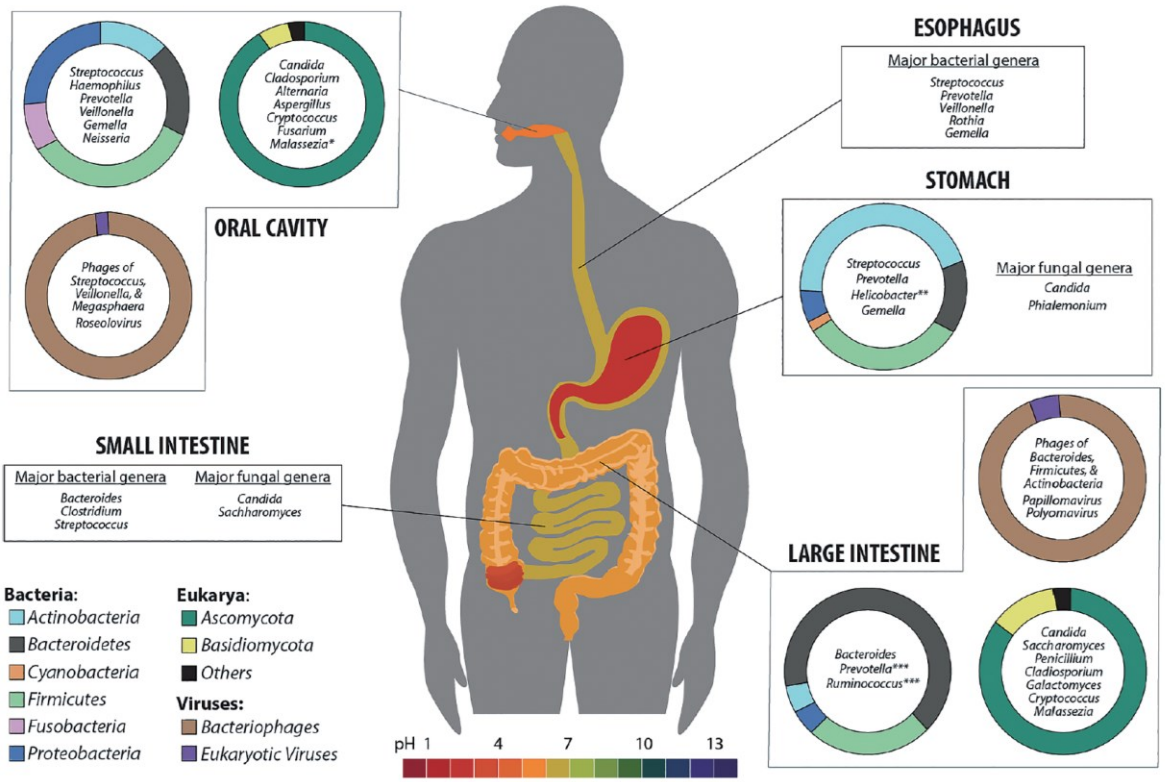

Figure 2: Human microbiome composition
The gastrointestinal tract and its different compartments conserve different microbial species. Among the physiological niches of the GI tract, the human microbiome refers to bacteria, eukarya, and viruses. The colors of the GI tract represent a defined pH according to the pH scale [18]. Figure from Hillman *et al.* (2017)

The most incredible variety of microbes that ferment non-digested carbohydrates (*e.g.*, soluble fiber) as substrates are also found in the colon [8, 19, 20]. Non-digested dietary products are complex polymerized carbohydrates that microbes break down into smaller oligomers. Further, fermentative microbes convert the oligomers into SCCs, H_2, lactate, succinate, ethanol, and carbon dioxide. SCCs, such as acetate (C_2), propionate (C_3), and *n*-butyrate (C_4), are quantitatively the most abundant fermentation products (**Figure 3**) [21-23]. SCCs typically have fewer than six carbon atoms in their carbon chain.

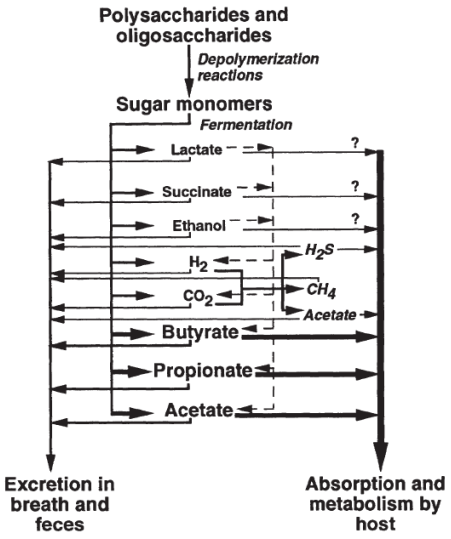

Figure 3: Carbohydrate fermentation in the human large intestine
The figure was adapted from Macfarlane and G.R. Gibson (1997)

During carbohydrate fermentation, anaerobic microbes have a cooperative metabolism: H_2 is generated by a diversity of hydrogenotrophic microbes and consumed by resident hydrogenotrophic microbes [8, 24]. H_2 is produced as molecular H_2 in the degradation process of carbohydrates *via* hydrogenases and is one of the most abundant metabolites in the colon. The production of molecular H_2 is coupled to the oxidation of reducing equivalents such as the redox protein Ferredoxin (Fd). In addition, electrons can be removed from the anaerobic environment in the gut by producing H_2. The main mechanisms by which H_2 is produced in the gut are explained in more detail in section 2.3 Cross-feeding and H_2 Metabolism of Human Colonic Microbiota. H_2 shapes metabolic homeostasis and microbial communities by creating a nice environment for microbes that can cross-feed on H_2.

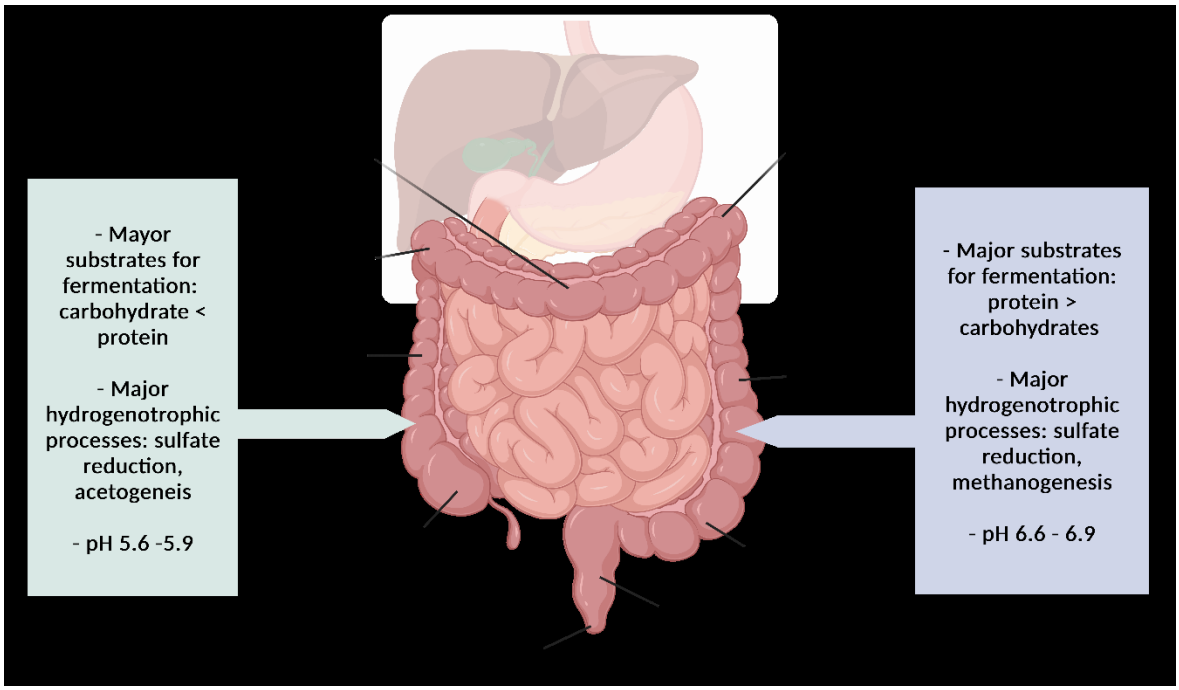

Figure 4: Characteristics of ascending and descending colon

The hydrogenotrophic processes are driven by the pH gradient and the differences in the fermentation of proteins and carbohydrates [8]. Figure adapted from Nakamura *et al.* (2010) and Payne *et al.* (2012) (created with BioRender.com)

The human colon is divided into four parts (**Figure 4**): the ascending colon (proximal), transverse colon, descending (distal) colon, and sigmoid colon. The considerable differences in the environment of the ascending and the descending colon influence the fermentation. The pH values throughout the colon vary from 5.6 - 5.9 in the ascending colon to 6.6 - 6.9 in the descending colon (**Figure 4**). This pH gradient affects the colon's microbial composition and the fermentation pattern. H_2 production is assumed to be affected by the change in pH, different microbial substrates, and other hydrogenotrophic processes. Slightly alkaline and neutral pH values are the optimal conditions for sulfate reduction and methanogenesis, which are hydrogenotrophic processes. As the third hydrogenotrophic process, acetogenesis appears to be maximal at acidic pH values [8]. Besides, the composition of hydrogenotrophic microbes changes along with the pH of the colon. For example, lower pH values (pH 5.6- 5.9) in the ascending colon promote the growth of acetogens and sulfate-reducing bacteria and support the production of *n*-butyrate by these microbes. With changes in the pH to less acidic values (pH 6.6 – 6.9) in the descending colon, methanogens exist in higher concentrations. In addition, sulfate-reducing bacteria are represent, besides of methanogens, the most abundant microbes in the part of the colon. In contrast, sulfate-reducing bacteria may colonize the whole colon.

Overall, the ascending colon is assumed to be the primary environment for hydrogenotrophic microbes and processes. Thus, it plays a pertinent role in H_2 disposal and further contributes to a homeostatic colon environment [25-29].

2.2. Energy Metabolism of the Human Gut Microbiota and their Production of Short-Chain Carboxylates

2.2.1. Microbe-Host Interactions

In the intricate ecosystem of the human gut microbiota, microbial fermentation processes yield substantial products, among which SCCs stand out prominently. The cecum and colon are the major sites for the production of SCC, with acetate, propionate, and *n*-butyrate is the most abundant aliphatic organic acid (>95%) in the intestine. Their approximate molar ratio of 60:20:20 in the colon and stool reflects a dynamic balance [22, 30-32]. The microbial community considers SCCs as essential waste products, contributing considerably to maintaining redox balance within the gut.

SCCs play a pivotal role in the interaction between microbes and their host. These organic acids, specifically acetate, propionate, and *n*-butyrate, have demonstrated therapeutic potential in the prevention and treatment of various diseases, including metabolic syndrome, Crohn's disease, ulcerative colitis, and antibiotic-induced diarrhea [32, 33]. The positive effects observed in clinical studies underscore the potential of SCCs in modulating host health. In the Western diet, humans, on average, consume approximately 20-25g of fiber/day in cases of fruit and vegetable-rich diets, the fiber content can increase up to 60g/day [34, 35]. Carbohydrate fermentation can lead to the total production of 400-600 mmol SCCs/day [36]. Since SCC production is challenging to monitor along the human gut and the fact that most of the fecal SCCs are taken up by the host, the reported SCC concentration might not reflect their actual concentrations and production rates in the intestine [37-39].

Despite the considerable impact of the gut microbiota on human health and its involvement in the development or progression of diseases, extensive research efforts have been directed towards unveiling that the influence of the gut microbiota is not restricted to the GI tract [40]. Moreover, recent revelations have demonstrated that the microbiota's impact extends beyond the gastrointestinal tract's confines, assuming a

considerable role in the bidirectional communication between the GI tract and the central nervous system. This concept is called the microbiota-gut-brain axis. [41-46]. Potential mechanisms through SCCs impact the communication between the gut and the brain are elucidated, too. SCCs, which are the primary metabolites generated by the microbiota during the anaerobic fermentation of indigestible polysaccharides, notably dietary fiber, and resistant starch in the large intestine (mainly the colon), may exert direct or indirect effects on gut-brain communication and brain function. Upon production, SCCs are absorbed by colonocytes, primarily through H^+-dependent monocarboxylate transporters (MCTs) or sodium-dependent monocarboxylate transporters (SMCTs) (**Figure 5**) [47].

Engaging with G protein-coupled receptors (GPCRs), including free fatty acid receptors 2 and 3 (FFAR2 and FFAR3), GPR109a/HCAR2 (hydrocarboxylic acid receptor), and GPR164, or inhibiting histone deacetylases, SCCs play a role in influencing intestinal mucosal immunity, barrier integrity, and function. GPR109a/HCAR2, GPR43, and GPR41 are expressed by a vast array of gastrointestinal mucose cells and the nervous and immune system [48, 49]. Interaction with receptors on enteroendocrine cells facilitates indirect signaling to the brain *via* the systemic circulation or vagal pathways. This signaling is mediated through the secretion of gut hormones, such as glucagon-like peptide 1 (GLP1) and peptide YY (PYY), as well as by the neurotransmitters gamma-aminobutyric acid (GABA) and serotonin (5-HT) by enteroendocrine and enterochromaffin cells [50-55].

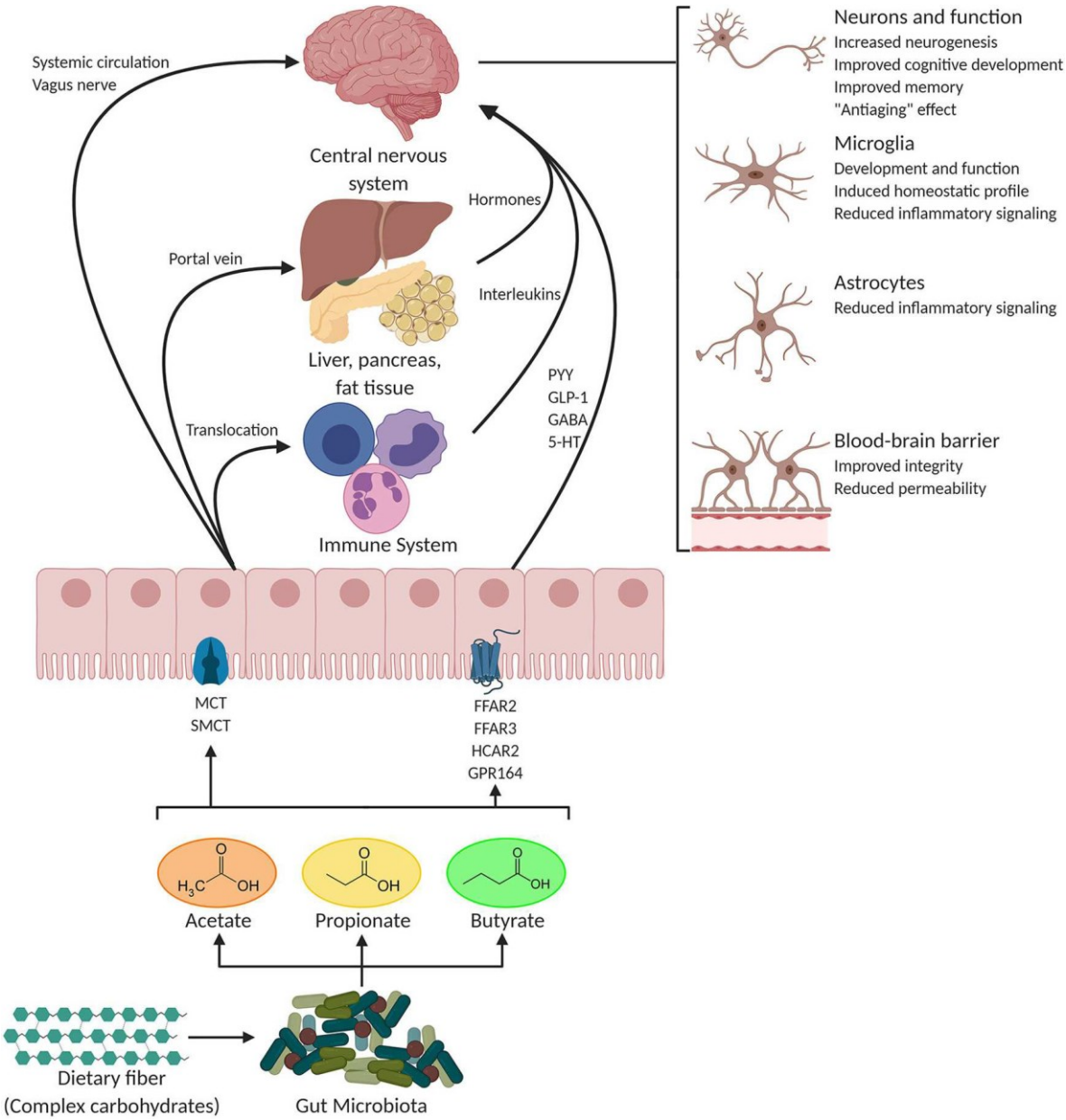

Figure 5: A simplified representation of the potential influences of SCC on the gut-brain communication

In the colon, microbes metabolize soluble and indigestible polymers from complex carbohydrates, such as dietary fiber and resistant starch, producing SCCs. In the microbiota-gut-brain crosstalk, it is speculated that SCCs play a pivotal role in the immune response and affect the central nervous system. The illustration is a simplified representation of the connection between SCCs and the gut-brain axis. It is not intended to provide a complete description of other functional groups. The figure was taken from [56].

SCCs originating from the colon reach the systemic circulation and various tissues, activating brown adipose tissue, regulating liver mitochondrial function, enhancing insulin

secretion by beta-pancreatic cells, and contributing to whole-body energy homeostasis [56].

Peripherally, SCCs impact systemic inflammation by promoting regulatory T cell (Treg) differentiation and regulating interleukin secretion. The effects of *n*-butyrate on the immune system were extensively studied. It induces Treg cell differentiation and controls inflammation [51, 57-59]. SCCs can traverse the blood-brain barrier (BBB) *via* monocarboxylate transporters on endothelial cells, influencing BBB integrity by downregulating tight junction proteins such as claudin and occludin. This affects the BBB integrity and the controlled passage of nutrients and molecules from the circulation to the brain. [60]. In the central nervous system (CNS), SCCs contribute to neuroinflammation by influencing glial cell morphology and function, modulating neurotrophic factors, increasing neurogenesis, participating in serotonin biosynthesis, and enhancing neuronal homeostasis and function [41, 53, 54, 61-63].

2.2.2. Microbe-Microbe Interactions and Metabolic Fluxes

In-vitro, production of SCCs differs from *in-vivo* studies due to changes in the microbiota caused by isolation and product accumulation during fermentation. The production of SCCs by the gut microbiota is influenced by the type of dietary fibers that change the microbiota composition. Furthermore, host genetics, environmental factors, the colonic milieu, and microbial composition affect SCC production [25, 26, 64, 65]. Dietary fiber intake considerably influences SCC production, with carbohydrate fermentation generating 400-600 mmol SCCs *per* day. In the context of the Western diet, where individuals consume approximately 20-25g of fiber daily, this production increases with a fruit and vegetable-rich diet [34, 36]. However, monitoring SCC concentrations along the human gut poses challenges, because most fecal SCCs are absorbed by the host, making reported concentrations potentially misleading [37-39].

Bacteroidetes, Firmicutes, and Actinobacteria are the most abundant phyla in the human intestine. Bacteroidetes mainly produce acetate and propionate, whereas Firmicutes are the dominant *n*-butyrate producers [66]. The availability of substrates is the highest in the proximal part of the colon and decreases towards the distal part. Therefore, the microbial activity is higher in the proximal site of the colon than in the distal part. In the proximal

part of the colon, nondigestible carbohydrates are fermented by saccharolytic microbes, mainly Bacteriodetes, which are primary fermenters. The fermentation products are SCCs and gasses such as H_2 and CO_2 [67]. Bacteriodetes are part of a syntrophic community that mutually cross-feeds with other microbes that take up these gasses as substrates. In the distal part of the colon, bacterial proteins and amino acids derived from primary fermenters, such as Bacteriodetes, are fermented by secondary fermenters, which are proteolytic bacteria and result in medium-chain carboxylates (MCC). MCCs have carbon chains containing 6 to 12 carbon atoms. In addition, toxic metabolites, such as phenolic and volatile sulfur compounds and amines, are products of the secondary fermenters [68].

The gut microbiota plays a crucial role in converting nondigestible carbohydrates *via* hydrolysis into oligosaccharides and monosaccharides. The latter are getting fermented into SCCs through intricate anaerobic processes. Key metabolic routes involve the Embden-Meyerhof-Parnas glycolytic pathway for six-carbon sugars and the pentose-phosphate pathway for five-carbon sugars, ultimately converting monosaccharides into phosphoenolpyruvate (PEP) [69]. Subsequently, PEP is converted into fermentation products, such as organic acids or alcohols.

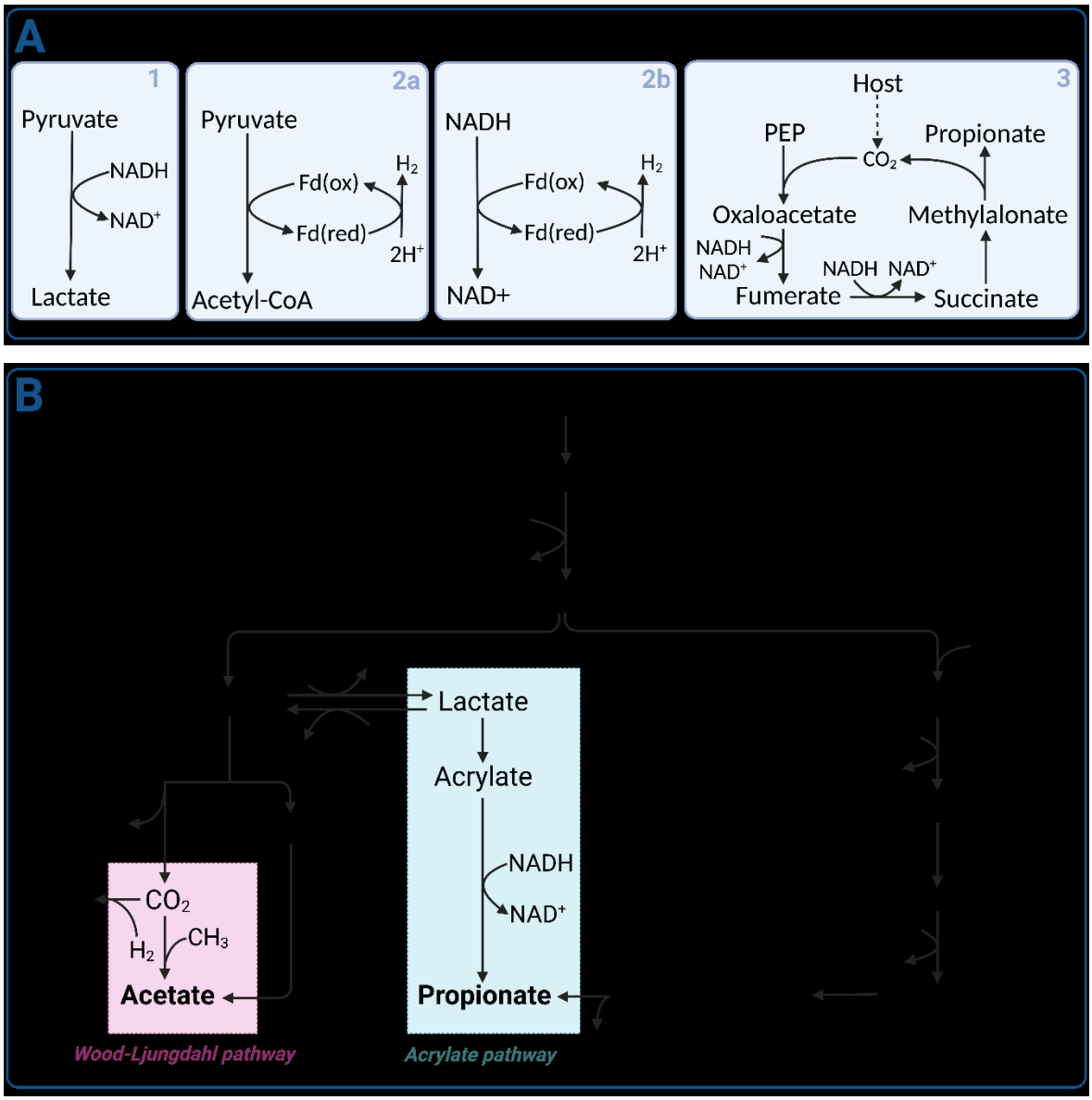

Figure 6: Bacterial pathways of anaerobic SCC production and concomitant formation of H_2 and CO_2

See the explanation on the next page.

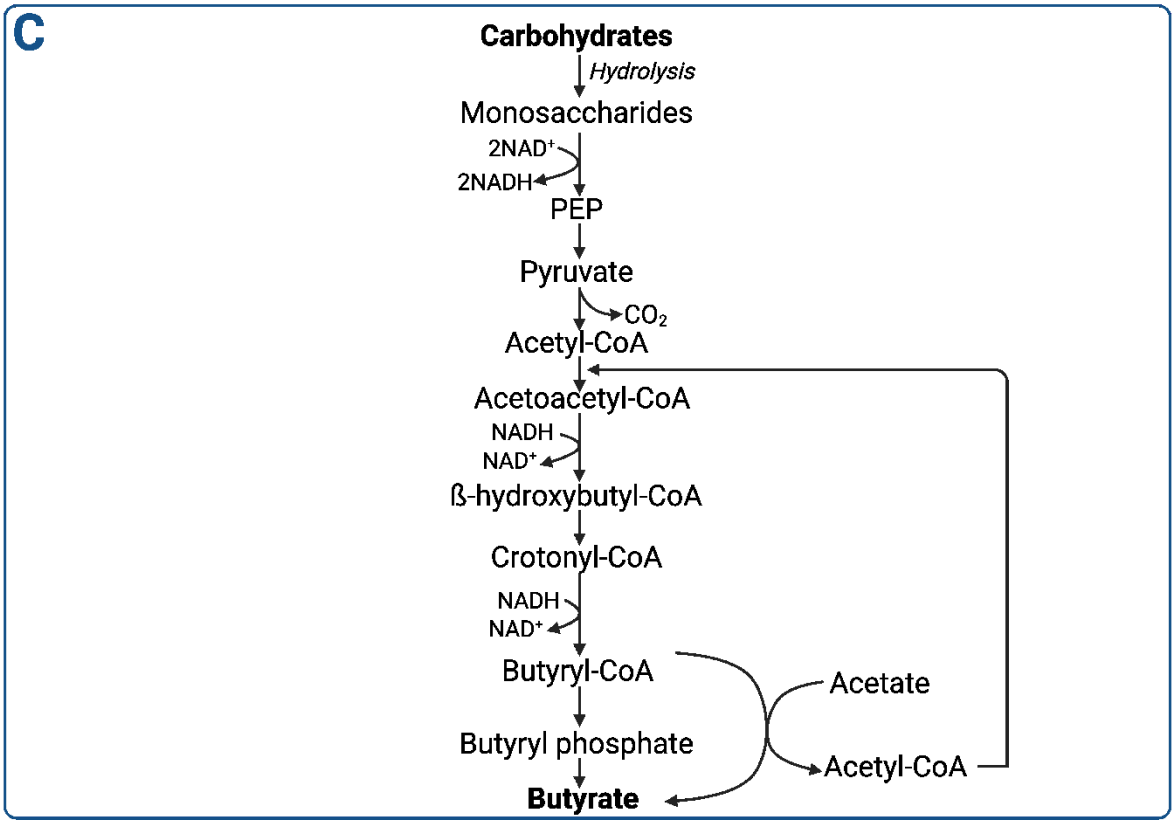

Figure 6: Bacterial pathways of anaerobic SCC production and concomitant formation of H_2 and CO_2

Gut microbes use three pathways to eliminate excess reducing equivalents when converting monosaccharides into SCCs. (A) *Via* the classical fermentation pathways (1), where pyruvate is reduced to either lactate or ethanol (not shown) and NADH is oxidized to NAD^+. Primary fermenters produce molecular H_2 to sink reducing equivalents *via* two routes (2a+2b). The exergonic (2a) route involves the pyruvate: ferredoxin oxidoreductase and ferredoxin hydrogenase enzymes. Meanwhile, the endergonic route (2b) goes *via* NADH: ferredoxin oxidoreductase and ferredoxin hydrogenase. In the third pathway type (3), SCCs are produced from the electron transport chain, starting from the carboxylation of PEP into propionate and CO_2. Production of acetate, propionate, and *n*-butyrate from carbohydrates. (B) Acetate is the product from either the Wood-Ljungdahl pathway using formate or directly produced from acetyl CoA. Propionate is produced from PEP by the succinate decarboxylation pathway or *via* the acrylate pathway, where lactate is reduced to propionate. (C) *n*-Butyrate is being produced from condensation of two moles of acetyl-CoA by butyrate-kinase or by butyryl-CoA:acetate-CoA-transferase which uses exogenously derived acetate to form *n*-butyrate. The figure was adopted from den Besten *et al.* (2013) [70]and was created with BioRender.com.

At the glyceraldehyde-3-phosphate dehydrogenase level within the glycolytic pathway, glyceraldehyde 3-phosphate is transformed into glycerate-1-3-bisphosphate combined with the formation of the electron carrier NADH. Anaerobically, NADH needs to be reoxidized to NAD^+ for reuse as an electron carrier for glycolysis. Three pathways exist to eliminate excess reducing equivalents (Fehler! Verweisquelle konnte nicht gefunden werden.**A**). The first is the classical fermentation pathway, where pyruvate is reduced to lactate or ethanol, oxidizing NADH to NAD^+. Second, some primary fermenters channel excess reducing equivalents into molecular H_2 through two major routes: an exergonic route ($\Delta G_0' < 0$) *via* pyruvate: ferredoxin oxidoreductase and ferredoxin hydrogenase, and an endergonic route ($\Delta G_0' > 0$) *via* NADH: ferredoxin oxidoreductase and ferredoxin hydrogenase, the latter operating at low H_2 pressure in the large intestine lumen. H_2-consuming bacteria, in turn, influence primary fermenter metabolism by depleting H_2 [66]. The third pathway involves a primitive anaerobic electron transport chain starting with PEP carboxylation, leading to the reduction of oxaloacetate to fumarate. Fumarate, in turn, accepts electrons from NADH through a simple electron-transfer chain, ultimately contributing to chemiosmotic ATP synthesis. Succinate, which is the product of fumarate reductase, is converted into methylmalonate and further into propionate only when the partial pressure of CO_2 is low. *Via* carboxylation, CO_2 can be recycled into PEP to form oxaloacetate [70-72].

The primary end products of fermentation pathways, described previously, are SCCs. Pyruvate conversion to acetyl-CoA results in the simultaneous formation of H_2 and CO_2. Acetate is formed either by acetyl-CoA hydrolysis or *via* the Wood-Ljungdahl pathway (**Figure 6B**), where CO_2 is reduced to CO, converted with a methyl group and coenzyme A to acetyl-CoA [73, 74]. Propionate can be generated through the primitive electron transfer chain or by lactate reduction to propionate, known as the acrylate pathway (**Figure 6B**) [69]. Both pathways involve additional NADH reduction compared to lactate fermentation. *n*-Butyrate production initiates with the condensation of two acetyl-CoA molecules, followed by reduction to butyryl-CoA (**Figure 6C**). Lactate-utilizing bacteria can contribute to *n*-butyrate production through acetyl-CoA generation from lactate. In the classical pathway, phosphotransbutyrylase and butyrate kinase convert butyryl-CoA to *n*-butyrate and coenzyme A, accompanied by ATP formation. An alternative pathway involving butyryl-

CoA: acetate CoA-transferase utilizes exogenously derived acetate, generating *n*-butyrate and acetyl-CoA. This pathway, supported by labeling studies, suggests cross-feeding between acetate and *n*-butyrate producers, with the alternative pathway dominating the human gut microbiota [75].

Collaborative functioning of the gut microbiota is essential for SCC production and symbiotic associations with the host. Other bacteria must utilize molecular H_2 produced during acetate formation to prevent H_2 accumulation, which can hinder primary fermenters' NADH oxidation. The host partly supplies CO_2 needed in the primitive electron transfer chain, as humans produce approximately 0.7 kg of CO_2 daily. This CO_2 is excreted into the gut lumen as HCO_3^- in exchange for SCC anions, serving as a crucial pH regulatory mechanism. Despite extensive knowledge about the biochemistry of carbohydrate conversion into SCCs by the microbial community, there is a lack of data on SCC production rates by the gut microbial community. The challenge lies in sampling the large intestine, emphasizing the need to measure SCC production rates accurately and understand the impact of specific carbohydrates and microbiota on SCC mass and composition [70]. Syntrophy is classically defined as obligatory mutualism between cooperative microbial partners that cross-feed on each other's products. Grasping the full scope of mutualistic cross-feeding interactions within the gut microbiome is essential for elucidating key features: the remarkable diversity of species and the extraordinary stability in maintaining consistent taxa over periods spanning years to decades [76]. Two groups of metabolites are cross-fed by microbes: sugars and electron donors/acceptors are directly used in the central metabolism, whereas essential nutrients, such as amino acids, cofactors, and vitamins, require direct uptake mechanisms [77].

2.3. Cross-feeding and H_2 Metabolism of Human Colonic Microbiota

Diversity, as well as community, describe the human gut-intestinal microbiome. The diverse and complex anatomical shape of the gut, its pH gradients, and nutrient supply, as well as the host genetics and secretions, continuously influence the composition of the gut microbiome. Due to different physical characteristics and nutrient supply, different microbial populations are found in different specific microhabitats. These microhabitats

serve as niches for distinct microbial groups and are diverse regarding presented substrates and physical characteristics [18, 78, 79]. This diverse ecological landscape comprises trillions of microbial cells and controls a person's health and disease status [24, 80, 81]. In detail, the colonic microenvironment is composed of bacteria, viruses, archaea, and eukaryotes that interact with each other and the host's immune system. A holistic approach to understanding the microbiome composition, host physiology, and disease susceptibility must include dynamic interactions, community characterization, and microbiome-host interactions (*e.g.*, epithelial cells and innate lymphoid cells).

In nature, microorganisms seldom exist in monoculture under constant conditions; rather, they create intricate communities capable of enduring fluctuating environments. The interplay among these microbes yields synergistic effects, often unpredictable when examining individual species. Competitive and antagonistic interactions limit the growth of certain members, while the collective metabolic activity of the community provides resilience against nutrient stress. Many of these ecological dynamics rely on diffusible metabolites, which serve as nutrients and play crucial roles in mediating interactions. Cross-feeding, which involves the exchange of metabolites as energy among various microbes, plays a pivotal role in forming stable communities of gut commensals that exhibit resistance to invasion and resilience against external disturbances. Metabolites engaged in cross-feeding within the microbiome can be broadly categorized into two groups: those directly utilized in central metabolism such as sugars and electron donors/acceptors, and those essential nutrients necessitating biosynthesis or uptake like amino acids, cofactors, and vitamins. Regarding the central metabolism, cross-feeding establishes trophic levels, where primary degraders hydrolyze complex polysaccharides, releasing oligo- and monosaccharides accessible to other species.

Primary fermenters either liberate these sugars independently or obtain them from other microbes. They channel these sugars through glycolysis, where the resulting PEP is utilized for substrate-level phosphorylation for SCCs (formate, acetate, succinate) or alcohols (*e.g.* 1,2-propandiol) generation. Subsequently, secondary fermenters utilize these by-products through various fermentative or respiratory pathways of their own, producing SCCs (acetate, *n*-butyrate, propionate) including acetate, butyrate, and propionate. Lastly, H_2

generated by primary/secondary fermenters acts as an electron donor for sulfate-reducing bacteria, methanogens and acetogens [77].

In the colon, carbohydrate fermentation is the central energy-generating process for most intestinal microbes, which also in the results in incompletely oxidized organic compounds and reduced fermentation products serve as terminal electron acceptors. Terminal electron acceptors are needed to recycle energy carriers (ATP, NAD^+, FAD^+). The whole metabolism is based on redox reactions, where the oxidation of one metabolite is coupled to the reduction of another one. During the colonic fermentation process, the reoxidation of reduced coenzymes NADH and $FADH_2$ maintains the redox balance and leads to the formation of H_2 [3]. During the microbial metabolism of carbohydrates and proteins, the production of H_2 is an efficient mechanism to dispose of the generated reducing power. In parallel, any accumulation of H_2 needs to be avoided because a rise in the partial pressure thermodynamically restricts further anaerobic fermentation in the colon. As described in section 2.2.2 Microbe-Microbe Interactions and Metabolic Fluxes, H_2 from bacterial fermentation is primarily derived from three different reactions (**Figure 6A**). One reaction is the reoxidation of pyridine and flavin nucleotides, which involves the ferredoxin oxidoreductase and hydrogenase enzymes. The other two reactions are the cleavage of pyruvate to formate by the formate hydrogen lyase and the generation of H_2 from pyruvate through the enzymes pyruvate: ferredoxin oxidoreductase and hydrogenase [3, 70].

H_2 can be efficiently removed with H_2 excretion in flatus and breath (15-20% of H_2 for each route). In addition, H_2 accumulation and a rising partial pressure can also be prevented by H_2-consuming (hydrogenotrophic) microbes. Generally, any metabolic process aims to generate products with a high energy yield. Thus, H_2 must be removed to shift the fermentation to more oxidized end products. Briefly, a sufficient exergonic reaction is enabled by an interaction of microbes that produce H_2 to maintain the redox balance and other microbes that utilize H_2 to keep the H_2 partial pressure low. This effect is called H_2 syntrophy and relies on the production and the removal (consumption) of H_2.

2.3.1. Interspecies H_2 Transfer

During the fermentation of organic matter, interspecies H_2 transfer is a mutually beneficial and unidirectional process where molecular H_2 (reducing equivalent) produced by hydrogenogenic microbes is transferred to and oxidized by a group of hydrogenotrophic microbes. Because very little energy is available from specific substrates, microbial communities have adapted to conserve small quantities of energy across a charged membrane from one microbe to another microbe(s). This is the principle of a syntrophic microbial relationship [8]. The classic definition of syntrophy refers to a metabolic interaction between dependent microbes (= microbial partners) and is based on close proximity in a microbial community. In other words, syntrophy is obligatory mutualistic catabolic metabolism where microbes share essential metabolic products. The metabolic product of one microbe serves as a substrate for another microbe. Besides substrates, a syntrophic microbial community shares growth factors, vitamins, and electrons. Furthermore, removing toxic products or thermodynamic constraints can also define microbial syntrophy [82, 83].

Molecular H_2 serves as a crucial electron sink in numerous pathways facilitating anaerobic growth. In these microbes, proton reduction is linked to the oxidation of ferredoxin, formate, NADH, and $FADH_2$, leading to H_2 production. However, the low redox potential of H^+/H_2 implies that these reactions are favorable only under low H_2 partial pressure, as its accumulation can impede or hinder growth, typically by restraining NADH oxidation. The elimination of H_2 by partner bacteria or archaea, known as interspecies H_2 transfer, holds paramount importance for the growth of these bacteria and stands as a classic illustration of syntrophy. In H_2 syntrophy, H_2 never joins the dissolved H_2 pool due to interspecies H_2 transfer [83, 84]. Thus, the whole anaerobic fermentation process is thermodynamically feasible. Methanogenesis and sulfate reduction are processes for terminal electron acceptance where H_2 is oxidized and the electrons are transferred to CH_4 (methanogenesis) or H_2S (sulfate reduction). These reactions consume less energy (**Table 1**). Thus, several microbes share available energy products. During reductive acetogenesis, H_2 and CO_2 are taken up and synthesized into acetyl-CoA, whereas energy and assimilating CO_2 are conserved into cell carbon. This process is called the Wood-Ljungdhal pathway.

Table 1: The competition between hydrogenotrophs in the human gut [8, 29]

	Methanogens		**Sulfate-reducing Bacteria**	**Acetogens**
	Methane producers	Non-Methane Producers		
CFU/g in human feces	10^9	10^4	10^3 to 10^{11}	10^2 to 10^8
Utilization of H_2	$4H_2 + CO_2 \rightarrow CH_4 + 2H_2O$		$4H_2 + SO_4^{2-} + H^+ \rightarrow HS^- + 4H_2O$	$4H_2 + 2CO_2 \rightarrow CH_3COO^- + 2H_2O + H^+$
$\Delta G^{0'}$ [kJ/mol]	-131.0		-152.2	-95.0
H_2 Threshold [ppm]	30-100		10-20	400-950

In the colon, oxidation of H_2 by sulfate-reducing bacteria ($\Delta G^{0'}$ = -152.2 kJ/mol) is energetically more favorable than by methanogenesis ($\Delta G^{0'}$ = -131.0 kJ/mol). An important acetate production resulting from H_2-dependent CO_2 reduction is only observed without methanogenesis. H_2/CO_2 acetogenesis ($4H_2 + 2CO_2 \rightarrow CH_3COO^- + H^+ + 2H_2O$) has a $\Delta G^{0'}$ of -95.0 kJ/mol and is, thus, less efficient than either sulfate reduction or methanogenesis (**Table 1**) [29, 85-88].

2.3.2. Hydrogeneses – Metalloenzymes for H_2 Disposal in the Human Gut

Hydrogenotrophic microbes are the major players of the central molecular H_2 cycle in the human gut and thus are responsible for the GI tract's metabolic homeostasis. The evidence is rising that imbalances in the colonic H_2 metabolism influence colorectal cancer, gastrointestinal infections, obesity, and inflammatory bowel diseases [3, 8, 89]. Thus, investigations of the human colonic H_2 metabolism are becoming increasingly important. The reversible oxidation of molecular H_2 is performed by metalloenzymes called hydrogenases. Archaea, bacteria, and eukarya possess these ubiquitous enzymes and their variants adapted to anaerobically and anaerobic environments [90, 91].

Hydrogenases have great phylogenetic diversity and can be subdivided into three distinct classes. The subdivision is based on the metal side of the hydrogenases. Therefore, [NiFe],

[FeFe], and [Fe] hydrogenases are distinguished. A comprehensive classification, which correlates the primary phylogeny of these enzymes with their functions, showed that these three main groups can be further distinguished. It was found that [NiFe]-hydrogenases can be subdivided into four groups, including 22 subgroups. In the case of [FeFe] –hydrogenases, three groups and six subtypes can be functionally distinguished [91]. [FeFe] –hydrogenases represent a small homogenous group of these enzymes, whereas the diversity of hydrogenases from the classes of [NiFe]- and [FeFe]–hydrogenases is much larger. Their functions in anaerobic environments are hydrogenotrophic respiration, hydrogenogenic respiration, hydrogenogenic fermentation, electron bifurcation, and sensing. Due to the enzymatic functionality, these hydrogenases will likely be located in the human colon [91]. Wolf *et al.* (2016) showed that two-thirds of all microbial species (343) included in the Human Microbiome Project Gastrointestinal Tract harbor hydrogenases. 60% of the investigated microbes encode for [FeFe] –hydrogenases and 21% for [NiFe]–hydrogenases (**Figure 7**). All representatives of Clostridiales and Bacteroidaceae harbor [FeFe] –hydrogenases genes, as well as some microbes of the kingdom Proteobacteria, Fusobacteria, Actinobacteria, and Synergistetes (**Figure 7**).

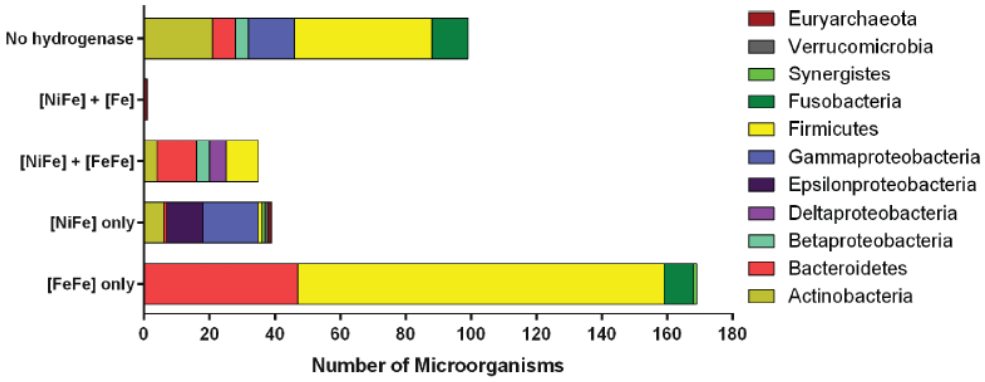

Figure 7: Microbial phyla from the human colon that encode hydrogenases
From the Human Microbiome Project Gastrointestinal Tract genome database, it was determined that, in total, 343 microbial species from 11 different phyla harbor hydrogenase sequences. Figure from [24]

Furthermore, it was found that [NiFe]–hydrogenases genes are present but unevenly distributed in all microbial phyla relevant to the human gut microbiome, except Fusobacteria. In contrast, Bacilli and Bifidobacteria do not harbor hydrogenase genes. Wolf *et al.* (2016) also showed that the most abundant hydrogenase genes encoded for [FeFe]–

hydrogenases mediate H_2 production, flavin-based electron-bifurcation, and possibly H_2 sensing. The analysis of [NiFe]–hydrogenases showed that the functionalities of the encoded genes are more diverse. These genes are involved in the H_2 oxidation coupled with physiologically relevant electron acceptors (sulfate and fumarate). In addition, enterobacteria-type hydrogenlyases were detected, a subgroup of [NiFe]–hydrogenases, and couple formate oxidation to H_2 production and methanogenic Eha, Ehb, and Ech hydrogenases. These methanogenic hydrogenases form proton/sodium-translocation respiratory chains, which couple ferredoxin oxidation to proton reduction reversible. The study showed that the H_2 cycle is dominated by [FeFe]–hydrogenases from Bacteroidetes and Firmicutes from the human gut, while Bacteroidetes hydrogenase genes are more abundant than those in Firmicutes [24].

2.4. Bioelectrochemistry: An Approach to Study Hydrogen Syntrophy

2.4.1. Introduction to Compartments of a BES

In bioelectrochemistry, BESs convert chemical energy into electric energy. This process can be used for energy storage and bioelectrosensors, but also to study microbial interactions [92]. Any BES is divided into a working chamber and a counter chamber. In the working chamber, when operated in the anodic mode, oxidation of an organic compound takes place, which results in the formation of protons and electrons. Simultaneously, protons are being reduced in the counter chamber while the electrons (negative charge) travel from the anode to the cathode *via* a connection site (*e.g.*, silver wire). An ion transport system enables the transport of protons and cations (positive charge) from the anode to the cathode chamber through an electrolyte. This guarantees electroneutrality and expresses the fact that zero net charge is carried. It is also possible to transfer anions from the cathode to the anode. To manage the transfer of either cations, protons, or anions from one chamber to the other, the working and counter chambers are separated by a membrane barrier. This barrier only allows selective ions, such as protons, to pass. Furthermore, the resulting electron stream is measured against a reference electrode. The reference electrode is the third principal part of a BES [93].

2.4.2. Electrode Materials

Depending on the application, various electrode materials are available. An electrode material needs to fulfill the following characteristics: i) electrical conductivity; ii) corrosion resistance; iii) high mechanical strength; iv) biocompatibility; v) developed surface area; vi) environmentally friendly; and vii) low costs [94, 95]. Mainly, carbonaceous- and metallic-based materials are used as electrodes. Carbonaceous materials include carbon brushes, carbon cloth, carbon veil, carbon paper, carbon rods, carbon mesh, carbon felt, carbonized cardboard, granular activated carbon, and graphite plates [96]. The most common carbonaceous material is carbon cloth. Its major advantages are the high surface area, relatively high porosity, and high electrical conductivity. Besides that, flexibility, mechanical strength, and complex 3D structures contribute to many applications in BESs [97, 98].

On the one hand, microbial electrochemistry relies on biocompatibility, which describes the interaction of microbes with the electrode surface. On the other hand, electron transfer mechanisms and environmental parameters of microbial colonization shape the performance of a BES. The general idea of a BES is the exchange of microbial-generated electrons with solid substrates (electrodes). Specifically coated electrodes in the anode compartment, for example, with platinum, can act as a (metal-) catalyst to oxidize H_2 produced from microbes, which leads to the generation of protons and electrons [99-101].

2.4.3. Metal Catalysts that Enable H_2 Oxidation

One essential component of a BES is the anode. Structurally and functionally, it can act as a site for bacterial attachment in, for example, microbial fuel cells and as an intermediate electron acceptor. The major limitation of the anode is often the interior conductibility. Commonly used anode materials are, besides the previously named materials, for example graphite, activated graphite felt, graphite foil, graphite felt, carbon-cloth, carbon paper, activated carbon-cloth, Pt, Pt-black, tungsten carbide, and reticulated vitreous carbon. Its inherent hydrophobic character can limit the anode function from functioning correctly and prevent microbial adhesion. However, lab protocols, such as autoclaving, have been developed to circumvent this problem.

Besides the insufficient electron transfer, surface fouling can also be a considerable challenge. By using different anode materials in combination with material modifications, for example, by coating with conductive materials, the problems have been solved to lead to a better bacterial attachment and increase the electron transfer rate. Thus, substrate metabolism and extracellular electron transfer are enhanced by material modifications to improve electrical conductivity. [102-104].

Pt and Pt-black electrodes perform better in comparison to carbon-cloth or graphite variants. Besides improving the overall electrode performance, metals, such as Pt, can also act as catalysts. These specifically coated electrodes are called electrocatalytic electrodes. Niessen *et al.* (2006) showed in their experiments with *Escherichia coli*, *Clostridium butyricum*, and *Clostridium beijerinckii* that electrodes coated with Pt-PFFA have a better catalytic property towards H_2 oxidation in comparison to Pt-coated electrodes [101, 105].

2.4.4. Mechanisms Involved in Electron Transport

The interaction of a microbial cell and an electrode can be of a capacitive or Faraday nature. In a capacitive interaction, the double-layer capacity of an electrode is changed by the attachment or detachment of a microbial cell. The lipid layer of the cell membrane displaces water molecules and ions from the double layer of the electrode due to microbial cell attachment. It leads to a flow of the charge-balancing (capacitive) electric current. Oxidation and reduction processes of microbial cells or molecular species are part of microbial extracellular electron transfer and belong to Faraday's nature. Microbial extracellular electron transport defines electrons as exchanging between an electrode and an intracellular electron transfer chain.

In a BES, electrons can be either transferred directly (**Figure 8**) or indirectly (= mediated, **Figure 9**) to the electrode. Direct electron transfer occurs between the outer membrane of an electro-active microbe and the electrode. Synonyms for electro-active microbes are electricigens, anode-respiring bacteria, and exoelectrogenic bacteria at anodes, and electrotrophes at cathodes [99, 106-108]. The microbe is near the electrode, which means a permanent attachment at the electrode in the form of a biofilm formation (**Figure 8A**). Mediated electron transfer is based on molecular redox compounds that act as electron carriers (**Figure 9A**-**B**). In technical systems, microbial redox mediators (*e.g.,* flavins or phenazines) are more common than artificial redox mediators.

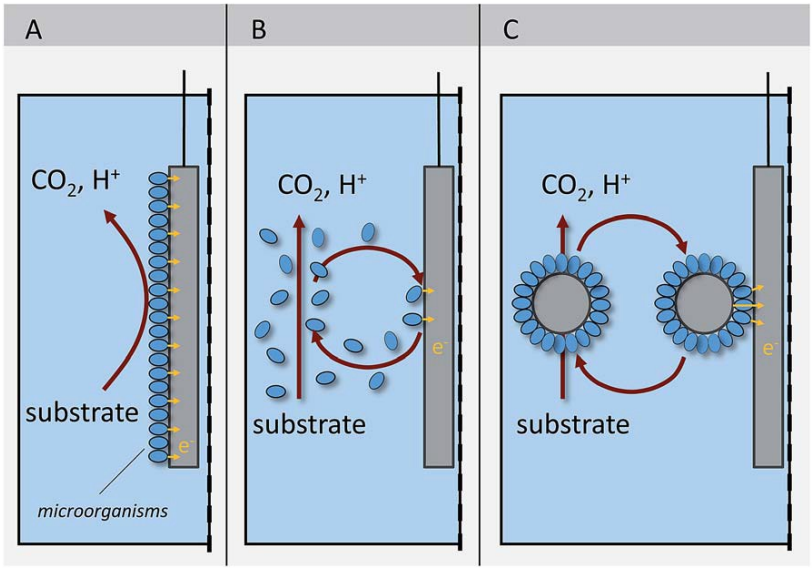

Figure 8: Direct electron transfer in anodic bioelectrochemical half-cell

(A) Electron transfer at a biofilm anode, (B) *via* microbes in suspension, or (C) *via* capacitive microbes in biofilm particles. Figure was adapted from Schröder, Harnisch and Angenent (2015)

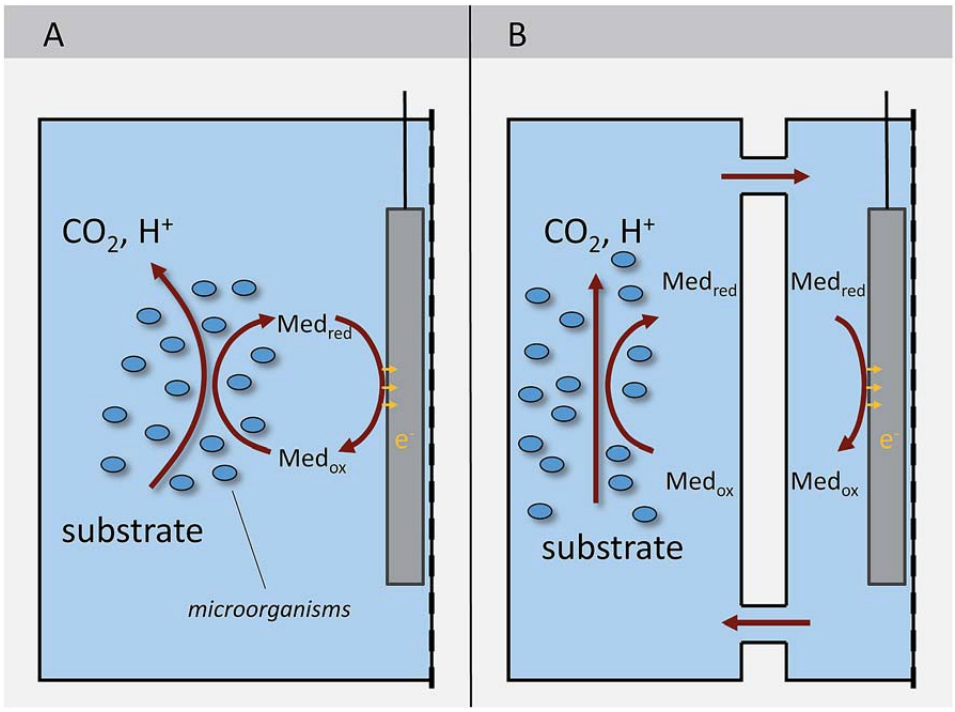

Figure 9: Mediated electron transfer in different anodic bioelectrochemical half-cell

(A) Integrating microbes in the bioelectrochemical half-cell, or (B) separating microbes from the bioelectrochemical half-cell. Figure was adapted from Schröder, Harnisch and Angenent (2015)

Type-c cytochromes and conductive pili or bacterial nanowires are known for the direct transfer of electrons across the membrane. One example of a direct electron transfer was demonstrated with *Geobacter sulfurreducens*. It could be clearly demonstrated by the model microbes that direct transfer is accomplished by cytochrome c membrane proteins (*e.g.,* MacA, PpcA, OmcB, OmcA, and OmcS) across the inner membrane, the periplasm, and the outer membrane to the electrode surface [106, 109-111]. The knowledge about direct electron transfer can be used to study microbial syntrophic relationships that rely on interspecies H_2 transfer. Guzman *et al.*, 2019 designed a BES that allows the investigation and the enrichment of H_2-producing syntrophic bacteria [112].

2.4.5. Design and Development of a BES to Oxidize H_2

The idea of a BES is to study and enrich H_2-producing syntrophic microbes by Guzman *et al.* (2019) was to develop a design based on the concept of a close physical contact of the microbe with the anode. The anode oxidizes the biologically produced H_2, and the resulting electrons can be recorded as generated current. This approach is called H_2-removing anode and was implemented to compete with the methanogen in the syntrophic microbial partnership.

BESs are used in environmental and biotechnological applications for waste treatment as a biotechnology platform for producing valuable chemicals and energy generation. Furthermore, electrochemical activity within the microbial culture can be studied using a BES. The development of a BES to study microbial syntrophy was developed by Guzman *et al.* (2019) in three steps. First, the maximum H_2 concentration to select for syntrophic bacteria was determined by mathematical modeling. The H_2 threshold is 51 nM in the bulk liquid, where both the syntrophic bacterium and the methanogenic partner could grow at identical rates. Thus, a lower H_2 concentration (< 51 nM) would promote the growth of the syntrophic bacterium, and higher H_2 concentrations (> 51 nM) the growth of the methanogen. Second, the maximum distance of the microbe away from the H_2-oxidizing electrode was evaluated by mathematical modeling to provide a growth advantage for the syntrophic (H_2-producing) microbe over the methanogen (H_2-consuming) within the BES. The model showed that 1 mm is the maximum space away from the anode. The third step was to enrich a syntrophic (H_2-producing) bacteria. Here, the microbial-produced H_2 can be

measured as current and relies on oxidation at a Pt-coated anode. The basic idea of this system was to separate the never-before-separated co-culture of *Syntrophomonas zehnderi* and *Methanobacterium formicicum* where *S. zenderi* grows only in the presence of *M. formicicum*. Guzmann *et al.* (2019) were able to enrich *S. zenderi* from the co-culture in the electrochemical system and a detectable increase in electric current was found when microbial H_2 was provided to the electrode (**Figure 10**). To ensure that the electrical current was generated due to anaerobic conditions, O_2 was introduced into the system, and a decrease in the current was detected (**Figure 10**). A short and minimal exposure to O_2 did not harm the activity of both microbes [112].

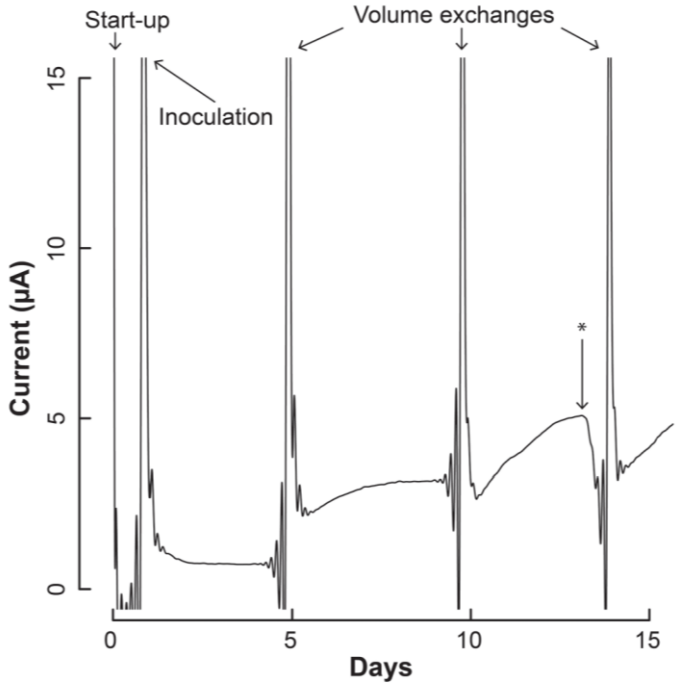

Figure 10: Current production during co-culturing a syntrophic acetogen *Syntropus aciditrophicus* and its methanogenic partner *Methanobacterium formicicum*. The asterisk marks the O_2 introduction into the BES to check if the generated electrical current is genuinely generated from microbial hydrogen. Figure from Guzman *et al.* (2019)

The increased detected current verified that the syntrophic acetogens, *S. zenderi*, provided H_2 to the anode rather than to the methanogen. The baseline current was measured at about 7.5 $*10^{-1}$ µA and increased throughout the batch operation period to 3.2 µA at the end of the first batch period. However, the performance of the BES need to be improved to achieve a statically relevant data set. Furthermore, an upgraded reactor architecture is necessary that allows continuous enrichment while maintaining a close interaction of the

microbes with the electrode to adhere to the ultimate goal to isolate syntrophic microbes from a natural microbiota.

2.4.6. Microbial Electrochemistry

The interaction of living microbial cells and electrodes defines microbial electrochemistry. This research field utilizes microbial fuel cells that convert chemical energy from, for example, wastewater into electric power. Furthermore, microbial electrochemical technology also uses the know-how of derivative technologies such as microbial electrolysis cells, photomicrobial fuel cells, microbial electrosynthesis, desalination cells, and biocomputing [113].

The nature and the degree of interaction define the type of microbial electrochemical technology. A distinction is drawn between primary and secondary microbial electrochemical technology. Primary microbial electrochemical technology belongs to the field of microbial electrochemistry (*e.g.*, Faraday or capacitive interactions of microbes and electrodes). Extracellular electron transfer (direct or mediated) to an electrode by such as electroactive microbes is one of the extensively studied processes in this field [99, 106, 108, 114-118]. Nowadays, BESs are used as a synonym for primary microbial electrochemical technology. Still, BESs also consider the fields of enzymology, microbiology, DNA, protein chemistry, and neuro-electro-chemistry. In secondary microbial electrochemical technologies, the biological system is connected to an electrochemical cell to control microbial processes or environmental parameters. Secondary microbial electrochemical technology focuses on indirect interactions. Here, the reaction environment of microbes and electrochemical processes is indirectly influenced by pH, oxygen partial pressure, and metabolites, such as microbial substrates and products. Besides, the electrochemical system must be close to the microbial system to be counted as a secondary microbial electrochemical technology. The applied electrode potential can differentiate between primary and secondary microbial electrochemical technology. Strong positive or negative potentials (high voltages) indicate secondary microbial electrochemical technology. In contrast, primary microbial electrochemical technology only considers electrode potentials within the physiological and thermodynamical range of the microbe or microbial

community. For both systems, any microbial electrochemical technology consists of at least two electrodes – an anode for oxidative reactions and a cathode where reduction occurs.

The field of microbial electrochemistry can be used to study and explain processes observed in, for example, geomicrobiology. The interaction of microbes with electron conductors can be either capacitive or Faraday´s nature. If microbes attach to the electrode, water molecules and ions are displaced from the double layer, which leads to a diminishing electrochemical (double layer) capacity. This leads to a flow of a charge-balancing (capacitive) electric current. Microbial oxidation and reduction reactions are the major characteristics described by Faraday´s process. Thus, any microbial species involved in microbial extracellular electron transfer can be investigated theoretically. All microbes require a physiological environment to live and grow. Therefore, microbial electrochemistry should occur at physiologically important potentials and depends on the microbes used in the setup. In detail, the applied potential should not be either too positive for anodic activities or too negative for cathodic activities. Both approaches would cause the degradation of physiologically essential biomolecules and harm the microbe or a whole microbial community. Aerobic and anaerobic systems need to be distinctively considered because the presence of oxygen leads to high redox potential, which anaerobic microbes cannot tolerate. Aerobic systems can manage an anodic potential of +0.6 V vs. SHE. This potential would cause a degradation of cytochrome c proteins in the microbial cell wall of anaerobes. To overcome this discrepancy, METs are designed as physiological technology, which unites electrochemical interactions with the environmental physiology of microbes [113, 117, 119].

2.5. DNA Sequencing

2.5.1. DNA-Sequencing Approaches

Studying the smallest building blocks of microbes living in the BESs is necessary to understand the underlying metabolic pathway and the different protein expression levels. Nucleic acids in a polynucleotide chain are arranged in genes and further translated into amino acids that are the building blocks of proteins, regulate the lives of every organism, and make up the DNA. Thus, DNA sequencing tells us about gene availability to identify and classify microbes. Furthermore, the identification of genes allows us to manipulate the

genetic information to knock out, overexpress, or mutate a gene to achieve a particular characteristic or expression of a foreign gene.

After Watson and Crick successfully solved the three-dimensional structure of the DNA molecule in 1953 and understood the function of ribonucleases, Robert Holley and Fred Sanger developed a technique based on radiolabeled partial-digestion fragments. Further sequencing techniques had been developed following the first steps of DNA sequencing. DNA sequencing strategies are divided into first-, second-, and third-generation DNA sequencing. First-generation sequencing comprises Sanger, Maxam-Gilbert, and Sanger´s chain-termination sequencing. These techniques are based either on radio- or fluorescent-labelled ddNTP nucleotides. If one ddNTP was incorporated into the consensus DNA strand, the reaction of DNA polymerization was stopped, and base by base could be detected to encode the base sequence. The major feature of first-generation sequencing is the read-length ability of 1000bp with 99.999% accuracy. [120, 121].

Due to the disadvantages of high costs and low throughput, second-generation sequencing became more popular. Here, no radio- or fluorescent-labeled dNTPs or oligonucleotides were used. Besides the increases in sequencing throughput, the read length of the sequenced DNA was much shorter than that of the first generation. The principle behind this approach is a luminescent methodology, where pyrophosphate synthesis during DNA polymerization is used to visualize and realize the base sequence [122]. Sanger´s dideoxy and the second-generation pyrosequencing method are categorized as sequence-by-synthesis techniques, which require the reaction with the DNA polymerase and limit both approaches.

Finally, third-generation sequencing is the third and latest approach for DNA sequencing. Third-generation sequencing is also known as long-read sequencing. It is characterized by single-molecule sequencing (SMS), real-time sequencing, simple divergence from previous technologies, and circumventing the requirement of DNA amplification [123]. Pacific Bioscience (PacBio) and Oxford Nanopore Technologies are two examples of companies that have developed different third-generation sequencing technologies. PacBios´ sequencing platform does single molecule real-time sequencing (SMRT), where DNA polymerization occurs in arrays of microfabricated nanostructures called zero-mode

waveguides (ZMW). These ZMW nanostructures are tiny little holes in a metallic film on a chip platform and allow the visualization of single fluorescence molecules close to the bottom of the ZMW. These processes will enable the sequencing of single DNA molecules in a very short time. The potential of nanopore sequencing, where DNA and RNA molecules can be driven across a lipid bilayer through large α-hemolysin ion channels by electrophoresis, was known before second-generation sequencing had emerged. In principle, detecting bases that pass through the ion channel blocks the current flow by decreasing the current for a length of time proportional to the length of the nucleic acid molecule. Oxford Nanopore Technologies was the first company to offer nanopore sequencing. More information about nanopore sequencing can be found in section 2.5.3, Nanopore Sequencing.

2.5.2. 16S rRNA Gene Sequencing

Besides the claim, having an entire genome sequenced, microbes can be differentiated by 16S rRNA gene sequencing. This approach is mainly applied to bacteria and archaea and uses the 16S gene locus of the rRNA. 16S rRNA gene sequencing is used for phylogenetic surveys of microbial communities. Here, the similarity of a ribosomal gene, whose sequence is known and stored in a database, decides whether one microbe is taxonomically the same, closely related, or far related to another microbe in a phylogenetic tree. A phylogenetic or evolutionary tree is a branching diagram (=tree) demonstrating the similarities and differences of various microbes in their genetic characteristics and evolutionary relationship. By evolution, microbess have either 16S or 18S rRNA genes that are conserved. Conserved genetic sequences across the entire genome are found in housekeeping genes and are widely distributed among different organisms. One of these genes is the small subunit (16S) ribosomal RNA gene, representing a taxonomic genomic marker [124]. The 16S rRNA gene subunit is divided into variable regions, flanked by conserved stretches in most microbes. Conserved regions are used as a target for PCR primers during sequencing, whereas variable regions provide species-specific information necessary for identification. The length of these RNA genes is around 1500 base pairs, and the characteristics are merged to be specific enough for the identification and differentiation of microbes and short enough to allow easy sequencing.

The identification of unknown microbes follows the protocol of: 1) amplification of the conserved stretch within the 16S rRNA gene locus by specific primers; 2) calculation of the genetic distance between pairs of microbes in the dataset gives a matrix of similarities; 3) construction of a phylogenetic tree by aligning sequences from different microbes; and 4) further analysis of the matrix by, for example, neighbor-joining method. [125].

The major advantages of 16S rRNA gene sequencing are the abundance of 16S rRNA gene locus and the existing methodologies to develop phylogenetic trees across different taxa. On the other hand, 16S rRNA gene sequencing also has some disadvantages. The variation of the 16S rRNA gene copy number *per* genome among strains, the amplification bias, which leads to un-reliable relative abundances, and the overestimation of the diversity of genes. Furthermore, if the resolution of the 16S rRNA gene is too low, differentiation of closely related species is impossible. Nowadays, the microbiome research area is moving away from 16S utilizing sequencing to more comprehensive and functional sequencing approaches of whole genome and shotgun metagenomics sequencing to overcome the disadvantages of 16S rRNA gene sequencing.

2.5.3. Nanopore Sequencing

Nanopore sequencing is, perhaps, the most anticipated area in the field of third-generation sequencing. This technique uses nanopores to detect and quantify biological and chemical molecules. A lipid-bilayer of large α-hemolysin ion channels is the primary interaction site for this methodology. By electrophoresis, RNA or DNA molecules that pass through the channel block the ion flow. This decreases the current for some time proportional to the length of nucleic acids [126, 127]. The principle of nanopore sequencing is based on the differences in the bases, where each of them prevents the membrane's ion flow distinctively (when the molecule passes through the nanopore) (**Figure 11**). By monitoring the current, the sequence of the DNA molecule can be inferred at each channel of the nanopore sequencing device [123, 128, 129].

The MinION and GridION platforms of Oxford Nanopore Technologies (ONT) were the first nanopore sequencing devices on the market [130-132]. A gigabase of DNA reads can be generated by the MinION instrument, whereas the GridION is designed for genome-scale sequencing. Both provide individual nanopores embedded within a synthetic membrane.

Changes in the current caused by different nucleotides are further translated into base sequence data (**Figure 12**) [130].

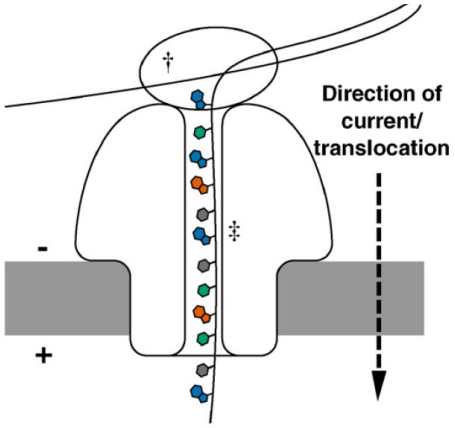

Figure 11: Nanopore DNA sequencing
The possessive enzyme (†) denatures the double-stranded DNA, which further ratchets one of the strands through a biological nanopore (‡). The nanopore (in grey) is embedded in a synthetic membrane where a voltage is applied. Figure from Heather and Chain, 2016

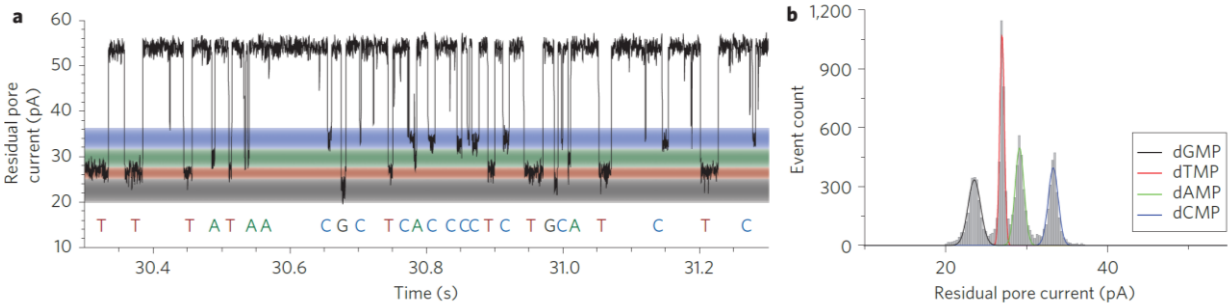

Figure 12: Separation and detection of nucleotides during nanopore sequencing
(a) Recording of residual pore current in pA of a single channel: nucleotides that pass the nanopore and induce a change in the current of the electric field. (b) The colored bands represent the residual current distribution for each nucleic acid, the Peak position of DNA bases. The residual current histogram of a nucleotide bound in a single channel. Figure from Clarke *et al.* (2009)

The MinIon platform can obtain ultra-long reads of up to 100 kb. In comparison, by Sanger sequencing, up to 1200 bp can be achieved, and MiSeq Illumina systems can achieve up to 300 bp. Besides that, ultra-long reads can be generated by MinIon sequencing; the circumventing of DNA or RNA amplification, rapid real-time of 48 h, ultra-long DNA reads,

and high-quality results are the key features of Oxford Nanopore MinION sequencing [130, 131, 133]. All these advantages together, in combination with high read depth and accuracy afforded by short-read sequencing, nanopore sequencing represents the best opportunity for decentralized sequencing away from core services that are common today. Core facilities offer a full sequencing service from DNA extraction to the data analysis of the sequencing output.

Chapter 3
Development of the BES and Proof of Concept of H_2 Removal with *C. minuta*

3.1. Abstract

Very little is understood about the H_2 economy of the human gut; therefore, interspecies H_2 transfer and microbial syntrophy have become increasingly important to fill one gap in understanding the entire human gut microbiome. *C. minuta*, which is one prominent member of the *Christensenellaceae* family, was already isolated from the human gut and is an H_2-producing microbe. In co-cultures of *C. minuta* and *M. smithii*, H_2 production supports CH_4 formation by the methanogen [4]. Due to thermodynamic limitations, H_2 accumulation predicts a microbial syntrophy in which carbohydrate degradation can only occur when a microbial partner consumes H_2 simultaneously [134]. The major questions are: how do these syntrophic microbes transfer molecular H_2 in the gut, and how do they benefit from it? We developed a BES for this investigation, mimicking a syntrophic microbial partner that takes up H_2. The BES provides a Pt/C-doped working electrode and a close interaction site of microbes with the working electrode where H_2 is actively removed by oxidation. Thus, it provides an environment favored by H_2-producing, carbohydrate-degrading bacteria. For proof of concept, *C. minuta* was used as an H_2-producing microbe. We found a shift of the fermentation products of *C. minuta* towards more acetate and less *n*-butyrate under conditions when the BES removed H_2. Furthermore, we found by scanning electron microscopy that *C. minuta* adhered to the Pt/C-doped working electrode as a biofilm. The outcomes of this study are essential to developing an isolation approach for gut microbes without requiring a microbial (syntrophic) partner. Culturing *C. minuta* in the BES will help further investigate and potentially isolate gut microbes that hide from lab cultivation. Furthermore, this supports our ultimate goal of understanding human gut microbes better.

3.2. Introduction

Besides the considerable knowledge about the interactions of gut microbes with the host, less is understood about the microbe-microbe interactions—especially in the human gut's H_2 economy. H_2 is one of the end products of carbohydrate fermentation and plays a central role in microbial metabolism because it acts as an electron sink. In addition, H_2 can also be used as a source of energy by other microbes in the gut. Therefore, to fill a gap in our understanding of the entire human gut microbiome, interspecies H_2 transfer and microbial syntrophy have become increasingly important. There is a need to fill this gap with knowledge about microbes that are not accessible to standard laboratory cultivation. These microbes have the potential to give us a better understanding of interspecies H_2 transfer and a deeper insight into human gut metabolism and its overall community function. Syntrophic microbes are difficult to culture and study because they rely on the metabolic activity of other microbes in their community. Therefore, we need cultivation systems that mimic the natural environment of the human gut or that give only certain uncultivated microbes a growth advantage over others.

Colonic H_2 metabolism is predominantly driven by fermentative H_2 production from hydrogenogenic microbes and interspecies H_2 transfer [1, 2]. Research on mouse disease models reveals that microbial-derived H_2 exhibits potent anti-oxidative, anti-apoptotic, and anti-inflammatory properties [3]. Colonic H_2 metabolism imbalances may lead to H_2 accumulation, disrupting gut function and harming humans, necessitating preventive measures [1]. In colonic microbiome models, the group of microbes that metabolize and cross-feed H_2 are underrepresented and challenging to study due to inconsistencies and a low relative abundance in the human population [135]. Demonstrated and hypothesised effects of hydrogenotrophs on both the microbiota and the host are reported, with effects on carbohydrate fermentation, host adiposity, and correlations with the development of irritable bowel syndrome, inflammatory bowel disease, and colorectal cancer The main question is: How can H_2 syntrophy with bioelectrochemistry be revealed? Guzman *et al.* (2019) designed a BES to investigate and enrich syntrophic H_2-producing microbes. The BES is based on the concept of close physical contact between the microbe and the working electrode. The working electrode oxidizes the H_2 from anaerobic fermentation, and the resulting electrons can be recorded as generated current. This approach was implemented

to compete with the methanogen in the syntrophic microbial partnership. Mathematical modeling was used to determine the maximum H_2 concentration that would select for syntrophic microbes. The H_2 threshold was found to be 51 M in the bulk liquid, where both the syntrophic bacterium and the methanogenic partner could grow at identical rates. Therefore, a lower concentration of H_2 (< 51 nM) would promote the growth of the syntrophic bacterium, while higher concentrations of H_2 (> 51 nM) would promote the growth of the methanogen. The study evaluated the maximum distance of the microbe from the H_2-oxidizing electrode. This gives a growth advantage to the syntrophic microbe that produces H_2 compared to the methanogen that consumes H_2 in the BES. According to the model of Guzman *et al.* (2019), efficient H_2 oxidation takes place at a distance of 1 mm from the working electrode. By enriching a syntrophic bacteria that produces H_2, Guzman *et al.* (2019) were able to measure the electric current produced by the bacteria's H_2 through oxidation at a Pt-coated working electrode. This resulted in a confirmed increase in electric current, indicating that the syntrophic acetogens provided H_2 to the working electrode instead of to the methanogen.

We continued this project, further optimizing the BES for the microbes to study of H_2 syntrophy. To demonstrate the concept, we used *C. minuta* as the H_2-producing microbe to test the ability of the BES to consume H_2 and to observe if *C. minuta* responded with a metabolic change to the H_2 removal by the BES. After the BES removed H_2, *C. minuta* shifted its production towards less *n*-butyrate and more acetate. In comparison to the operating condition where H_2 was added, in addition to the H_2 produced by *C. minuta*, more *n*-butyrate was produced. In addition, biofilm formation was detected at the working electrode, demonstrating the biocompatibility of the BES.

3.3. Material and Methods

3.3.1. Setup of the BES

The experimental setup of a BES consisted of two glass chambers equipped with a three-electrode configuration (**Figure 13**). The two glass chambers are the working chamber equipped with a working electrode and a counter chamber containing a counter

electrode(**Figure 13**). An ion exchange membrane separated the working electrode and the counter electrode, ensuring that *C. minuta* was only in contact with the working electrode in the working chamber of the BES. A three-electrode configuration of working electrode, counter electrode, and Ag/AgCl reference electrode was used to control the electrochemical potential, where it was set to E_i=350 mV *vs*. Ag/AgCl for H_2 removal by oxidation or to E_i=-650 mV *vs*. Ag/AgCl for H_2 evolution at the working electrode. Both electrodes, working electrode and counter electrode, were made of carbon cloth and had a size of 122 cm². The working electrode was doped with 4 mg/cm² of platinated carbon (10%) which was spray-coated on both sites of the carbon cloth for oxidation or evolution of H_2 from or to the microbes. For the reference electrode, we used an Ag/AgCl reference electrode composed of a metallic silver wire coated with silver chloride embedded in 3 M potassium chloride and 0.7 g agarose. The Nafion 117 membrane was activated by 1 M sulfuric acid for 24 h and equilibrated in a salt solution (85.5 mM sodium chloride, 16.9 mM disodiumphosphate *$2H_2O$, 41.9 mM sodium bicarbonate) for 24 h before the assembly of the BES to ensure good chemical stability *prior* the assembly.

The BESs (n=3), including the electrodes and the ion-exchange membrane, were assembled in their sandwich configuration and sterilized at 121°C for 20 min under aerobe conditions. After autoclaving, the chambers of the BESs were filled with anaerobic, reduced media and sparged with N_2:CO_2. The BES has a working volume of 21 mL in both, working and counter, chambers (**Figure 13**). The BES was designed to minimize the space between the microbes and the working electrode. Therefore, the distance between the microbes and the electrode was approxumately 1 mm.

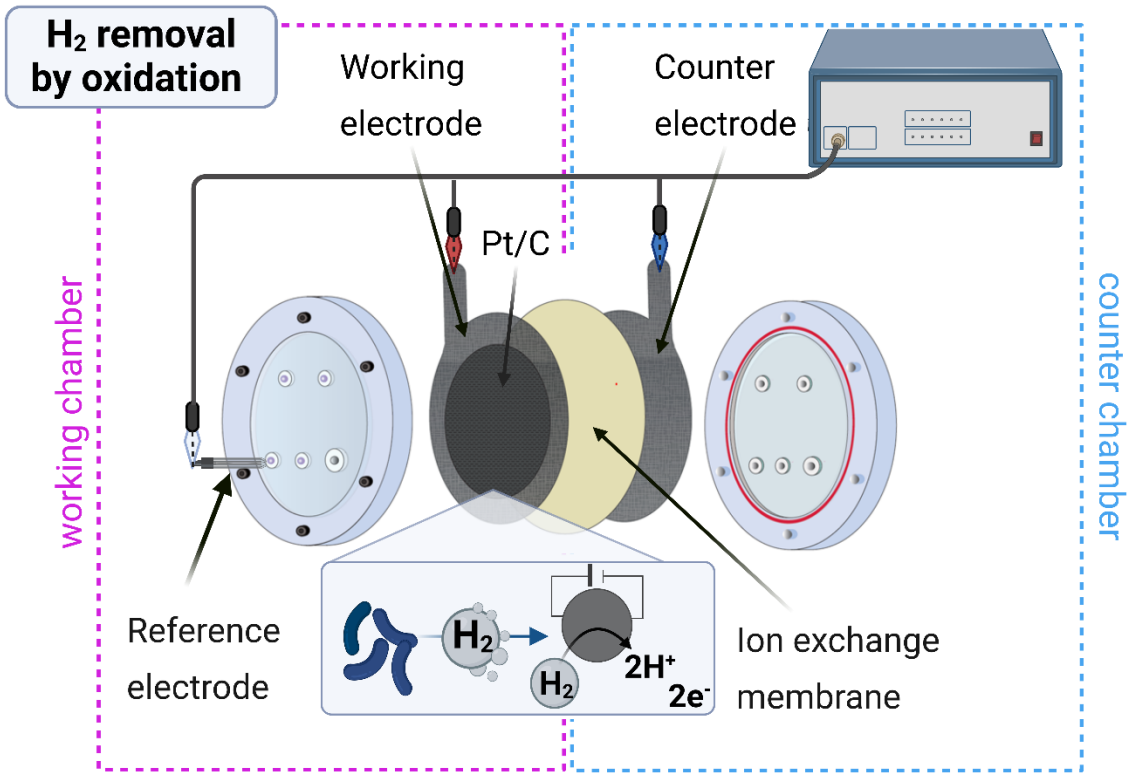

Figure 13: BES reactor setup for the cultivation of *C. minuta* under H_2 oxidation or evolution reactions at the working electrode

The BES consists of a working and counter chamber, separated by an ion exchange membrane (Nafion-117). Equipped with a three-electrode configuration, a working electrode (E_{we}), counter electrode (E_{ce}), and a reference electrode (E_{ref}), a constant potential can be applied to the BES for either H_2 oxidation (E_i = 350mV *vs.* Ag/AgCl) or evolution (E_i = -650mV vs. Ag/AgCl). A potentiostat controls the electrode potential. The working electrode is coated with Pt/C (10%) for catalytical H_2 oxidation or evolution reactions. *C. minuta* was cultivated in the working chamber at the working electrode.

3.3.2. Cultivation and Growth of *C. minuta*

C. minuta was thawed from -80°C cryo stocks and precultured in anaerobe 50 mL Brain Heart Infusion Broth (BHI) (VWR) media in serum bottles with one transfer *prior* to inoculation to the BESs. Brain Heart Infusion Broth (pH 7.4) was buffered with 15g/L PIPES (Sigma) and sparged with N_2:CO_2. After sparging with N_2:CO_2, L-cysteine-HCL (Sigma) was added to a final concentration of 5 mM to obtain reduced media conditions. The start OD was calculated to be 0.01 from a growing preculture that we measured spectrophotometrically (NanoDrop Photometer NP80, Implen).

3.3.3. Operation of the BES

Three BESs (R1-R3) with *C. minuta* were operated for more than 1704 h, where different operation conditions with regard to the removal or supply of H_2 were applied (**Figure 14** and **Figure 15**). In the establishment phase (before 1343 h), all three BESs (R1-R3) were operated under the same experimental setting. In the operating phase (after 1343 h) of the experiment, each BES was operated under a different operating condition to compare simultaneously different experimental settings. The experiment started with an enrichment phase, where we tested the operation conditions of with H_2 removal, with H_2 supply, and without electrochemistry (**Table 2**) in parallel in all three BESs and how *C. minuta* respond to the different operating conditions. In the beginning of the enrichment phase we started with a batch cultivation with *C. minuta* of 96 h without electrochemistry, where the BESs are not connected to the potentiostat. After 96 h all BESs ran in continuous cultivation, and we switched between H_2 removal, H_2 supply, and without electrochemistry. Due to the high bubble formation by H_2 at the working electrode under the operating condition of with H_2 supply, we decided to run these phases for a shorter operation period than the with H_2 removal phases.

Table 2: Operating conditions and electrochemical potentials

Operating condition	Abbreviation	Electrochemical potential
With H_2 removal	$-H_2$	E_i = 350 mV *vs*. Ag/AgCl
With H_2 supply	$+H_2$	E_i = -650 mV *vs*. Ag/AgCl
Without electrochemistry	w/o	Electrodes are disconnected from the potentiostat

After the batch cultivation, we switched to continuous cultivation and H_2 supply for 216 h. In the next phase, H_2 was removed for 456 h and a follow-up with H_2 supply phase of 96 h. The phase without electrochemistry ran for another 120 h. Afterward, we cultivated *C. minuta* again at with H_2 removal for 287 h, which followed by another operation phase without electrochemistry for another 72 h. Over a period of 1343 h, we switched between the conditions of with H_2 removal, with H_2 supply, and without electrochemistry. This phase was the establishment phase for the *C. minuta* culture and the BESs.

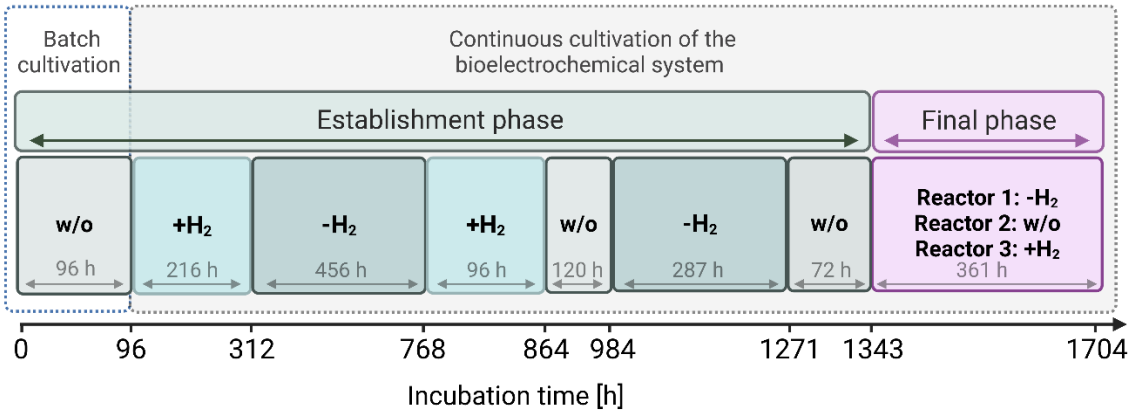

Figure 14: *C. minuta* cultivation in the BES
C. minuta was cultivated in three BESs under different operation conditions: without electrochemistry (w/o), with H_2 supply (E_i = -650mV *vs*. Ag/AgCl) (+H_2), or with H_2 removal (E_i = 350mV *vs*. Ag/AgCl) (-H_2). The three BESs ran as triplicates in the establishment phase, and the same operation condition was applied. In the final phase, R1 was set to -H_2, R2 to w/o, and R3 to -H_2.

Before 1343 h of cultivation, all three BESs were operated with the same experimental conditions (**Figure 14**). In the final phase (after 1343 h) of this experiment, each BES was operated under a different condition. R1 was operated with H_2 removal, R2 with H_2 supply, and R3 without electrochemistry. The final operation period had a duration over 361 h. The feed rate with BHI medium was set either to 1.75 ml/h (before 1488 h) or to 5 mL/h (after 1488 h)

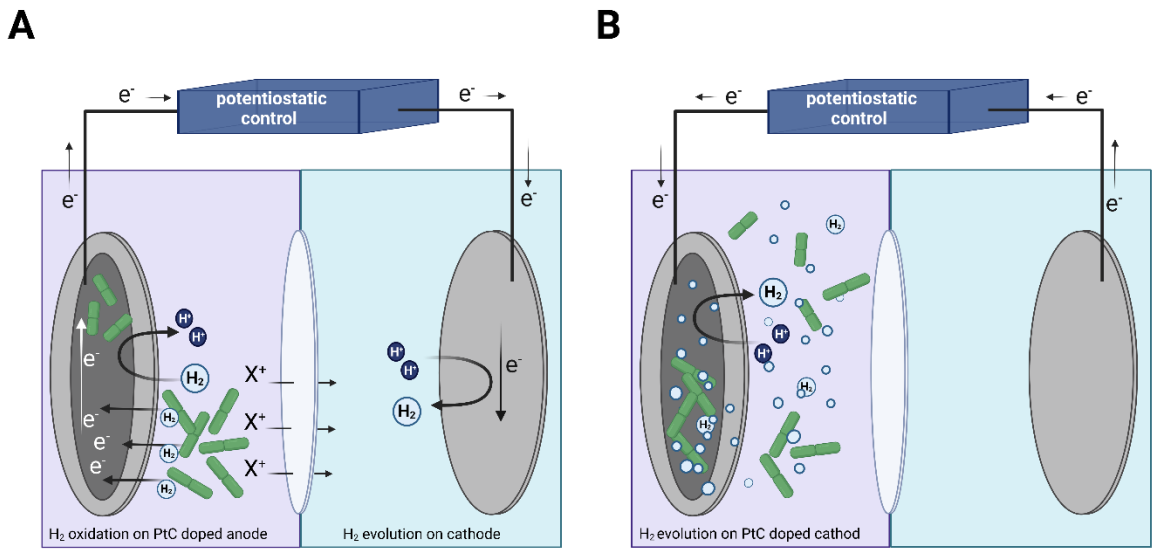

Figure 15: Potentiostatic operation conditions of the BES
The cultivation of *C. minuta* was carried out under two different operating conditions: (A) with H_2 removal by oxidation (E_i = 350mV *vs*. Ag/AgCl), and (B) with H_2 supply by reduction (E_i = -650mV *vs*. Ag/AgCl). Both operating conditions took place at the Pt/C-doped working electrode.

3.3.4. Monitoring of Metabolic Product Formation by *C. minuta*

The production of SCCs and the presence of H_2 were monitored over the entire operation period of 1704 h. 300 µL of gas from the BES was analyzed by an SRI gas chromatograph for trace concentrations of H_2 (6´13x Molsieve column, UV RDG detector, SRI Instruments). 1 mL was sampled from the cultivation broth and centrifuged at 19000 × *g* to separate biomass from supernatant containing SCCs. The supernatant was stored at -20°C for later analysis of SCC. SCCs (acetate and *n*-butyrate) were measured by gas chromatography (DB-FATWAX UI column, Agilent Technologies) using a six-level standard calibration curve where each standard contained 25 µL of 30mM ethyl-lactate as internal standard and 475 µL of a mixture of SCCs (Supelco) as external standards ranging from 0.475 - 9.5 mM for each SCC standard mixture. The SCC standard mixture contained acetate, propionate, iso-butyrate, *n*-butyrate, iso-valerate, *n*-valerate, iso-caproate, *n*-caproate, *n*-heptanoate, and *n*-caprylate. *Prior* analysis, 50 µL samples were mixed with 425 µL 2% formate and 25 µL internal standard (1.5 mM ethyl-lactate). The pH was monitored using autoclavable, optical pH sensor spots (SP-HP5v3-D10-US-SA, Presens), which we attached to the inner side of the BES glass. O_2 concentrations were detected using autoclavable, optical O_2 senses

(SP-PSt3-YAU-D10-YOP, Presens) to ensure anaerobic operating conditions. We glued both sensors on the glass with durable and heat-stable silicon glue (PreSens).

3.3.5. Scanning Electron Microscopy (SEM) Imaging

SEM was used to investigate biofilm formation of *C. minuta* at the working electrode in all three BESs. Electrode pieces of 1x1 cm were placed into separate wells of a 6-well plate, each containing 2 mL of PBS. 25% electron microscopy-grade glutaraldehyde (GA) was added to each well for a final 2.5% concentration. The well-plate was covered with a lid that was secured with parafilm to avoid contamination or spillage. The samples were incubated for at least 24 h at 4°C to allow for thorough fixation of the bacterial cells. After incubation, the fixative solution was removed, and 25% ethanol was immediately added to each well. Note that the plate was always covered with a lid during incubations to prevent evaporation. The samples were incubated for 15 min at room temperature (ca. 21°C) after which the ethanol solution was removed. This dehydration procedure was repeated with 50, 75, and (3x) 100% ethanol with 15 min incubations for each concentration. A solution containing a 1:1 ratio of 100% ethanol and hexamethyldisilazane (HMDS) was then added to each well and incubated for 30 min. The ethanol: HMDS solution was removed after incubation, immediately replaced with 100% HMDS, and incubated for an additional 30 min. After incubation, the well-plate lid was placed slightly open to allow the HMDS to evaporate overnight. Once dry, each sample was attached to a 25 mm diameter aluminum stub using Tempfix adhesive (Plano GmbH) and coated with ca. 8 nm of gold using a BAL-TEC™ SCD 005 sputter coater. The electrodes were imaged in secondary electron mode using a Zeiss Crossbeam 550L Focused Ion Beam – Scanning Electron Microscope operating with an acceleration voltage of 2 kV.

3.4. Results

The growth behavior of *C. minuta* was studied in different operating conditions (H_2 removal, H_2 supply, and without electrochemistry) under continuous cultivation. Switching between different operating conditions affected the H_2 concentration in the BES and *C. minuta´*s production of acetate and *n*-butyrate (**Figure 16**).

3.4.1. Establishment of the BES Setup

The BES was designed to fulfill two aims. The first aim was to provide a close interaction between the microbes and the electrode and grow the microbes to a maximum distance of 1 mm away from the electrode. The second aim was the sufficient removal or supply of H_2 from or to *C. minuta* by the BES. Therefore, together with Helmut Kammerlander from the MPI-IS Stuttgart, we designed and built a glass disk-like reactor system made out of borosilicate glass, where the stack of electrodes and Nafion-117 membrane perfectly fit inside. It needed five different versions of BESs to fulfill all requirements. The final version of the BES can be sterilized by autoclaving, is fully liquid- and gas-tight up to 1 bar overpressure, and prevents contamination from the outside environment. In addition, it keeps the electrodes separated, and its five connection ports can be used for sampling or to connect feed and effluent lines to the BES for continuous cultivation. For the efficient H_2 removal in parallel to a sufficient biofilm formation, we provided a large electrode surface area of 122 cm^2. Both glasses of the final BES version had two sets of o-ring sealings. The inner sealing ring kept the electrode and ion exchange membrane layers in place. In contrast, the outer sealing ring tightened the BES and prevented contamination with microbes from the outside. The sampling ports were designed not to create a dead volume next to the electrode to prevent the enrichment of microbes at a more considerable distance to the electrode. The feeding of the BES at the working electrode with media was performed through one sampling port at the bottom of the BES to ensure sufficient mixing and supply with nutrients. The port for the effluent sat on top of the BES. The design of the inlet and outlet ports supported a continuous flow of media and therefore homogeneous biofilm formation over the entire electrode area. The feeding and effluent port configuration was the same for both chambers. We needed to ensure that the volume in both chambers of the BES is constantly the same; otherwise, the Nafion membrane would bend due to more or less volume on one side. Therefore, the feeding rate (the flow of the medium) was always the same for both chambers to prevent influences on the cultivation volume and space for *C. minuta* at the working electrode.

3.4.2. The H_2 Concentration Can Be Controlled by the BES (Proof-of-Concept)

The experiment was divided into two phases: the establishment phase (cultivation between 0 h and 1343 h) and the final phase (cultivation between 1343 h and 1704 h) (**Figure 14**). Within the establishment phase, we tested the performance of all BESs, R1, R2 and R3, for operating conditions of with H_2 removal or with H_2 supply. The concentrations of H_2 are lower under with H_2 removal than under with H_2 supply (**Figure 16A**). At 1008 h, we were not able to set the potential on R2 to the next operation condition. Therefore, we disconnected this reaction from the potentiostat and ran without electrochemistry until the end the experiment.

In the BES final phase, we detected a clear difference in the H_2 levels between the operation conditions of with H_2 removal in R1 and with H_2 supply in R3. The H_2 level during the operating condition of with H_2 removal in R1 was lower than during with H_2 supply in R3 and without electrochemistry in R2. The levels of H_2 detected under the operating conditions of with H_2 supply in R3 and without electrochemistry in R2 were found to be very similar. This led to the conclusion that there is an upper limit of H_2 that can be produced by *C. minuta* and the working electrode of the BES, which can be maintained under continuous operating conditions.

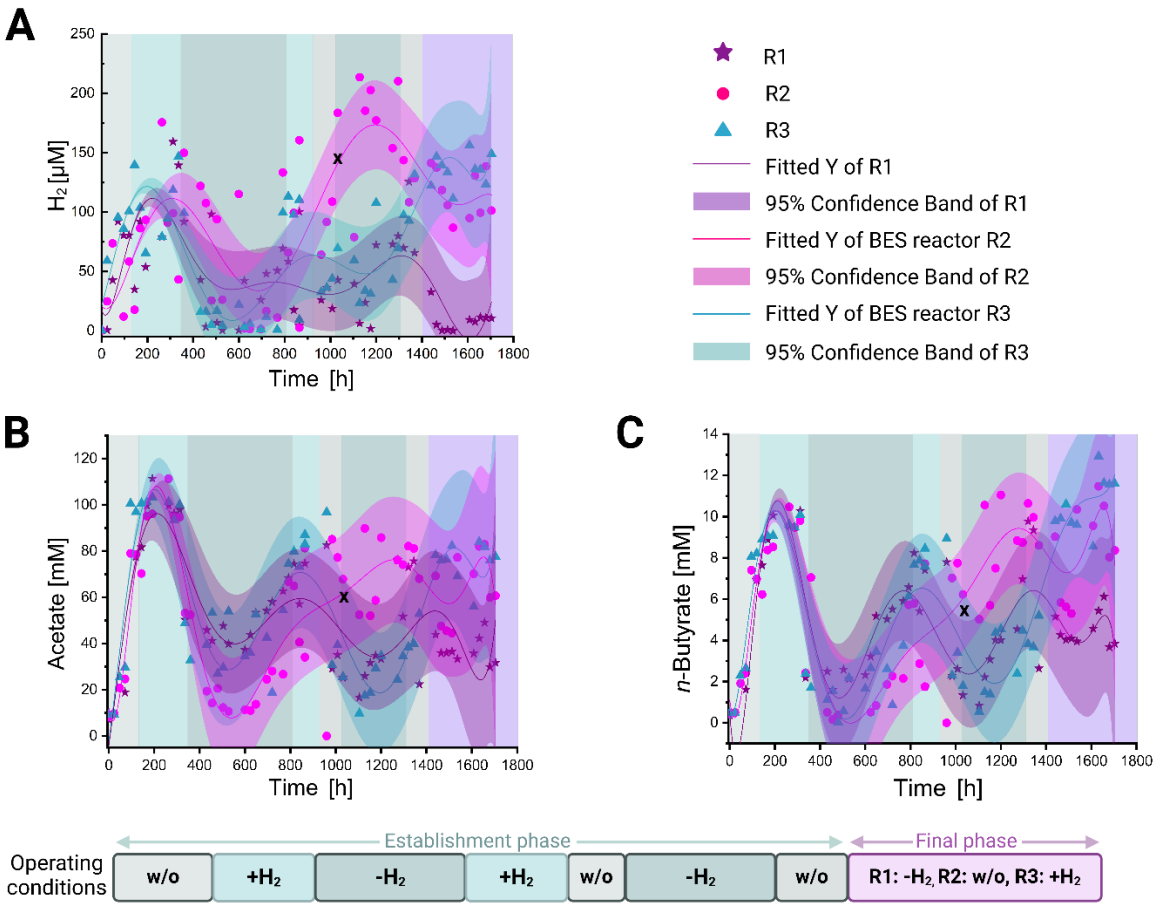

Figure 16: H_2, acetate, and *n*-butyrate concentrations of *C. minuta* from different operating conditions

(A) H_2, (B) acetate and (C) *n*-butyrate were measured in three BESs (R1-R3) throughout different operating conditions: without electrochemistry (w/o), with H_2 removal. ($-H_2$), and with H_2 supply ($+H_2$). For R2: x indicates an error in potentiostatic control at t=1008 h. Therefore, R2 was disconnected from the potentiostat and ran without electrochemistry until 1704 h.

3.4.3. SCC Production of *C. minuta* Was Affected by the H_2 Concentrations in the BES

In the BES establishment phase, acetate and *n*-butyrate production depends on the H_2 concentration (**Figure 16**). In particular, during the with H_2 removal operating condition, less acetate and *n*-butyrate were produced compared to the with H_2 supply condition. (**Figure 16BC**). To prove our hypothesis that the availability of H_2 influences the production of *n*-butyrate, where *C. minuta* produces less *n*-butyrate under reduced H_2 concentrations, we applied multiple statistics on the data of the final BES phase. Therefore, we investigated *n*-butyrate-to-acetate ratios in detail (**Figure 17**). A low ratio of *n*-butyrate: acetate means

that more acetate and less *n*-butyrate was produced, whereas higher values represent a higher concentration of *n*-butyrate.

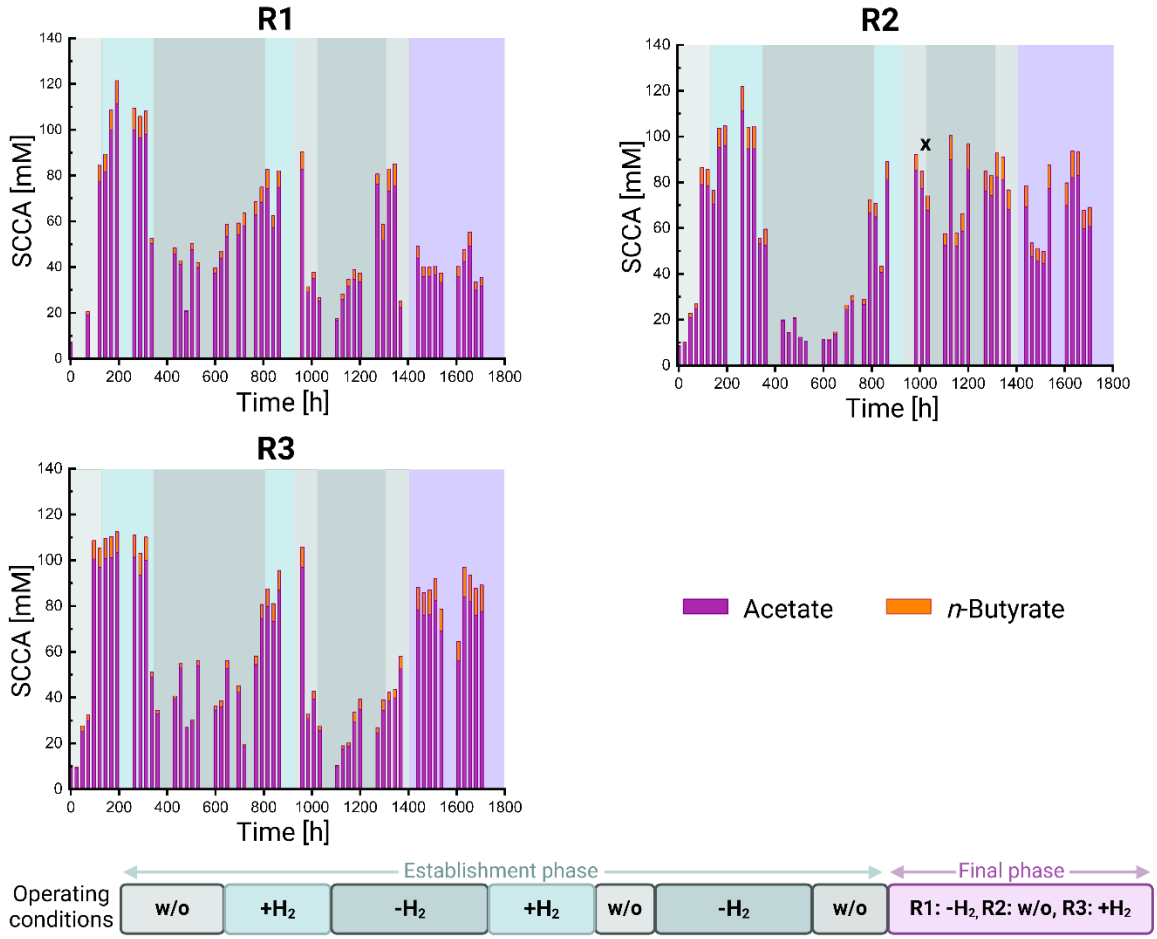

Figure 17: Stacked concentrations of acetate and *n*-butyrate
C. minuta produced acetate and *n*-butyrate in the BES (R1-R3) throughout different operating conditions: without electrochemistry (w/o), with H_2 removal. (-H_2), and with H_2 supply (+H_2). For R2: x indicates an error in potentiostatic control at t=1008 h. Therefore, R2 was disconnected from the potentiostat and ran without electrochemistry until 1704 h.

In the final phase, we compared the linear correlation of the *n*-butyrate: acetate ratios to H_2 concentrations between the three different operating conditions. We found that lower H_2 concentrations correlate negatively with *n*-butyrate: acetate ratios, resulting in a negative slope of the linear regression curve (**Figure 18A**). In the case of with H_2 supply in R3, higher H_2 concentrations and positive slope of *n*-butyrate: acetate ratio to the concentration of H_2 was found. Even though there was no statistical difference in the linear correlations of *n*-butyrate: acetate ratio and H_2 concentration between the three operating conditions of the final phase, tendencies were detected.

Higher concentrations of H_2 led to higher *n*-butyrate: acetate ratios, which were observed during the operating conditions without electrochemistry in R2 and with H_2 supply in R3 (**Figure 18B**). By applying an unpaired t-test of the means of *n*-butyrate: acetate (90% confidence interval), we detected significant differences between the *n*-butyrate: acetate ratios rations for with H_2 removal *vs.* with H_2 supply (P=0.0079), and for with H_2 removal *vs.* without electrochemistry (P=0.0013) (**Figure 18A-B**). No significant difference was found between the operating conditions with H_2 supply *vs.* without electrochemistry (P=0.2793), where higher H_2 concentrations were detected (**Figure 18B-C**). To investigate and prove further that the concentration of *n*-butyrate to acetate changed when the levels of H_2 changed, we performed a cluster analysis. The cluster analysis shows that low amounts of H_2 lead to a reduced *n*-butyrate: acetate ratio, whereas higher H_2 concentrations increase this ratio. The operating conditions with H_2 removal did not show a clustering pattern together with the operating conditions without electrochemistry and with H_2 supply for which higher concentrations of H_2 were present (**Figure 18C**). The concentrations of H_2 in R2 and R3 reached similar levels in the final phase, and therefore the values for *n*-butyrate: acetate cluster in the same area of the scatter plot (**Figure 18C**).

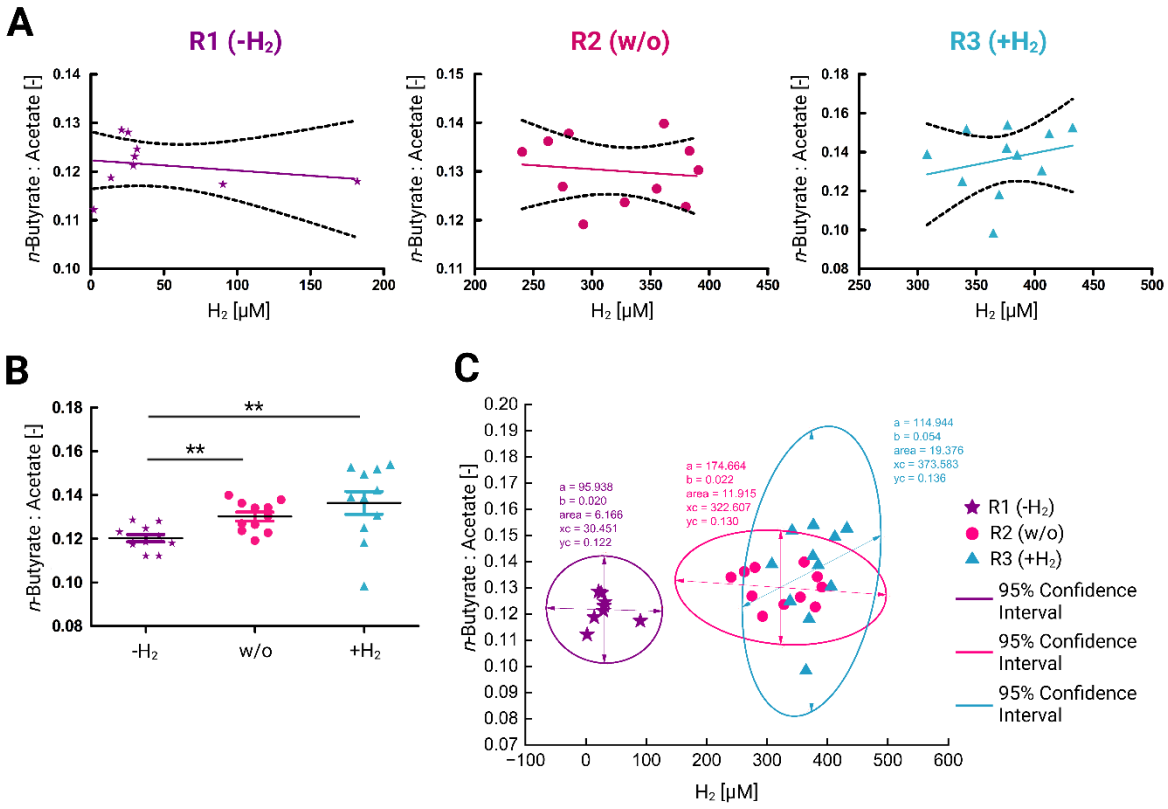

Figure 18: *n*-Butyrate to Acetate ratio of the BES final phase.
Different operation conditions were applied to each reactor in the final phase (between t=1343 h and t=1704 h). R1 was set to with H_2 removal (-H_2), R2 to without electrochemistry (w/o), and R3 to with H_2 supply (+H_2). Different statistical approaches investigated the *n*-butyrate: acetate ratio in relation to H_2 concentration in the BES. (A) Linear regression between *n*-butyrate: acetate ratio and H_2 concentrations. (B) Unpaired t-test of means from *n*-butyrate: acetate ratios from the final BES phase (C) Cluster analysis (2D Confidence ellipse with 95% confidence interval) of *n*-butyrate: acetate ratios in relation to H_2 concentrations. The statistical analysis was done by GraphPad Prism 9 (Version 9.5.1); n.s., $P > 0.10$; *, $P \leq 0.05$; **, $P \leq 0.01$; ***, $P \leq 0.001$,

3.4.4. *C. minuta* Attaches to the Pt/C-doped Working Electrode

After 1704 h cultivation of *C. minuta*, 1 x 1 cm pieces of the working electrode were collected from R1, R2, and R3 at the end of the final phase to investigate the biofilm formation of *C. minuta* at the Pt/C-doped carbon cloth material. The working electrode sample was collected from the same electrode position from R1, R2, and R3. The SEM micrographs indicate that during the entire operation period, some Pt/C coatings detached from the carbon cloth, and thus some uncoated fibers of the carbon cloth were exposed (**Figure 19**). Nonetheless, the working electrode looked still fully coated with Pt/C to remove or supply H_2 from or to *C. minuta*. Several factors can contribute to the structural

variation of the Pt/C coating, ranging from different electrode potentials to the resulting different H_2 concentrations. The H_2 gas formation under the operating condition of with H_2 supply could explain the different shapes of the Pt/C coating. Furthermore, the cell length of *C. minuta* observed at the working electrode in R3 increased from 4 to 8 µm compared to in R1. For R1, we found shorter cell lengths of *C. minuta* between 1 to 2 µm. In R2, cell lengths of *C. minuta* were similar to those for R3. With SEM imaging, we showed that with H_2 removal or supply caused by different electrode potentials, affected the cell size of *C. minuta*, where greater cell sizes were detected for the operating conditions of with H_2 supply and without electrochemistry.

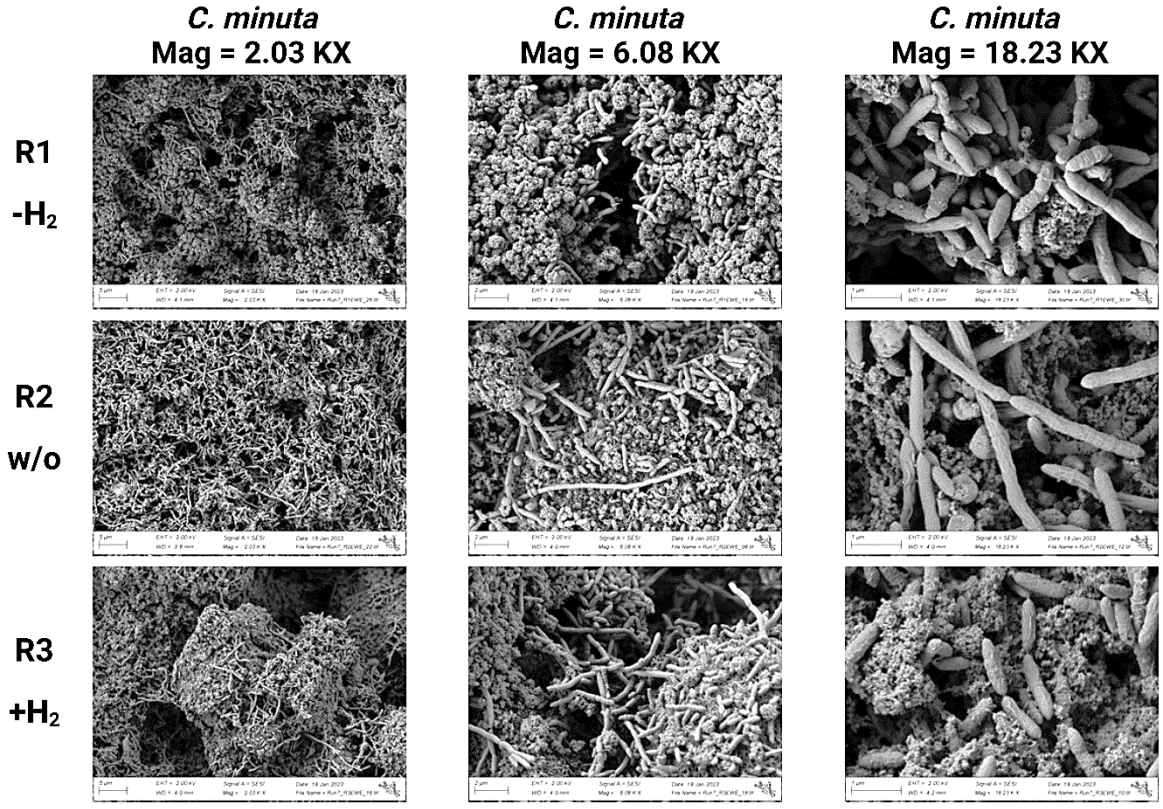

Figure 19: SEM micrographs of *C. minuta* growing at the Pt/C-doped working electrode of the final phase (t=1704 h)

During the final phase (between t=1343 h and t=1704 h). R1 was set to with H_2 removal ($-H_2$), R2 to without electrochemistry (w/o), and R3 to with H_2 supply ($+H_2$).1x1 cm² pieces of the working electrode were investigated for *C. minuta* growing at the electrode material at magnifications of 2.03KX, 6.08KX, and 18.23 KX.

3.5. Discussion and Outlook

The first part of this experiment was to design a BES that provides optimal growth conditions for an anaerobic gut microbe, such as *C. minuta*, and can be operated as a continuous operating setup. We had to redesign the BES reactor five times until we solved the problems of sterility, leaking, durability, dead volumes in the sampling ports, and a close electrode-membrane setup. We established a BES in this experiment that can remove H_2 that was produced by *C. minuta* or it can be operated under with H_2 supply to *C. minuta* in continuous operating conditions. This BES also enabled a close interaction of the microbes with the working electrode and led to a biofilm formation of *C. minuta*. The maximum gap of 1 mm between the microbes and the electrode enabled sufficient H_2 removal within the entire volume. The biofilm formation enhanced these processes and

brought the microbes closer to the reaction site. Floc formation was observed in a co-culture of *C. minuta* and *M. smithii*, which enhanced the syntrophic H_2 transfer between these two microbes [4]. Besides the syntrophic interaction that is related to adhesion *in-vitro*, the adhesion of beneficial bacteria on the intestinal mucosa enhances the intestinal barrier function and modulates the immune system *in-vivo* [139-141].

Furthermore, we were able to switch back and forth between three operating conditions: with H_2 removal, with H_2 supply, and without electrochemistry. The H_2 concentration in the BES influenced the SCC production of *C. minuta*, where less *n*-butyrate was produced under operating condition of with H_2 removal, where we kept the H_2 concentrations to a minimum. Higher *n*-butyrate concentrations were found when H_2 was not removed electrochemically under operating condition of without electrochemistry or under with H_2 supply. *n*-Butyrate is produced from crontonyl-CoA, which is reduced to butyryl-CoA by the butyryl-CoA dehydrogenase electron-transferring flavoprotein complex. This complex couples the reduction of crotonyl-CoA to the endergonic reduction of ferredoxin (oxidized) and oxidation of NADH by electron bifurcation, making the reaction thermodynamically feasible [142, 143]. By reducing protons to H_2, ferredoxin (reduced) is reoxidized by the ferredoxin hydrogenase [144, 145]. In the metabolism of microbes that produce *n*-butyrate in the human GI tract, *n*-butyrate production is favored over acetate at higher gut H_2 concentrations. Also, *C. minuta* produced more *n*-butyrate under high H_2 levels [4]. The limitation of this experiment in terms of H_2 removal comes from the BES itself, where we could not completely remove all H_2 from *C. minuta* electrochemically. Due to the attachment of the microbes to the electrode surface, we cannot control the cell density. Thus, with increasing cell concentrations in continuous cultivation, more H_2 may be produced by *C. minuta* than the electrode´s capacity can oxidize. Therefore, fluctuations in cell density can lead to fluctuations in the amount of H_2 that the BES can remove electrochemically and to changes in the acetate and *n*-butyrate production rate produced by *C. minuta*.

Further research is required to determine the maximum cell density in relation to the amount of H_2 produced by *C. minuta* that can be removed by the BES. This also included control over the cell density that forms a biofilm on and within the electrode surface. Surfaces, such as biomaterials, provide more excellent growth conditions for microbes than

suspension cultivation can provide. Microbial adhesion, which defines the adhesive junction between microbes and surfaces, is driven by physicochemical interactions, the target surface material, environmental factors, and microbes' characteristics. Microbes have a diverse repertoire of adhesins for different surfaces [7, 146]. In addition, the combination of Lifshitz-van der Waals interactions, acid-base bonds, and electrostatic double-layer interactions are present in the first phase of adhesion. In the second phase of adhesion, microbes create a connection to the surface *via* external appendages on the bacterial surface, such as flagella, pili, or fimbriae, and the production of extracellular polymeric substance [147-152]. In addition, surface properties such as wettability, stiffness, topography, surface charge and roughness can influence microbial adhesion and surface sensing, and it is important to note that these factors provide physical support for the microbes. [153]. Since we detected a massive colonization of *C. minuta* at the Pt/c-coated electrode, we can conclude that this setup of the BES mimics physiological growth conditions and provides an environment leading to biofilm formation with an evenly distributed microbial colonization on and within the electrode material.

We also detected that acetate and *n*-butyrate productions are less in the beginning of the operating phases with H_2 removal compared to with H_2 supply. The production always dropped by switching to the operating phases of with H_2 removal but recovered to almost the same level. Therefore, it would be helpful to compare the proteomes of electrode-attached cells and supernatant cells under different H_2 concentrations and investigate whether specific proteins from catabolic pathways are up- or down-regulated under high or low H_2 concentrations.

Chapter 4
Can the H_2 by the BES compete with a Syntrophic H_2 Consumer?

4.1. Abstract

In Chapter 4, we wanted to study whether the H_2 removal by the BES can compete with a syntrophic partner of *C. minuta*, such as *M. smithii*. Therefore, we had planned to perform two bioelectrochemical experiments, where both microbes would be cultivated together at the cathode in the BES or separated into the anode and the cathode chamber of the BES. Here, we were only able to perform the first of two experiments. In the second experiment, which still needs to be performed, *C. minuta* would grow at the anode and *M. smithii* at the cathode so that both microbes would be technically separated but in a connected electrochemical fashion with electrons flowing from the anode to the cathode and ions crossing the proton-exchange membrane. The preliminary results of the first experiment showed that, when *M. smithii* is growing, the *n*-butyrate: acetate ratio changes and decreases throughout the operating period when *M. smithii* is present in co-culture with *C. minuta*. Unfortunately, in one BES, *M. smithii* was not growing in co-culture with *C. minuta* in the last operating period; therefore, only the results of two BESs were used. This experiment gave insight into the potential of the BES as a research tool and how it can be used to study the H_2 syntrophy of already isolated microbes. To get a more detailed understanding, this experiment needs to be repeated, and the second experiment needs to be performed to verify (or falsify) the hypothesis that separated syntrophic partners in a BES can outcompete the co-culture in a similar experimental conditions.

4.2. Introduction

Goodrich *et al.* (2014) reported that the abundances of many microbial taxa are shaped by host genetics, and that especially the *Christensenellaceae* family co-occurred in humans with methanogenic archaea and other heritable bacteria in humans with a low body mass index. The positive association of *Christensenellaceae* and lean BMI was studied in mice,

where an obese-associated microbiome from a human donor was supplemented with *C. minuta*, which is a cultured member of *Christensenellaceae*, and transplanted to germ-free mice. Here, adding *C. minuta* before transplantation reduced the level of adiposity in the test group compared to the mice in the control group that had not received *C. minuta* [154].

Methanobacteriaceae are often reported as part of the *Christensenellaceae* co-occurrence consortium, whereas *M. smithii* is the most abundant methanogen in the human gut microbiome [155-158]. In addition, both families correlate *via* physical and metabolic interactions. Ruaud and Esquivel-Elizondo *et al.* (2020) studied specific interactions of two abundant species of each family. They showed that the H_2 production of *Christensenella* spp. have supported the growth of *M. smithii*. This effect is coupled with the immediate consumption of H_2 by the methanogen (which uses it to make methane) and shifts the metabolic activity of *Christensenella spp* towards acetate rather than *n*-butyrate production. In addition, *C. minuta* and *M. smithii* were found to co-localize in dense flocs throughout the operating period, whereas *M. smithii* has better access to H_2 produced by *C. minuta* [4].

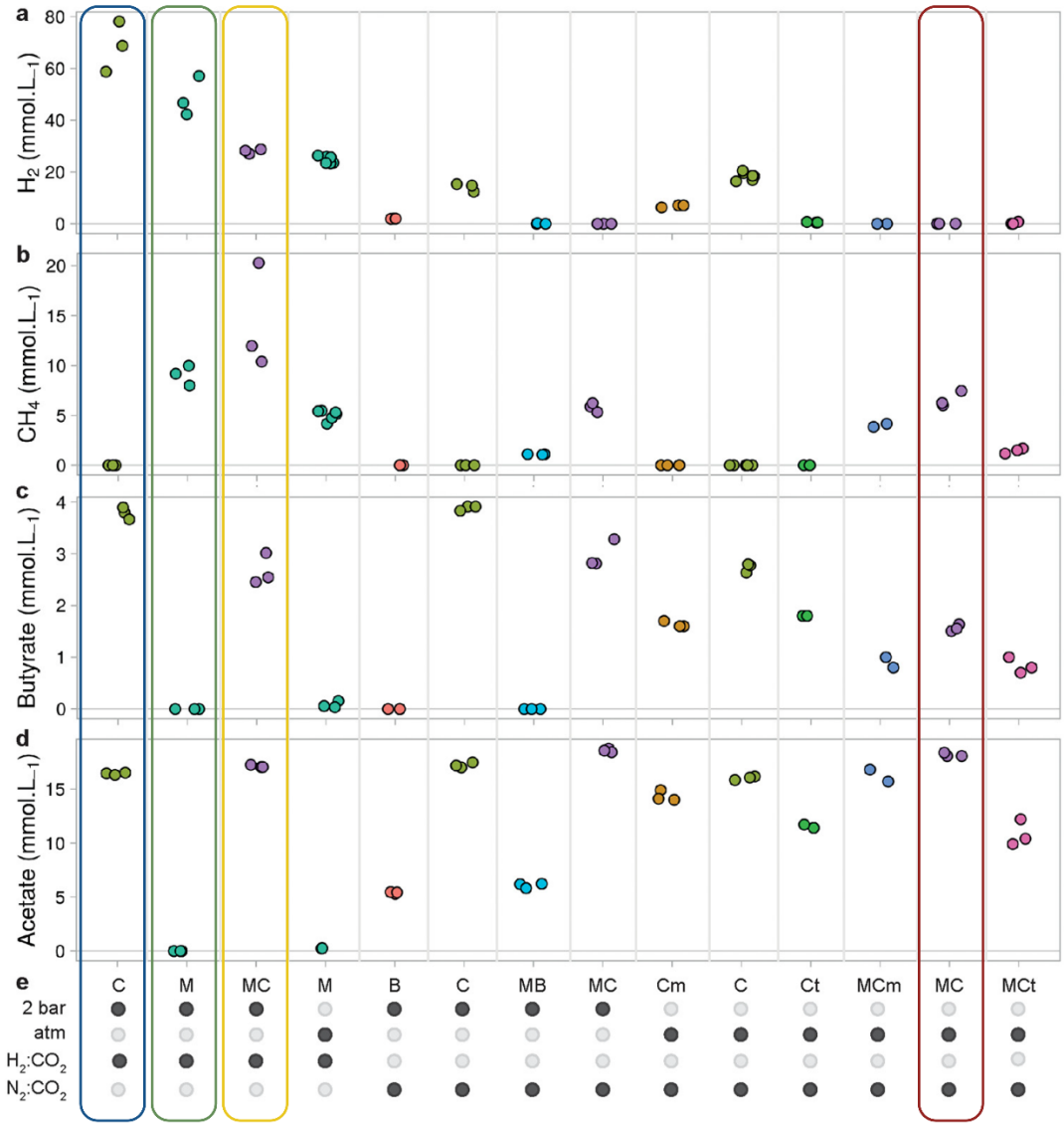

Figure 20: Metabolic activity of *C. minuta*, *C. timonensis*, *C. massiliensis*, *B. thetaiotaomicron*, and *M. smithii* after six days of growth (gas and SCCs production) from Ruaud and Esquivel-Elizondo *et al.* (2020)

Blue border: *C. minuta* (C); green border: *M. smithii* (M)*;* yellow border: *M. smithii* and *C. minuta* at 2 bar (MC); red border: *M. smithii* and *C. minuta* (MC) at atmospheric pressure (atm)

Furthermore, H_2:CO_2 was provided in excess to the co-culture of *C. minuta* and *M. smithii* at different pressure conditions to prove that the close contact between *M. smithii* and *C. minuta* gave a growth advantage to the methanogen (**Figure** 20). Here, the CH_4 production was supported by *C. minuta* to similar extents independent of the pressure of additional H_2:CO_2, which was either atmospheric or 2 bars overpressure. In all cases for the

co-culture, with and without additional H_2:CO_2, *M. smithii* aggregated with *C. minuta* (**Figure 21**).

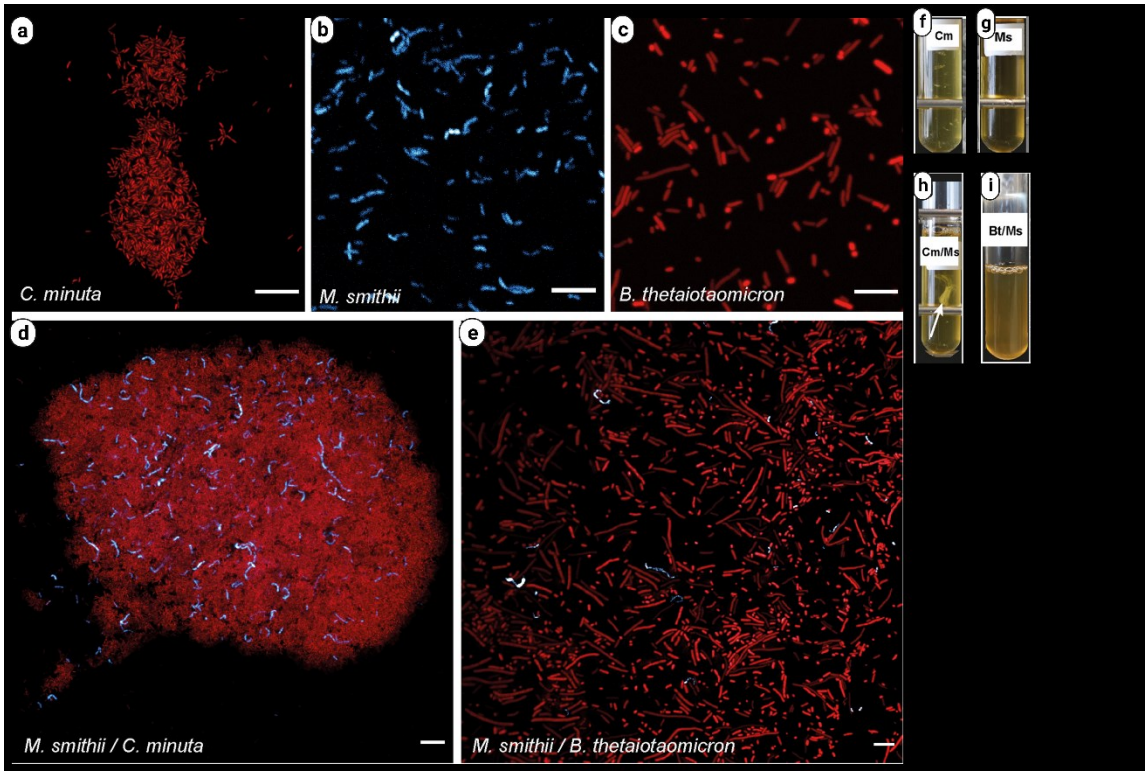

Figure 21: Confocal images of *C. minuta, M. smithii*, and *B. thetaiotaomicron* (after 3 days of growth in pure and co-culture) from Ruaud and Esquivel-Elizondo *et al.* (2020)
(a) and (f) *C. minuta* in pure culture, (b) and (g) *M. smithii* in pure culture, (c) *B. thetaiotaomicron* in pure culture, (d) and (h) *M. smithii* / *C. minuta* co-culture, (e) and (i) *M. smithii* / *B. thetaiotaomicron* in co-culture and. For confocal imaging, microbes were visualized by staining with SYBR green I fluorescence (DNA staining, red), and *M. smithii*´s was visualized by its autofluorescence coenzyme F_{420} (blue). Scale bares represent 10 µm. All images were taken from Ruaud and Esquivel-Elizondo *et al.* (2020) publication and were configured by Biorender.com

Fick's law of diffusion can describe the flux of metabolites between microbes, which is directly proportional to the concentration gradient and inversely proportional to the distance between producer and consumer. In other words, the closer the microbes aggregate, the better the H_2 transfer. In all scenarios (with and without additional H_2:CO_2) for *C. minuta* in co-culture, the *n*-butyrate production was inhibited, and the carbon metabolism was shifted to acetate production [4]. It has been suggested that the consumption of H_2 by the methanogen decreased the H_2 partial pressure within the aggregation in close proximity to *C. minuta*. This favoured more oxidised fermentation products, such as acetate, resulting in increased CH_4 production. [66, 70, 144, 159, 160].

After the development of the BES and the proof of concept with *C. minuta*, we wanted to test the ability of the BES (removing H_2 at the anode) to compete with a syntrophic partner. Therefore, we planned to split this study into two experiments where C *minuta* and *M. smithii* are physically or not physically separated in the same environment (**Figure 22**). For the first experiment (**Figure 22A**), we planned to culture both *C. minuta* and M *smithii* in one of the chambers of the BES without current flow, where the H_2 was only removed by *M. smithii*. For the second experiment (**Figure 22B**), *C. minuta* would grow at the anode, where H_2 is removed by oxidation. The resulting protons cross the Nafion membrane and move to the cathode, where they are reduced back to H_2. *M. smithii* would grow at the cathode where H_2 is generated. In the Ph.D. dissertation, I will only focus on the first of the two experiments.

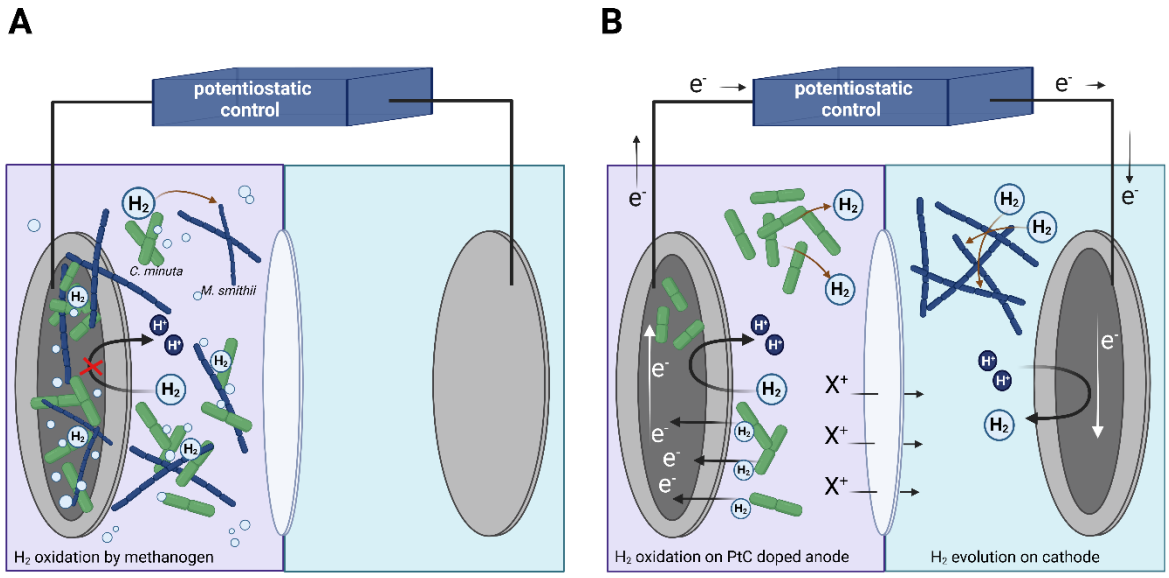

Figure 22: Setup of the BES to test whether the H_2 removal at the anode can compete with the H_2 removal by *M smithii*

(A) Co-culture of *C. minuta* and *M. smithii* together in one of the chambers of the BES. (B) Cultivation of *C. minuta* at the anode and *M. smithii* at the cathode in the same BES but then work with potentiostatic control.

In the first experiment, we want to investigate the H_2 removal by the methanogen. Therefore, we grew *C. minuta* under different operating conditions: i) without electrochemistry; ii) with H_2 supply for *C. minuta*; and iii) with H_2 supply for *C. minuta* plus *M. smithii*, where the H_2 is removed only by the methanogen.

4.3. Material and Methods

4.3.1. Setup and Operation of the BES

For the first experiment, where *C. minuta* and M *smithii* were co-cultured together at the cathode (**Figure 22A**), the BES was set up in a three-electrode configuration, as explained in section 3.3, Material and Methods. The two chambers of the BES were separated by a Nafion 117 ion exchange membrane (Sigma) to separate the working and counter electrodes and keep *C. minuta* and *M. smithii* only in contact with the working electrode. Both electrodes, the working electrode and counter electrode, were made of carbon cloth and had a size of 122 cm^2. The working electrode, reference electrode, and Nafion 117 membrane were prepared as described in section 3.3, Material and Methods.

Three BESs (R1-R3) were assembled in their sandwich configuration and sterilized at 121°C for 20 min under aerobe conditions. For the first experiment, we set up three BESs. The pH was monitored using an autoclavable, optival pH sensor spots SP-HP5v3-D10-US-SA (PreSens Precision sensing) attached to the middle of the inner glass side of the BES. O_2 concentrations were detected using an autoclavable, optical O_2 sensors SP-PSt3-YAU-D10-YOP (0-100% O_2, PreSens Precision sensing) to ensure anaerobic operating conditions.

We started this experiment by growing *C. minuta* in monoculture (between 0 h and 240 h) and later in co-culture with *M. smithii* (between 240 h and 432 h). The BES with *C. minuta* monoculture was operated first in batch cultivation without electrochemistry for an operating period of 72 h and later in continuous cultivation for 360 h (**Figure 23**). The continuous cultivation was split into two operating conditions: i) with H_2 supply for *C. minuta* (E_i = -650 mV *vs.* Ag/AgCl) for a period of 168 h; and ii) H_2 supply for *C. minuta* plus *M. smithii* (E_i = -650 mV *vs.* Ag/AgCl) for a duration of 192 h.

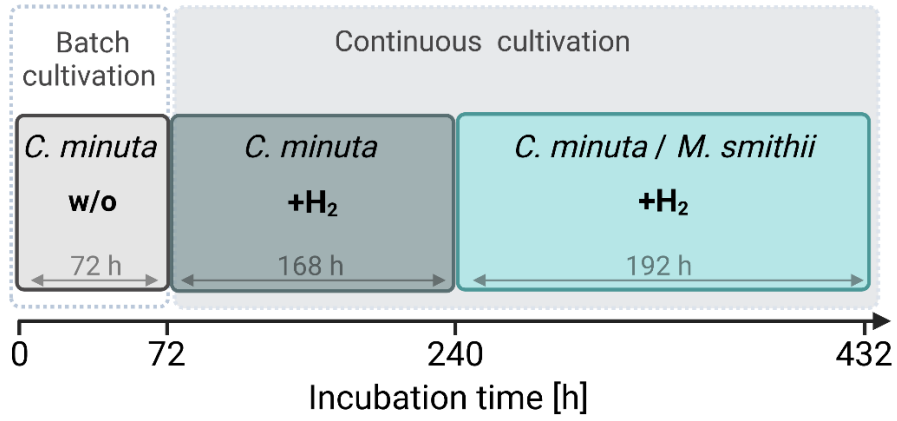

Figure 23: Operating periods and conditions for the co-cultivation of *C. minuta* and *M. smithii* in the BES
Operating conditions: without electrochemistry (w/o), with H_2 supply (+H_2) for *C. minuta*, with H_2 supply (+H_2) for *C. minuta* plus *M. smithii*

4.3.2. Media Preparation and Cultivation

The assembled BES was not completely tightened during autoclaving and under oxic conditions to prevent breaking the glass parts of the BES. After autoclaving, we carefully tightened all screws of the BES in the sterile bench and made sure that the sandwich configuration, consisting of electrodes and Nafion ion exchange membrane, stayed in place. Anoxic operating conditions of the BES were provided after autoclaving by adding a sterile BHI medium to both sites of the BES and by sparing with N_2:CO_2. Therefore, two bottles with each 200 mL medium were prepared for each of the three BESs.

For the cultivation and for filling of the BES, we used modified BHI (37g/L) that was supplemented with yeast extract (5 g/L), L-Cystein-HCL (5 mM, pH 7, adjusted with NaOH), and sodium bicarbonate (42mM, pH 7, adjusted with HCl). For filling the BES with modified BHI medium, after autoclaving, the medium bottles were connected to the BES and sparged with N_2:CO_2 for 1 h while the medium circulated between the medium bottle and the BES. Afterward, after sparging for 1 h, L-Cystein-HCl and sodium bicarbonate were added to the bottle to fill the BES while the medium circulation kept running for another hour. For the continuous cultivation, feed bottles were connected to both sites of the BES to prevent the accumulation of products on only one side of the BES and to avoid an imbalance in the BES volume, which might change the distance from the inner rector glass to the working electrode. The feed rate of the modified BHI medium was set to 2 mL/h.

4.3.3. Inoculation and Cultivation Times

C. minuta and *M. smithii* were precultured from cryostock in serum bottles using the same cultivation media. Both microbes were inoculated at a theoretical OD of 0.05 from an exponentially grown preculture. The actual OD in the medium of the BES was not determined after injection due to impurities of particles from the Pt/C-doped working electrode, which came off and would lead to an artificially elevated OD measurement. *C. minuta* was inoculated to the working electrode at t=0 h and was cultivated for 72 h in batch cultivation and for another 168 h in continuous cultivation. After an operating period of 240 h, M *smithii* was inoculated to the working (**Figure 22A**). Both microbes were co-cultured for 192 h.**Analytic of SCCs and Gasses**

The production of SCCs and the presence of H_2 and CH_4 were monitored once *per* day throughout the entire operating period of 430 h. 200 µL of gas taken from the BES were analyzed for the H_2 and CH_4 content by a gas chromatograph with a HayeSep D column (length 3 m, outer diameter 1/8”, SRI Instruments). The column temperature and pressure were set to 70°C and 20 psi. A thermal coupled detector (TCD) was used to measure H_2 and CH_4.

1 mL was sampled from the cultivation broth and centrifuged at 12000 rpm to separate biomass from supernatant containing SCCs. The supernatant was filtered through a 0.22-µm syringe filter and was stored at -20°C for later analysis of SCCs. SCCs were measured by gas chromatography (DB-FATWAX UI column, Agilent Technologies), using a six-level standard calibration curve where each standard contained 25 µL 30 mM ethyl-lactate as an internal standard and 475 µL of a mixture of SCCs as external standards ranging from 0.475 - 9.5 mM for each SCC standard mixture. The SCC standard mixture contained acetate, propionate, iso-butyrate, *n*-butyrate, iso-valerate, *n*-valerate, iso-caproate, *n*-caproate, *n*-heptanoate, and *n*-caprylate. *Prior* analysis, 50 µL samples were mixed with 425 µL 2% formic acid and 25 µL internal standard.

4.3.5. Statistical Analysis

To test whether the production of *n*-butyrate and acetate by *C. minuta* was affected by the H_2 consumption of *M. smithii*, the *n*-butyrate: acetate ratios were calculated for the operating conditions: i) with H_2 supply for *C. minuta* and ii) with H_2 supply for *C. minuta*

plus *M. smithii*. We tested whether the slopes of *n*-butyrate: acetate ratios produced by *C. minuta* differ in the last two operating conditions. We performed the statistical analysis with a simple linear regression analysis using Prism GraphPad (Version 9). Simple linear regression analysis fits a straight line through the data to find the best-fit value of the slope (slope = ΔX/ΔY) and intercept. The p-values were calculated from an F test, and a 95% confidence band surrounding the best-fit line defines the confidence interval of the best-fit line.

4.3.6. SEM Imaging

We investigated the biofilm formation of the co-culture of *C. minuta* and M *smithii* at the working electrode from all three BESs (R1-R3) by SEM. Electrode pieces of 1x1 cm were placed into separate wells of a 6-well plate, each containing 2 mL of PBS. 25% electron microscopy-grade glutaraldehyde was added to each well for a final 2.5% concentration. The well-plate was covered with a lid secured with parafilm to avoid contamination or spillage. The sample preparation and imaging procedure is described in Chapter 3.3.5, Scanning Electron Microscopy (SEM) Imaging.

4.4. Results

The experimental setup included the replicate BESs, R1, R2 and R3. Since we did not observe any growth of *M. smithii* after its inoculation to R3, we decided to discuss only the results of R1 and R2. Lower SCC production was detected in R1 during in the first two operating conditions, *C. minuta* without electrochemistry and with H_2 supply for *C. minuta*, in comparison to R2 (**Figure 24A**). We concluded that *C. minuta* grew less in R1 than in R2.

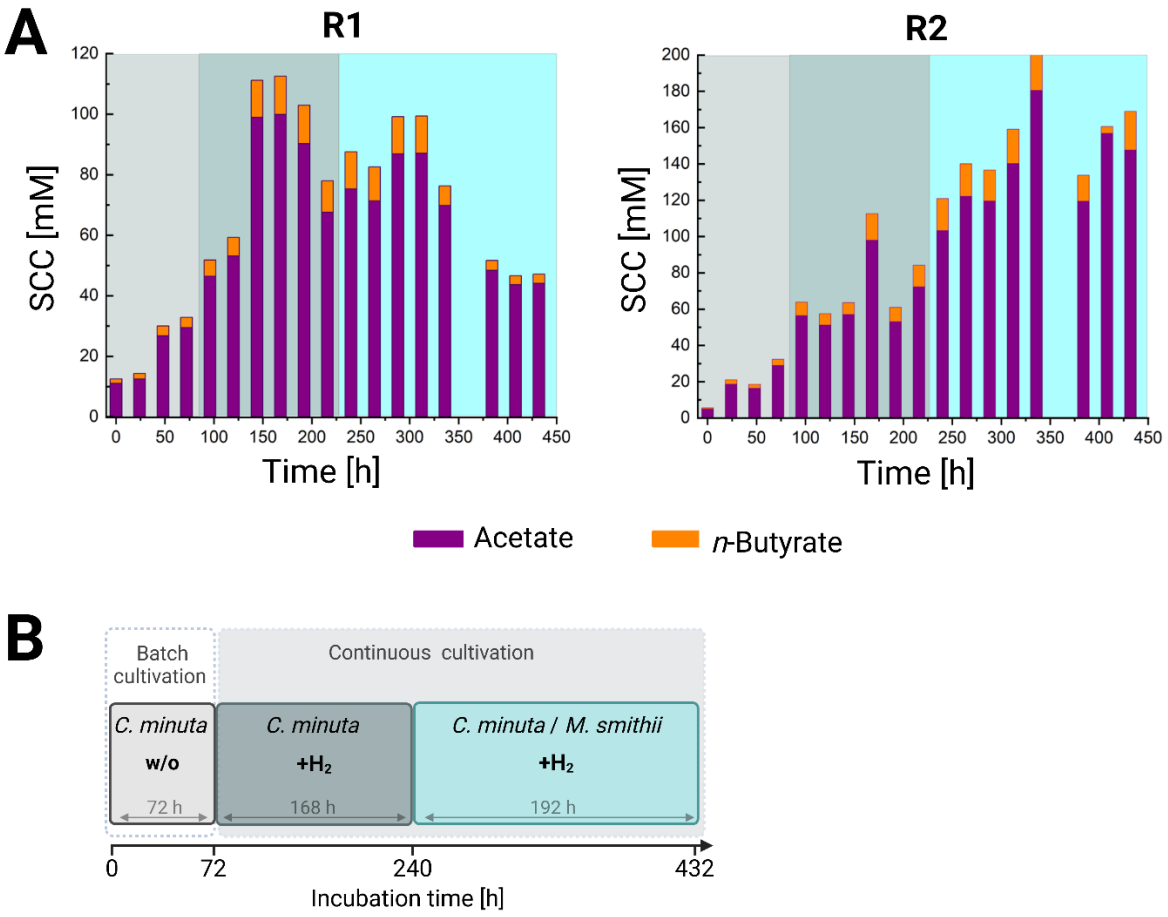

Figure 24: Production of acetate and *n*-butyrate by *C. minuta* in pure and co-culture with *M. smithii*

(A) Acetate (violet) and *n*-butyrate (orange) produced by *C. minuta* in R1-R2 throughout different operating conditions: *C. minuta* without electrochemistry (w/o), with H_2 supply ($+H_2$) for *C. minuta*, with H_2 supply ($+H_2$) for *C. minuta* plus *M. smithii*. (B) Operating periods of the experiment

Therefore, we decided to investigate the *n*-butyrate: acetate rations (**Figure 25C**). This ratio increased in the second operating condition, with H_2 supply for *C. minuta*, indicating that *C. minuta* produced more *n*-butyrate in the R1 and R2. After the inoculation of *M. smithii* at 240 h, the *n*-butyrate: acetate ratio dropped almost to the ratio in the BES phase *C. minuta* without electrochemistry in R1 and even more for R2. Therefore, less *n*-butyrate and more acetate was produced in the presences of *M. smithii*. In addition, the H_2 concentration in R1 and R2 decreased after inoculation with *M. smithii* and was almost completely consumed after 300 h (**Figure 25A**). After the inoculation of *M. smithii* to study the co-culture activity together with *C. minuta* in the BES, CH_4 was only detected in R1 and R2 (but not in R3) (**Figure 25B**).

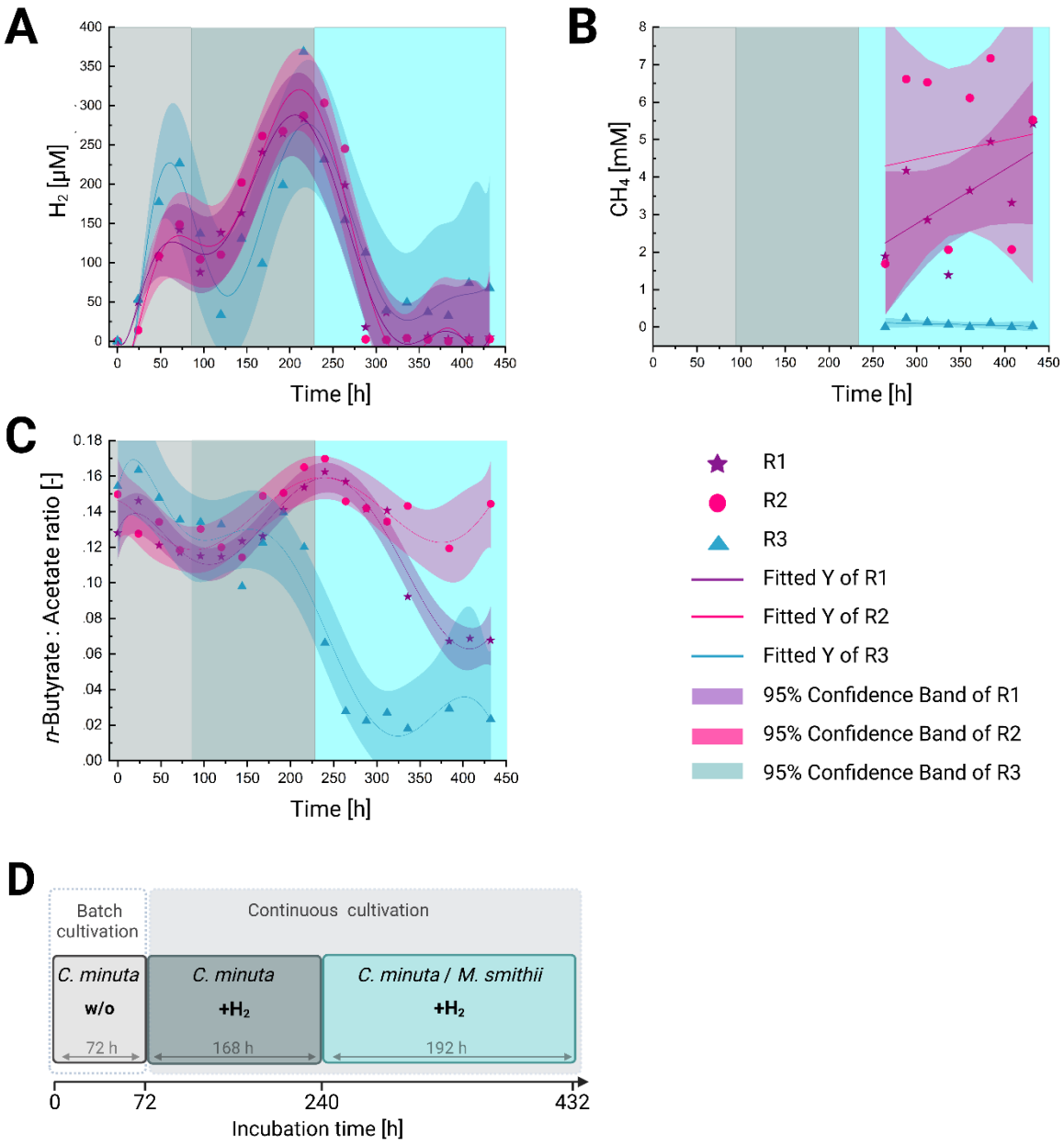

Figure 25: Production of H_2, CH_4, and *n*-butyrate: acetate ratios
(A) H_2, (B) CH_4 and (C) *n*-butyrate: acetate ratios of R1-R3 throughout different operating conditions: *C. minuta* without electrochemistry (w/o), with H_2 supply (+H_2) for *C. minuta*, with H_2 supply (+H_2) for *C. minuta* plus *M. smithii*. (D) Operation periods of the experiment. The plotting and curve fitting by polynomial interpolation (95% confidence band) were done with the software Origin (version 2023). The graphs were arranged using BioRender.com.

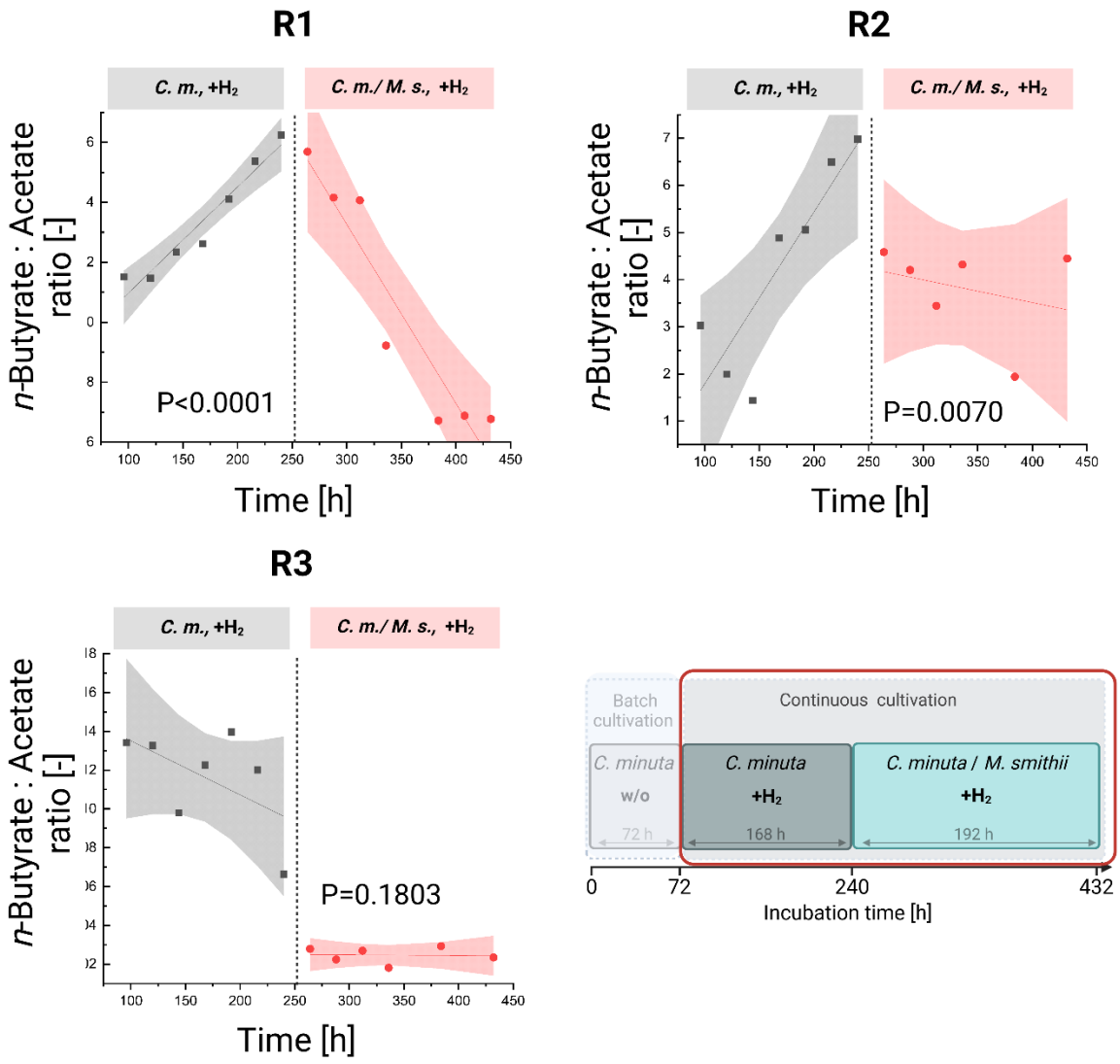

Figure 26: Statistical analysis of *n*-butyrate: acetate ratios
Linear regression test of *n*-butyrate: acetate ratios between the operating conditions with H_2 supply ($+H_2$) for *C. minuta*, with H_2 supply ($+H_2$) for *C. minuta* plus *M. smithii*. In R1 and R2, best-fit slopes in the phase with H_2 supply ($+H_2$) for *C. minuta* is significantly different from with H_2 supply ($+H_2$) for *C. minuta* plus *M. smithii* , R1: P<0.0001, R2: P=0.0070). R3's best-fit slopes are not significantly different without and with *M. smithii*. C. m., *C. minuta*, M. s., *M. smithii*, 95% confidence band. The statistical analysis was done by GraphPad Prism 9 (Version 9.5.1). The graphs were arranged using BioRender.com.

M. smithii completely consumed H_2 during the last operating condition (with H_2 supply for *C. minuta* plus *M. smithii*), resulting in the production of CH_4 (**Figure 25**). With linear regression, we tested *n*-butyrate: acetate ratios in R1 and R2 and compared the operating conditions with H_2 supply for *C. minuta* and with H_2 supply for *C. minuta* plus *M. smithii* (**Figure** 26). We found that the best-fit slopes are significantly different between these two operating conditions in R1 (P<0.0001) and R2 (P=0.0070) (**Figure** 26).

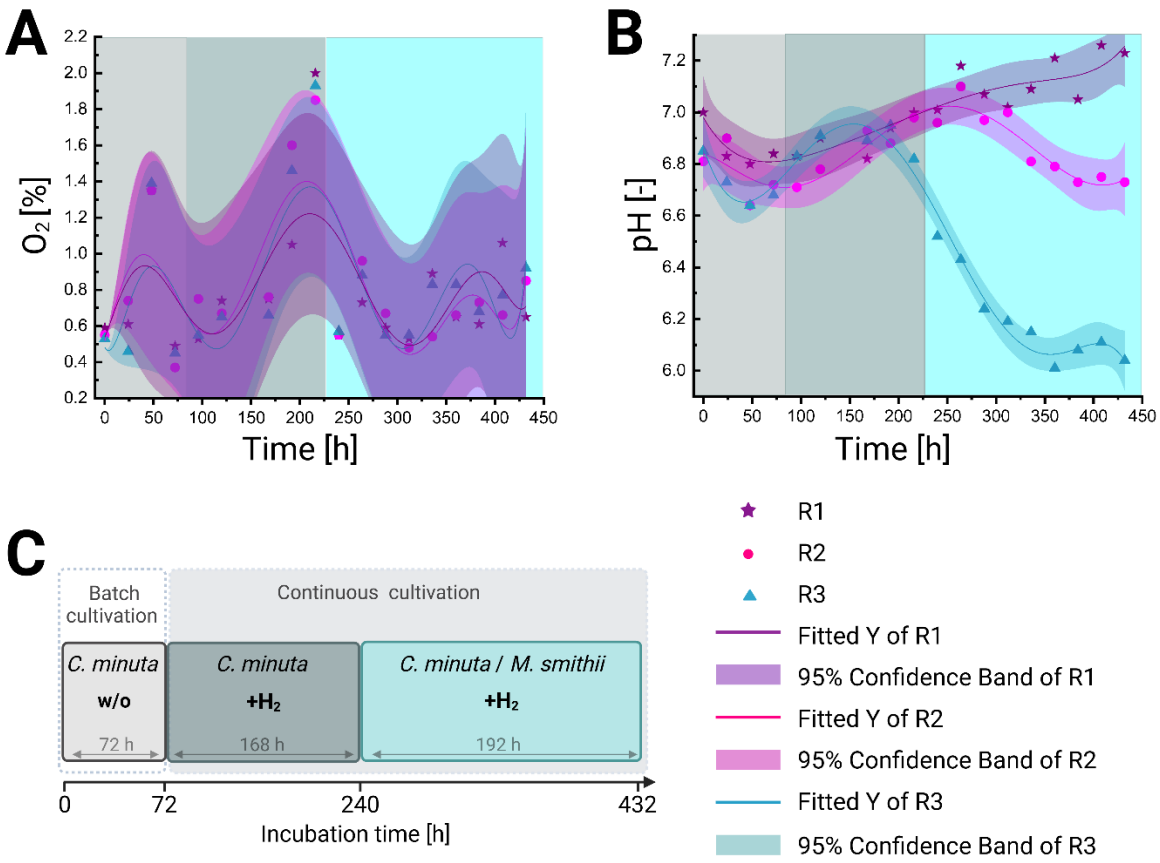

Figure 27: O_2 and pH from R1-R3
(A) O_2 and (B) pH were measured in R1-R3 throughout different operating conditions: *C. minuta* without electrochemistry (w/o), with H_2 supply ($+H_2$) for *C. minuta*, with H_2 supply ($+H_2$) for *C. minuta* plus *M. smithii*. (C) Operating periods of the experiment. The plotting and curve fitting by polynomial interpolation (95% confidence band) were done with the software Origin (version 2023). The graphs were arranged using BioRender.com.

Furthermore, we investigated the O_2 concentration and pH throughout all operating periods (**Figure 27**). O_2 concentration increased two times in the first two operating conditions above 1% in R1 and R2 (**Figure 27A**). We did not detect an effect on the production of acetate and *n*-butyrate and on the H_2 supply by the BES. The pH stayed for R1 and R2 in the physiological cultivation range of *C. minuta* and *M. smithii*, which is pH 6.0-9.0 for *C. minuta* and pH 6.5 to 8.0 for *M. smithii* [161, 162] (**Figure** 27**B**).

At the end of the operating condition with H_2 supply for *C. minuta* plus *M. smithii*, all BESs were disassembled, and 1 x 1 cm pieces from the working electrode were taken for investigation of the electrode-microbe interaction by SEM. For R1 and R2, a biofilm of *C. minuta* and *M. smithii* embedded in the Pt/C-coating was detected (**Figure 28**).

Furthermore, for both R1 and R2, we found that *C. minuta* was growing at a higher density than *M. smithii*.

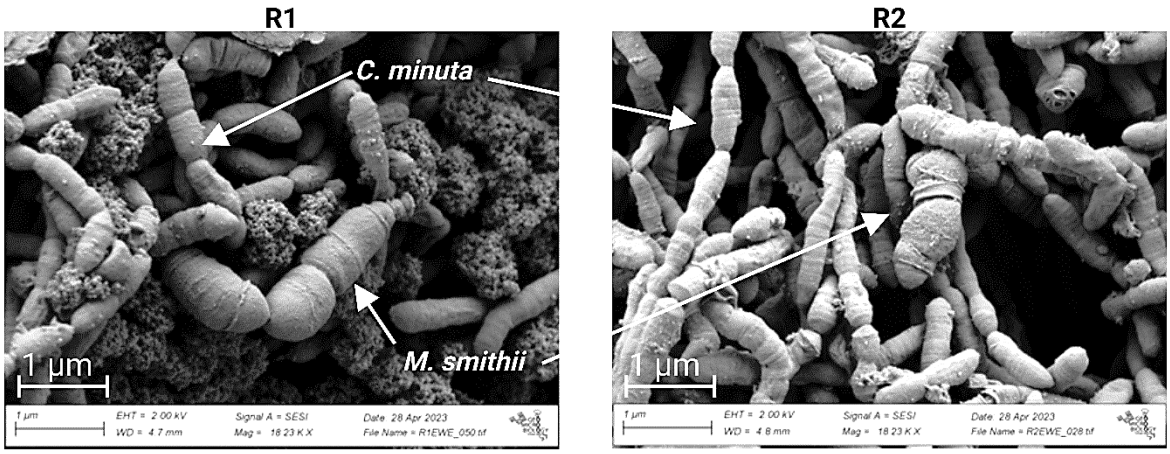

Figure 28: SEM from working electrode of R1 and R2 at t= 432 h
Biofilm formation of *C. minuta* and *M. smithii* from the end of the operating period with H_2 supply for *C. minuta* plus *M. smithii*. Magnification = 18.23 K*X*

4.5. Discussion and Outlook

In the experiment performed in Chapter 3, we showed that *C. minuta* also grows and forms a biofilm when H_2 is supplied by the BES (**Figure 19**). In this experiment, in which we co-cultured *C. minuta* and *M. smithii*, the two microbes grew as biofilm at the working electrode in the BES. Furthermore, we detected a drop in the *n*-butyrate: acetate ratios after the inoculation of *M. smithii*, where less butyrate was produced than in the operating period with H_2 supply for *C. minuta.* The change in the *n*-butyrate: acetate ratio and the close proximity of the microbes in the biofilm at the working electrode indicate that the BES is a suitable tool to study H_2 syntrophy between *C. minuta* and *M. smithii* and other microbial synthrophes, which are based on H_2 availability. Due to contamination observed in R3, the results of this BES are misleading, and the reduced production of acetate and *n*-butyrate throughout the entire operating period of R1 (in comparison to R2) led to the conclusion that the experiment with three BESs needs to be repeated to get reliable and reproducible results. We did not further investigate other metabolic products from R3, so we cannot conclude which type of contamination it could be. Furthermore, the pH slightly changed after *M. smithii* was inoculated in R1 and R2, ranging between pH 6.8 and 7.3. Therefore, a different buffer compound with a higher buffer capacity might be suitable to

minimize changes in the pH. Another technical approach could be adding more pH sensor spots across the chamber of the BES because we only used one spot *per* BES in the middle of each chamber. It was impossible to set up an automatic control until we experienced, that the pH slightly changed. There, we had only one pH meter for optical pH measurement for three BESs, and there was no controller set up available for continuous pH measurements and the automatic pH adjustment by adding acid or base. By adding additional ports to the BES and stacking up the technical equipment, the pH can be controlled more precisely, and its influence on the production of acetate and *n*-butyrate can be neglected. Besides the pH, the biofilm formation at the electrode might play a role and can influence the H_2 supply reaction.

The second part of the experiment needs to be performed to answer the question whether the H_2 supplied by the BES can compete with a syntrophic H_2 consumer. There, *C. minuta* would grow at the anode, where H_2 is removed by oxidation, and *M. smithii* will be cultivated at the cathode, where H_2 from *C. minuta* is reduced again to H_2. With these results, we will be able to answer whether the BES can compete with a methanogen in terms of syntrophic H_2 uptake and if the BES can be used to study the H_2 syntrophy of other microbes from the human gut or other environments. In addition to the second part of this investigation, we need to evaluate whether *M. smithii* can grow on the amount of H_2 produced by *C. minuta* in the BES or if an additional supply of H_2 is required to achieve suitable cell densities.

In addition, the SEM micrograph and the first preliminary data have already given us great insights into the biofilm formation at the electrode surface. The ability of biofilm formation *in-vitro* and its investigation can give us a better understanding of the action of syntrophic communities from the human gut, such as *C. minuta* and *M. smithii*, and might help to understand better the role of biofilms in the human intestinal tract. Biofilm formations in the human gut are found in the luminal and mucosal locations and may be a mechanism for bacterial retention in the gut [163]. In addition, they are organized in complex microbial communities and greatly impact the function of the intestinal microbiome, and therefore human health and disease [164]. Several studies showed that the microbial composition associated with particles/food residues in stool differs from the community extracted from the liquid phase [165]. Furthermore, in fermentation experiments, the biofilm population

was more efficient in digesting polysaccharides than non-adhering communities and produced mainly acetate. Higher amounts of *n*-butyrate were found for nonadhering microbial communities, and the biofilm population is metabolically distinct from a nonadherent population [166].

Chapter 5
A BES as a Tool for the Enrichment of Syntrophic H_2 Producers from the Human GI Tract

5.1. Abstract

In Chapter 3, we designed and operated a BES capable of mimicking the H_2 consumption of a methanogen as found in microbial H_2 syntrophy. Furthermore, in Chapter 4 we showed that the BES is a suitable tool to study the H_2 syntrophy of the co-culture of *C. minuta* and *M. smithii* as an example. Both microbes were grown together as a biofilm at the same electrode. By combining the outcomes from these two experiments, we wanted to test whether this BES can be used as a cultivation approach to enrich and isolate syntrophic H_2 producers from the human gut. Therefore, we add a bioinformatics pipeline to this experiment to continuously track the development of the microbial community based on full-length 16S rRNA gene sequencing. With this real-time monitoring approach, we could better define time points for microbial isolation in future experiments and understand interspecies H_2 transfer and microbial syntrophy.

Chapter 5 focuses on applying this BES setup to enrich microbial H_2 producers from a human feces sample and monitor microbial dynamics on the species level. These dynamic variations will be observed in the BES by next-generation sequencing of the 16S rRNA gene using the Oxford Nanopore sequencing platform. Nanopore sequencing is known to study complex microbial samples by sequencing long reads in real time using inexpensive and portable technologies. Therefore, a human fecal sample from the lab of Ruth Ley[3] was cultured in the BES with H_2 removal by oxidation at the working electrode. The dynamics of the community will be investigated throughout the entire operating period using

[3] Department Microbiome Science, Max Planck Institute for Biology Tübingen

continuously fed BESs and the MMonitor software developed by Timo Lucas[4] and the group of Prof. Daniel Huson[4].

Microbial fermentation products, such as SCCs and gasses, were monitored throughout the complete operating period. Further, we wanted to track the diversity of the microbial community by full-length 16S rRNA gene sequencing using the Nanopore MinIon sequencing platform. This combined approach using genomic information that was paired with the produced metabolites allowed us to have a fast answer about the relative abundance of specific microbes and their metabolic activity. In this study, we cultivated microbes from human feces in a BES and grew them as a biofilm. H_2 from microbial fermentation was removed at the working electrode, and only micro-molar concentrations were detected in the BES. Furthermore, we detected typical concentrations for SCCs and other organic acids, CO_2, and ethanol. No CH_4 was detected during the BES cultivation. The microbial community changed dynamically during the cultivation, but no uncultured H_2-producing microbes were detected by MMonitor using 16S rRNA gene sequencing and a 0.1% relative abundance threshold.

5.2. Introduction

5.2.1. Isolation Strategies for new Microbial Species from the human GI Tract

As understanding the human microbiome has become a popular topic in the scientific community and its role in health and disease has become critical, the potential for developing new therapeutic approaches is enormous. Sequencing approaches made considerable efforts to decipher and profile the composition of the human microbiota at different sites of the body. In addition, metagenomics have revealed the microbial diversity in the human gut and showed that only a few species can be cultivated in the lab. Until 2012, it was generally accepted that 80% of all classified bacteria were not cultivable due to the limitations of cultivation approaches. In order to find the best methods and appropriate tools for the cultivation and identification of unknown bacteria and to overcome the limited detection of minor microbial populations, a new cultivation approach was introduced by Lagier *et al.* (2015) [167-170]. This cultivation approach, which uses

[4] Research group Algorithms in Bioinformatics, University of Tübingen

multiple culture conditions in combination with matrix-assisted laser desorption/ionization-time of flight and 16S rRNA gene sequencing for identification. It has led to a tremendous increase in new microbial isolates from the human gut, expanding our understanding of bacterial diversity and broadening the scope of human microbiota studies and potential implications for human health [171].

5.2.2. Bioreactor Systems to Study Human Gut Microbiota *in-vitro*

Besides developing new isolation approaches, exciting new perspectives came up by studying the entire microbial community and its interaction with the host. Therefore, *in-vitro* fermentation systems were developed that allow precise control over many physiological parameters and exclude confounding factors from the human host. Different reactor models are available to study microbial community ecology and function. The Mini Colon Model is a low-cost, benchtop multi-bioreactor system that simulates the physiological relevant condition of the human colon environment where pH, temperature, and fermentation fluidics can be controlled automatically and runs independently of an anaerobic chamber [172]. Other reactor systems, such as Robogut, which is a single-stage bioreactor system that mimics the conditions of the distal human colon, but have the disadvantage of being litre-sized bioreactors. [173]. The most well-known bioreactor type is the Simulator of Human Intestinal Microbial Ecosystem (SHIME). This bioreactor consists of a 5-stage chemostat reactor replicating different human GI tract sections [174]. The disadvantages of this bioreactor are the lack of multiplexing, low experimental throughput, large footprint, and stabilization of the microbiota, which can take up to a few weeks. Besides the available bioreactor systems to study the microbiota of the human GI tract, there is no setup available that is able to mimic syntrophic interactions. Since the beginning of the great debate about the importance of direct electron transfer, our bioelectrochemistry research group has been developing different BESs for the intensive study of electrically connected microbial communities and the direct exchange of electrons with an electrode. Based on these bioelectrochemical technologies and the BES setup of Guzman *et al.* (2019), we developed BESs to study the H_2 syntrophy of microbes from the human GI tract to enrich and later isolate a syntrophic H_2 producer without its syntrophic H_2-consuming partner.

5.2.3. Bioinformatic Tools to Track Microbial Taxonomy

The complexity of bacterial communities can be characterized on the species level by 16S rRNA gene sequencing, which is a reliable way to characterize microbial diversity and is important in clinical applications such as diagnosis and treatment [175]. High-throughput sequencing is now mostly performed by Illumina sequencing, but the sequences are limited to approximately 500 nucleotides *per* joined paired-end read. Thus, Illumina sequencing is limited to only a portion of the 16S rRNA gene, which consists of nine hypervariable regions and targets only a selected subset of the 16S rRNA gene. Distinguishing between highly similar species and making reliable taxonomic classifications based on short-read data is a major limitation of Illumina sequencing. Furthermore, in most cases, taxonomic profiles are only classified to genus level [176]. To overcome this limitation, the assembly of short reads by the synthetic long read method and sample-specific barcoding are two approaches to increase accuracy - but also increase sample preparation time and sequencing costs. With long-read sequencing of the entire 16S rRNA gene, we can overcome this limitation and gain a higher resolution for species-level identification. In the past, long reads came with one notable drawback: high sequencing error rates [177, 178]. With the ongoing improvement in Oxford Nanopore Technologies kit chemistry and the reduction of error rates, the sequencing reads become less noisy, have better accuracy, and have a higher species classification. Comparing the Nanopore sequencing platform and Illumina for 16S rRNA gene sequencing, Nanopore shows a better species-level taxonomic resolution, enables the investigation of rare taxa, and gives a more accurate estimation of microbial richness [179].

Besides continuously monitoring the metabolic fermentation products from the microbiota in the BES, we will analyze the dynamics of the microbial community and how stable or fluctuating the community is with MMonitor developed by Timo Lucas[4] and the group of Prof. Daniel Huson[4] (**Figure 29**). MMonitor is a tool for metagenomic monitoring, taxonomic and functional insights, species-level microbiota monitoring and quality control using nanopore sequencing data. The software consists of a desktop application for data analysis and an accompanying webserver dashboard for result visualization. MMonitor provides real-time data analysis with immediate sample overviews and was developed in

collaboration with the Environmental Biotechnology Lab of Lars Angenent[5]. It can run on personal or lab computers or external servers to enhance processing capabilities. Furthermore, the software can assemble genomes from pure microbial cultures. Depending on the user, MMonitor can be operated through a user-friendly graphical interphase or the command tool on a remote server.

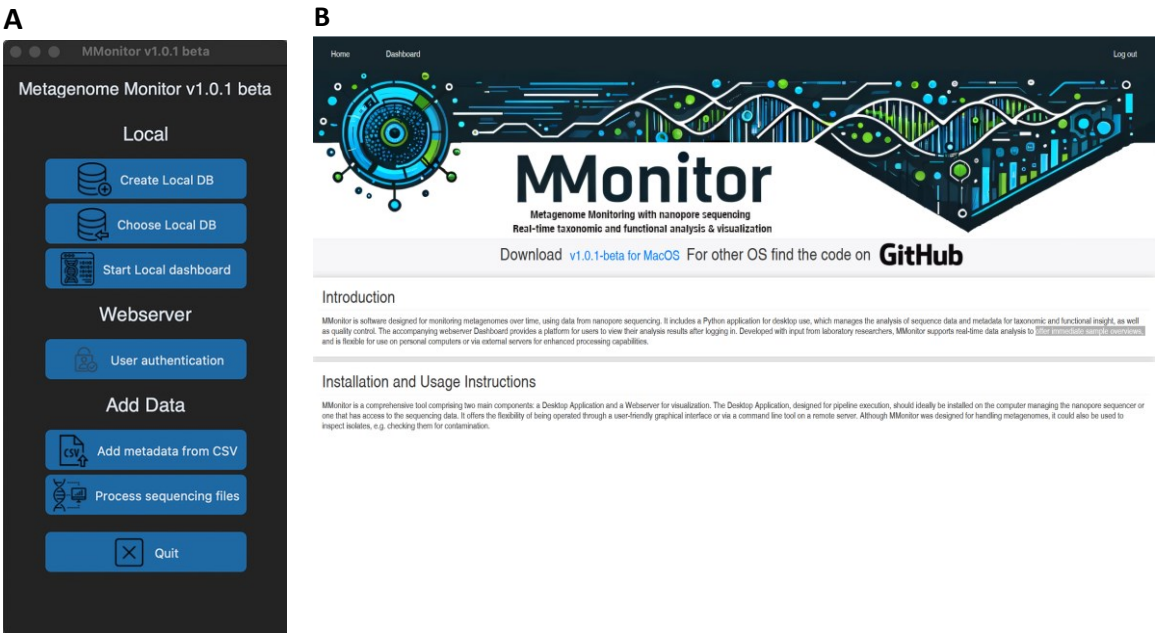

Figure 29: Graphical user interfaces of MMonitor using Nanopore sequencing data
(A) MMonitor consists of a desktop application for data analysis and (B) a web server dashboard for result visualization and quality control of the sequencing reads. MMonitor was developed by Timo Lucas[4] from the research group of Prof. Daniel Huson[4].

For the experimental part of this study, which included an enrichment study, we grew a human fecal sample in the BES with H_2 removal to enrich for microbial, syntrophic H_2 producers (**Figure 30**). We monitored the microbial community on an almost daily basis throughout the complete operating period. As a first step, we wanted to define sampling times to sample for H_2-producing microbes, which we wanted to gradually bring into pure culture in a follow-up experiment. Here, only the results on the enrichment part of Objective 3 are shown, and possible isolation strategies are discussed in the outlook part of Chapter 5.

[5] Research group Environmental Biotechnology, University Tübingen

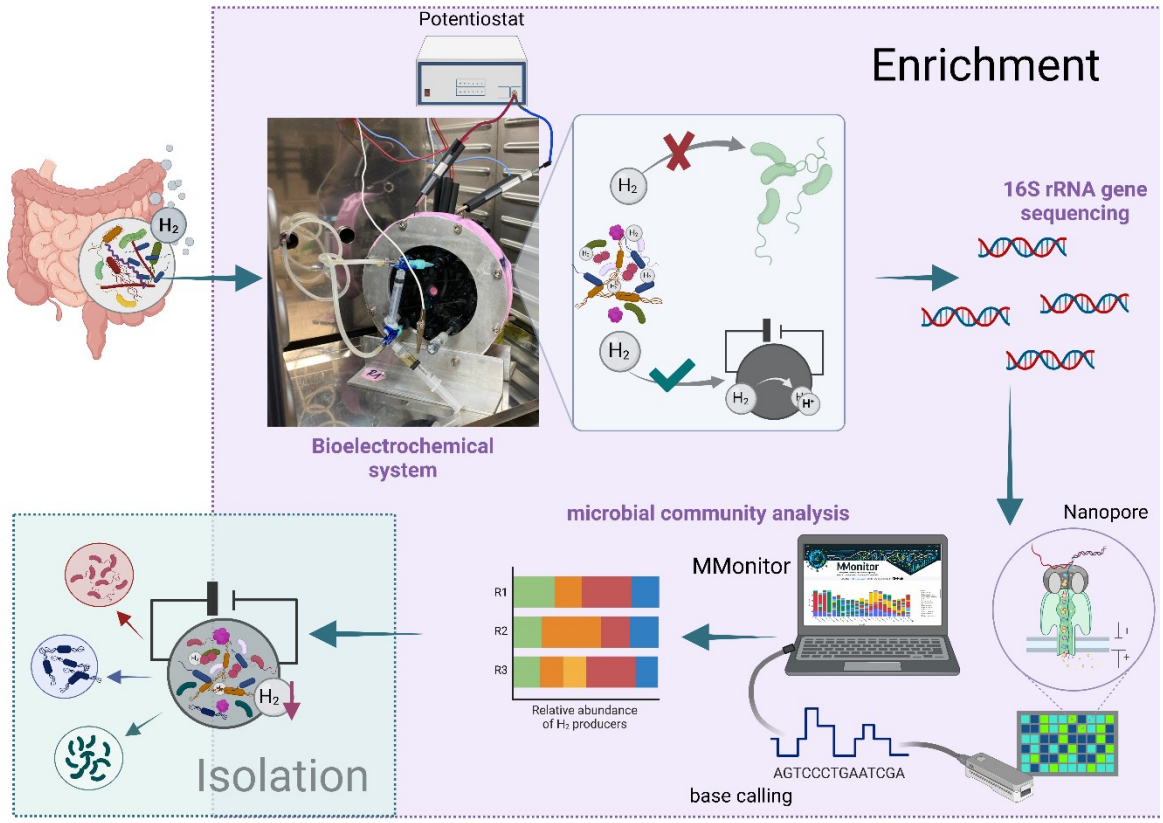

Figure 30: Schematic illustration of the experimental setup for Objective 3
Enrichment and isolation of syntrophic H_2-producing microbes from human feces in the BES

5.3. Material and Methods

We monitored the microbial community and its dynamics based on 16S rRNA gene sequencing during the enrichment of a human fecal sample in a BES with H_2 removal. The 16S Barcoding Kit will amplify the target gene with PCR using specific, universal bacterial 16S rRNA gene primers (27F and 1492R). There, universal primers are designed based on conserved regions (with slow evolution rates) of the 16S rRNA gene, which can amplify 16S rRNA genes across different taxa.

5.3.1. BES Setup

We used the same BES setup as described in section 3.3, Material and Methods. Three replicate BESs (R1= BES 1, R2= BES 2, and R3= BES 3) were set up for this experiment. The human fecal sample was consciously enriched under H_2 removal by oxidation (E_i= 350 mV *vs*. Ag/AgCl) at the working electrode for 559 h. After 24 h of batch cultivation period, the BESs were continuously operated with a 1 mL/min media feed rate.

5.3.2. Inoculum

We used a fresh human fecal sample for the experiment. After the fresh fecal sample was collected, it was placed directly in an anaerobic chamber because most microbial species are anaerobes and microaerophiles and are sensitive to O_2 exposure. We suspended the sample in PBS (32% w/v) and homogenized it by vortexing for 5 min. By centrifugation (550 × *g* for 5 min at room temperature), we separate all solid residuals (undigested food and fiber, bile, and bilirubin) and large cellular debris from the microbes in the supernatant. We then collected the supernatant containing the microbes. The BESs were inoculated at an initial OD of 0.01. Therefore, we calculated the volume from the supernatant needed to reach an OD of 0.01 in each BES. The appropriate volume + 25% of the microbe-PBS suspension was taken, and the microbes were pelleted by centrifugation. The pellet was resolubilised in the 800 µL media, and 200 µL was used as inoculum for each BES. The leftovers of the microbes from the fecal sample were stored in 25% glycerol stocks at -80°C.

5.3.3. Media and Cultivation Conditions

The BES media contained 28.4 g/L Schaedlers broth (Carl Roth, #5772.1), which was supplemented with 5% defibrinated sheep blood (Analytics shop, #OXSR0051E), 0.1 g/L Menadione sodium bisulfite (vitamin K3) from 1 M anoxic stock solution (Sigma-Aldrich, #M5750-25G), 0.3 g/L Polyanetholesulfonic acid sodium salt (PSS, Sigma-Aldrich, #444464-25G), 1 g/L α-lactose-monohydrate (Carl Roth, #8921.1), 5 g/L mucin from porcine stomach (Sigma-Aldrich, #M2378-100G), 2 mg/L β-Nicotinamideadenine-dinucleotide hydrate (β–NAD, Sigma-Aldrich, #N1511-250MG), 3.53 g/L sodium bicarbonate (from 1.13 M stock solution, Carl Roth, # 0965.2), and 0.5 g/L L-cystein-HCL (from 1 M L-cystein-HCl/NaOH anoxic stock solution, Carl Roth, # 3468.3. During the first step of the medium preparation, Schaedler's broth, PSS, mucin, β–NAD, and lactose were dissolved in MiliQ water and autoclaved. Defibrinated sheep blood was added under sterile conditions after autoclaving. The medium was sparged with N_2:CO_2 for 1 h. After sparging, vitamin K3, L-cysteine-HCl, and sodium bicarbonate were added from anoxic, sterile stock solutions. We set the pH to 7.5.

5.3.4. DNA Extraction

For DNA extraction, 500 µL were taken from the BES and centrifuged (19000 × *g*, 5 min at 4°C) to separate the microbes from the supernatant. The pellet containing the microbes was kept at 4°C for immediate DNA extraction or stored at -20°C for later use. For the DNA extraction, we used the AllPrep® PowerFecal Pro DNA/RNA kit (QUIAGEN). We used the FastPrep-24™ 5G bead beating grinder (MP Biomedicals) with 2 cycles of 6.0 m/s for 40 sec with break of 30 s (feces program) for the mechanical cell wall disruption. We followed the manufacturer's instructions with some exceptions: <450 µL instead of 300 µL of supernatant were taken in step 6 of the sample pretreatment where CD2 is added to the supernatant from cell disintegration. When taking a larger volume in this step, we followed the additional instructions for using higher supernatant volumes. After the DNA extraction, the DNA concentration was measured with a Qubit™ Flex Fluorometer (Invitrogen™), and the DNA quality was determined by the NanoPhotometer® N60/N50 (IMPLEN).

5.3.5. Monitoring of SCCs, Volatile Fatty Acids, EtOH, and Gasses from Microbial Fermentation

The production of SCCs, MCCs, volatile fatty acids, and gasses such as H_2, CO_2, and CH_4 were monitored once *per* day over the entire BES operation period of 558 h. 200 µL of gas from the BES gas phase were analyzed for trace amounts of H_2 by gas chromatography (6´13x Molsieve column, UV RGD detector, SRI Instruments), whereas CO_2 and CH_4 concentrations were detected by another gas chromatograph (0.3-m HayeSep D packed Teflon column, SRI Instruments).

The supernatant for SCC, MCC and EtOH monitoring was collected as described in section 5.3.4, filtered through a 0.22-µm syringe filter, and stored at -20°C for later analysis. SCCs were measured by gas chromatography (DB-FATWAX UI column, Agilent Technologies) using a six-level standard calibration curve, each standard containing 25 µL of 30 mM ethyl-lactate as internal standard and 475 µL of a mixture of SCCs and MCCs as external standards ranging from 0.475 mM to 9.5 mM. The SCC-MCC standard mixture contained acetate, propionate, iso-butyrate, *n*-butyrate, iso-valerate, *n*-valerate, iso-caproate, *n*-caproate, *n*-heptanoate, and *n*-caprylate. *Prior* to analysis, 50 µL of sample was mixed with 425 µL of 2% formate and 25 µL of internal standard.

A standard calibration curve was generated using HPLC (Aminex HP87H column, Shimadzu) for lactate, succinate, formate, and EtOH. The five-level external standard for lactate was in the range of 5 mM to 100 mM. An eight-level external standard ranging from 5 mM to 200 mM was used for succinate and formate. For the detection of EtOH, a five-level external standard ranging from 5 mM to 200 mM was used.

5.3.6. Nanopore Sequencing

For 16S rRNA amplicon sequencing, we used the 16S Barcoding kit 1-24 (SQK-16S024, Oxford Nanopore Technologies) and an R9.4.1 flow cell (FLO-MIN106). The 16S Barcoding kit enables a rapid and full-length 16S rRNA gene sequencing for microbe identification by using universal primers 27F (5'- AGAGTTTGATC**M**TGGCTCAG -3') and 1492R (5'- CGGTTACCTTGTTACGACTT -3'). For the 16S rRNA gene amplification *via* PCR, we mixed 10 µL of 10 ng DNA with 25 µL of LongAmp® Hot Start Taq 2x Master Mix (New England Biolabs), 10 µL of an individual 16S rRNA gene barcode and 5 µL of nuclease-free water. The PCR cycles were 1 min at 95°C, 25 cycles of 20 s at 95°C, 30 s at 51°C, 2 min at 65°C, and a 5 min final elongation step at 65°C. We then followed the manufacturer's protocol to clean the DNA by bead cleaning, prepare the purified DNA library using the Rapid Adapter, pool the samples, and prepare and load the flow cell. The sequencing run time was set to 2h *per* sample and adjusted for every library containing multiple samples. The MINKNOW software version 23.11.4 was used for data acquisition.

5.3.7. Data Processing and Statistical Analysis by MMonitor

Timo Lucas provided the method chapter about MMonitor. MMonitor consists of a user application for data input and analysis and a web server for data management and visualization. The user application offers a simple graphical user interface that lets users input data and select analyses based on their research questions. For processing a larger scale of data, MMonitor also offers a command line interface. The command line interface has the advantage that it can also be used remotely (*e.g.*, on a high-performance server) for better scaling. Besides a single-sample input, the graphical user interface and command line interface support multi-sample input by providing a CSV file with references to the associated data. After analysis, results (*e.g.*, taxonomic profiles) are sent to the web server *via* HTTP requests, which are stored in a database (**Figure 31**).

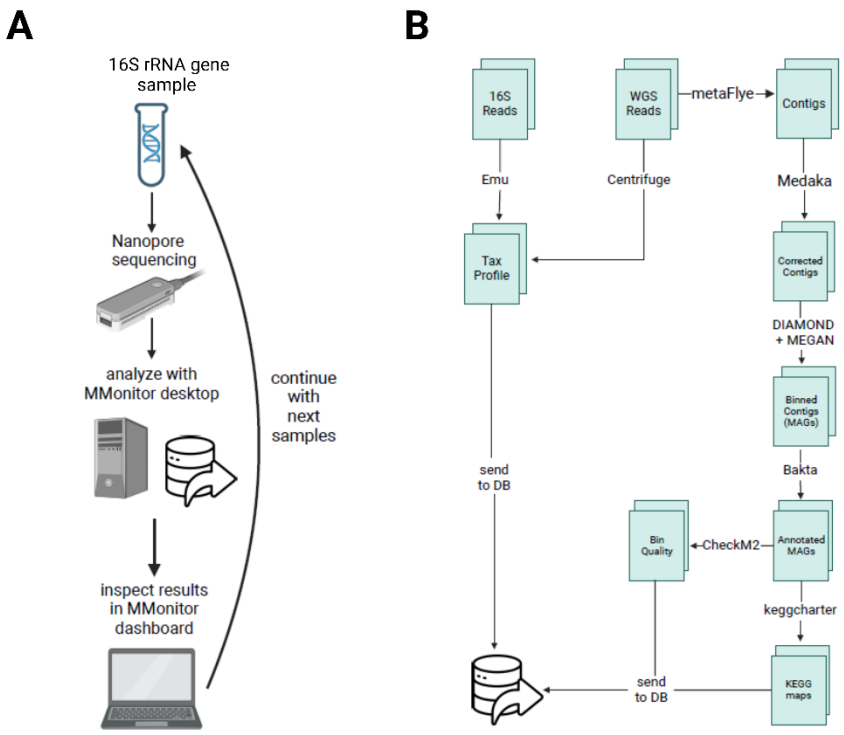

Figure 31: Analysis of 16S rRNA gene sequences by MMonitor
(A) Application of MMonitor in the lab. (B) The bioinformatics pipeline of MMonitor is used to process the input 16S rRNA gene reads before they are sent to the web server's database. The figure was adjusted after Timo Lucas[4] and was created by BioRender.com.

The desktop application handles data input and running pipelines, while the computations themselves are performed by external bioinformatics tools that are usually implemented in performant languages, such as C, for which benchmarks and methods can be found in the respective publications. Taxonomic analysis using 16S rRNA gene nanopore reads is performed by a novel microbial classification engine called Centrifuge, which is based on the Burrows-Wheeler transformation and the Ferragina-Manzini index [180].

For 16S rRNA gene taxonomic profiling by nanopore sequencing, MMonitor uses Emu [178], which uses minimap2 [181] for alignment and an expectation maximization (EM) algorithm [182] for computing taxonomic profiles. It needs to be mentioned that normalization of the reads was performed by sample size and not by rarefaction or other normalization approaches. Basic quality statistics for input reads were implemented by querying the input reads for quality score, read lengths, and number of bases using biopython seqIO [183]. For the statistical analysis, we used different methods. Normalized

counts in (**Eq. 1**) are calculated from raw counts *cr*, number of aligned bases *b*, and a scaling factor *f*.

$$\boldsymbol{n_c = \frac{c_r}{b} * f} \qquad \textbf{(Eq. 1)}$$

The scaling factor *f* ensures that raw and normalized counts have a similar magnitude and is the average number of aligned bases over all samples. Alpha and beta diversity are calculated using scikit-bio diversity (v0.5.9), using normalized counts on demand. Shannon (**Eq. 2)** and Simpson (**Eq. 3**) indices can be used for alpha diversity, where *s* is the number of unique taxa, and *p* is the proportion of the community represented by taxon i.

$$\boldsymbol{H = -\sum_{i=1}^{S}(p_i log_2 p_i)} \qquad \textbf{(Eq. 2)}$$

$$\boldsymbol{S = 1 - \sum p_i^2} \qquad \textbf{(Eq. 3)}$$

Beta diversity is determined by calculating the Bray-Curtis distance (**Eq. 4**) between all samples, where ui and vi are the proportions of taxon I in samples *u* and *v*.

$$\boldsymbol{d(u,v) = \frac{\sum_i |u_i - v_i|}{\sum_i |u_i + v_i|}} \qquad \textbf{(Eq. 4)}$$

5.3.8. SEM imaging

We used SEM to examine biofilm formation at the working electrode of all three BESs from the enriched human fecal sample. We took 1 x 1 cm pieces of the working electrode and placed them in separate wells of a 6-well plate, each containing 2 mL of PBS. To each well, 25% electron microscopy grade glutaraldehyde was added to a final concentration of 2.5%. Sample preparation and imaging procedures are described in section 3.3.5, Scanning Electron Microscopy (SEM) Imaging.

5.3.9. Ethics, Consent, and Permissions

This experiment was approved by the Ethics Committee of the Medical Faculty of the Eberhard Karis University of Tübingen (Project number: 456/2023A). Anonymized stool samples were collected with the permission of all human subjects.

5.4. Results

5.4.1. Results from Microbial Fermentation

Three BESs were operated at batch operation for 24 h and at continuous operation for 558 h. We wanted to get an overview of the products of microbial fermentation and to study the availability of H_2 in the BES. Therefore, we measured gases such as H_2 and CO_2 and the main SCCs, such as acetate, propionate, *n*-butyrate and lactate. In addition, we studied fermentation products produced at lower concentrations, such as formate, *n*-valerate, *n*-caproate, succinate, ethanol, and MCCs.

H_2 was only detected in micro-molar concentrations by gas chromatography. We found an increase and a highly fluctuating profile of H_2 in all three BESs throughout the operating period (**Figure 32A**). Furthermore, after half the operation, the H_2 concentration increased. Fluctuations in the H_2 concentration in the BESs and the increased concentrations in the second half of the operating period might result from changes in the microbial community and their growth as biofilm at the working electrode. This might decreased its performance and less H_2 was removed electrochemically. In addition to H_2, CO_2 was detected, but no CH_4. Therefore, we only show data on H_2 and CO_2 concentrations (**Figure 32A-B**). For CO_2, acetate, and propionate, we found fluctuation in the observed concentration throughout the complete operating period for all three BESs (**Figure 32B-D**). For R1, R2 and R3 fluctuations in the CO_2 production were observed (**Figure 32B**). In the case of acetate and propionate, very similar fluctuations were found for all three BESs (**Figure 32C-D**). The results for *n*-butyrate showed fewer fluctuations and more stable, increasing production throughout the entire operating period for all three BESs.

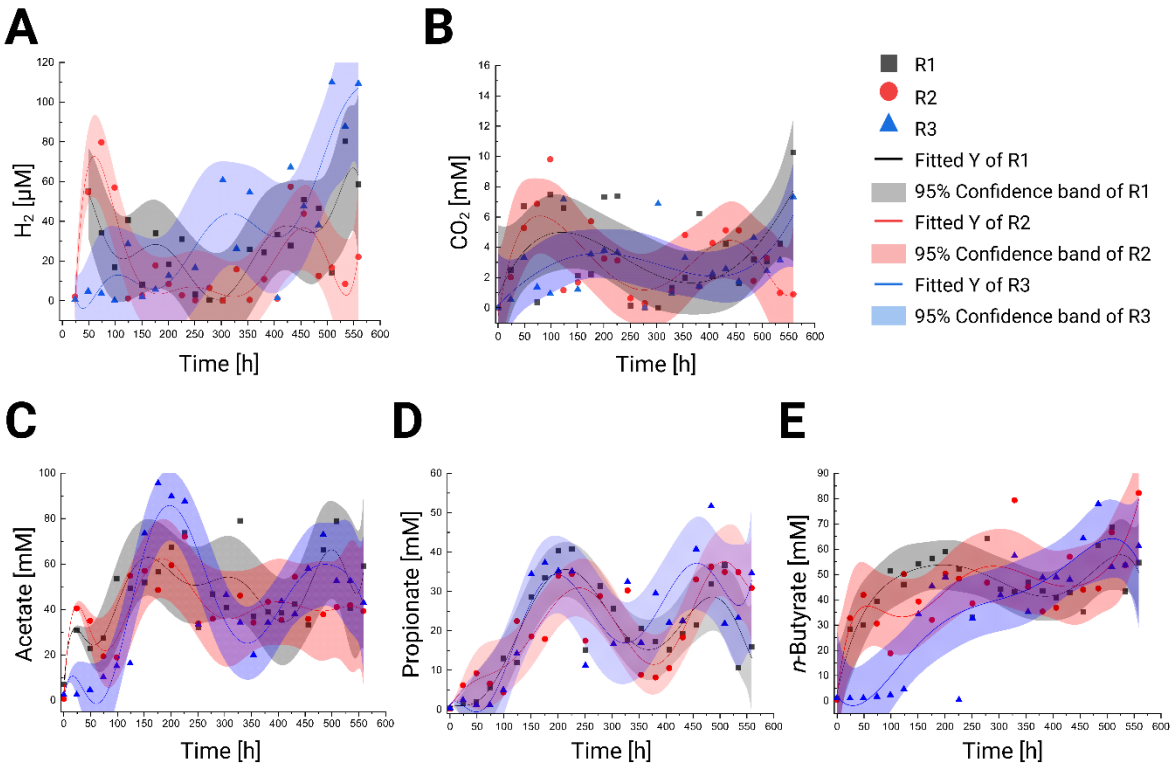

Figure 32: Gas and SCC production from enrichment of a fecal sample in a BES with H_2 removal under continuous operation

We have enriched a fresh human fecal sample in the BES with H_2 removal at the working electrode (E_i= 350mV *vs.* Ag/AgCl). Gas production of (A) H_2 and (B) CO_2 was detected during the operating period. SCCs, such as (C) acetate, (D) propionate, and (E) *n*-butyrate, were detected for all three BES throughout a continuous operating period of 558 h. The plotting and curve fitting by polynomial interpolation (95% confidence band) were performed with the software Origin Pro (version 2023). The graphs were arranged using BioRender.com.

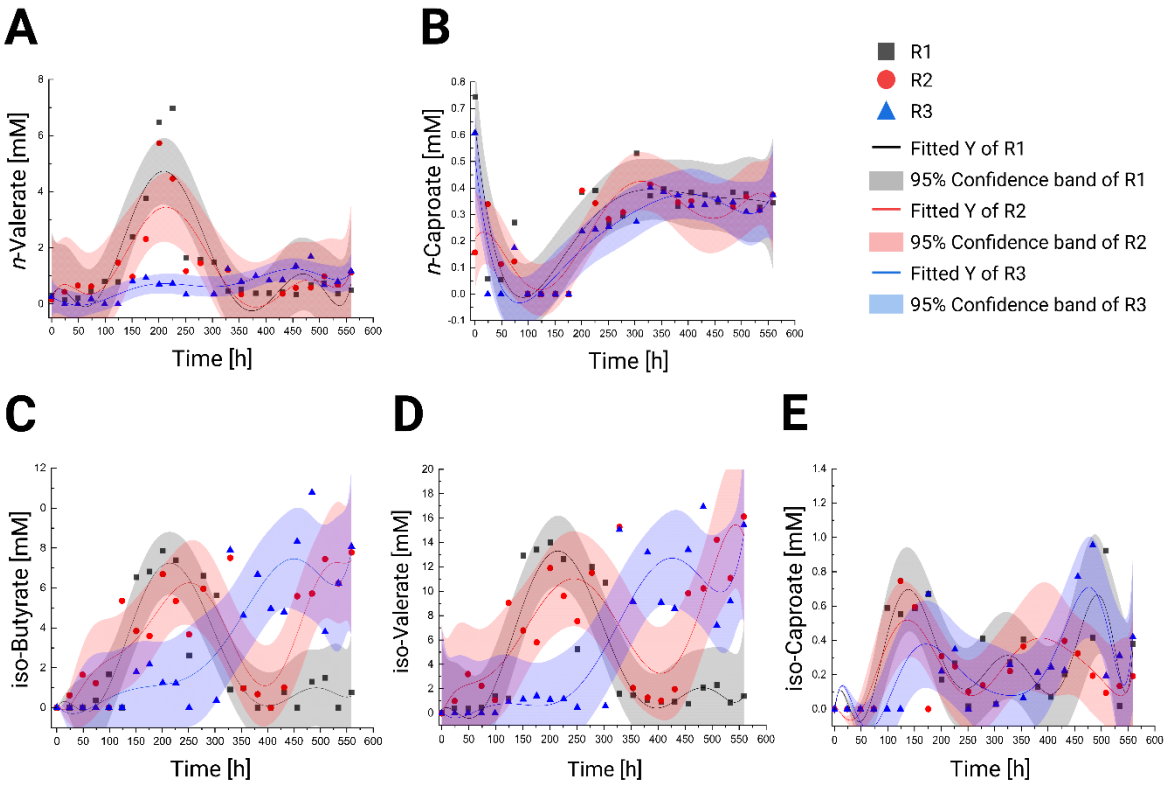

Figure 33: SCCs and MCCs production from enrichment of a fecal sample in a BES with H_2 removal under continuous operation

We have enriched a fresh human fecal sample in the BES with H_2 removal at the working electrode (E_i= 350 mV *vs.* Ag/AgCl). SCCs such as (A) *n*-valerate, (B) *n*-caproate, and MCCs, such as (C) iso-butyrate, (D) iso-valerate, and (E) iso-caproate, were detected for all three reactors throughout a continuous operating period of 558 h. The plotting and curve fitting by polynomial interpolation (95% confidence band) were done with the software Origin (version 2023). The graphs were arranged using BioRender.com.

Furthermore, the production of *n*-valerate showed fluctuations in the R1 and R2, with a maximum production after an operation period of 200 h (**Figure 33A**). For R3, we detected a stable and slightly increasing production of *n*-valerate (**Figure** 33**A**). In the case of *n*-caproate, a steady state production was detected after an operation period of 300 h (**Figure 33B**). All three BESs showed no stable production for the MCCs, which also differs between R1, R2, and R3. For all measured SCCs and MCCs, except for *n*-butyrate, *n*-caproate, fluctuations in the production were detected at an operation period of 200 h in R1 and R2 (**Figure 32-34)** After an operation period of 200 h, we detected a stable production of *n*-butyrate and *n*-caproate (**Figure 32E** and **Figure 33B**). These results led to the conclusion that either acclimation of the microbiota to the BES or changes in the

microbial composition, including biofilm formation, changed the microbial fermentation profile.

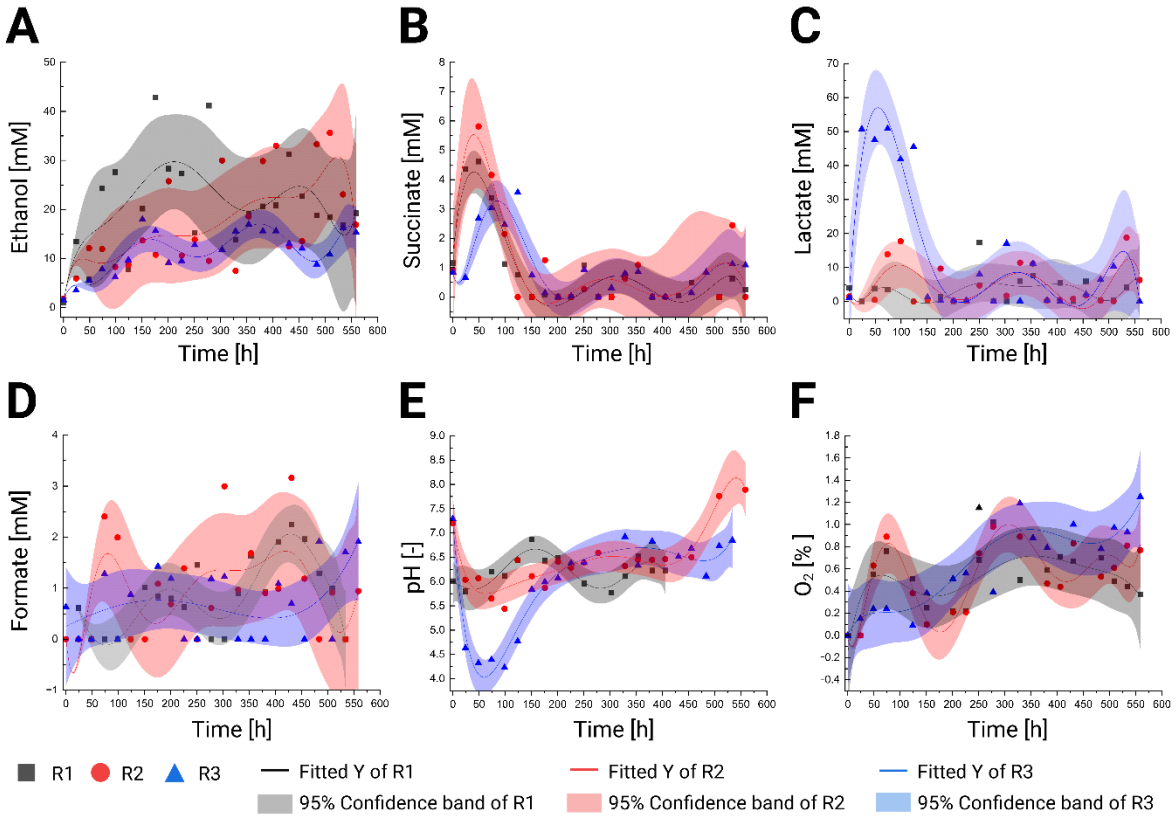

Figure 34: Ethanol, succinate, lactate, and formate production, and pH and O_2 concentrations from enrichment of a fecal sample in a BES with H_2 removal under continuous operation

We have enriched a fresh human fecal sample in the BES with H_2 removal at the working electrode (E_i= 350 mV *vs.* Ag/AgCl). (A) Ethanol, (B) succinate, (C) lactate, and (D) formate were detected for all three reactors throughout a continuous operating period of 558 h. In addition, we observed the (E) pH and (F) O_2 concentration in the BES. The plotting and curve fitting by polynomial interpolation (95% confidence band) were performed with the software Origin (version 2023). The graphs were arranged using BioRender.com.

We further investigated the production of ethanol, succinate, lactate, and formate (**Figure 34A-D**). Ethanol production increased in all three BESs with some fluctuations throughout the entire operation period (**Figure 34A**). High succinate concentrations were produced until an operation period of 124 h and decreased again afterward (**Figure 34B**). Lactate was produced in high amounts in R3 at the beginning of the operation period until 99 h, but not in R1 and R2. At an operation period 200 h, R1, R2, and R3 showed similar lactate concentrations (**Figure 34C**). All the reactors showed a very low and unstable production of formate (**Figure 34D**). The unstable and variable production of metabolites

such as lactate, succinate, and formate, as well as ethanol, must be interpreted separately because they all result from different pathways of microbial fermentation, such as the acylate, succinate, and Wood-Ljungdahl pathways.

To track the performance during the operating period of the BES, we also investigated the pH and the O_2 concentrations (**Figure 34E-F**). These parameters are important for evaluating the performance of the BES. The initial pH was set to 7.4. We used pH sensor spots inside the BES to monitor the pH during cultivation. Unfortunately, the spots were not working throughout the entire operating period, and therefore the pH was measured with a standard pH probe. The pH value dropped for all three BESs at the beginning of the operating period and stabilized in the physiological range after ~200 h (**Figure 34E**). The O_2 concentration in the BES was observed to monitor the anaerobic status of the BES. Throughout the operating period, the O_2 concentration slightly increased from 0%. up to 1-1.2% (**Figure 34F**). Sampling the BES under an aerobic atmosphere after obtaining a liquid sample may cause a slight increase in O_2.

5.4.2. Microbial Community Analysis

The objective of the experiment was to enrich H_2-producing microbes from a human fecal sample during an enrichment process in a BES. The microbial composition was evaluated by MMonitor using full-length 16S rRNA gene sequencing. Only bacterial species are shown in the taxonomic classification for this investigation because the primers of the 16S Barcoding kit 1-24 only target bacteria. The microbial composition changed along the enrichment in all three BESs (**Figure 35-37**). We also found differences in the amount of different species and their relative abundance in the inoculum (time = 0 h) of R1, R2 and R3. The inoculum originated from the same person, and each BES was inoculated with the same amount. Thus, the variability of species and their relative abundance in the inoculum may be due to insufficient sequence depth. Although the community varies a lot throughout the enrichment and also among R1, R2, and R3, some species were found in all three BESs. For R1, we detected two periods of enrichment with each had relatively different community composition. The first period of the enrichment was between 0 h and 226 h, while the second period of the enrichment was between 251 h and 559 h. Therefore,

we analyzed the top 10 most abundant species that were found in all three BESs in the first half and in the second half of the enrichment (**Table 3**).

Table 3: Top 10 dominant species detected in R1, R2 and R3 in the first half of the enrichment (between 0 h and 226 h) and in the second half of the enrichment (between 251 h and 559 h).

Species from the first half of the enrichment	Species from the second half of the enrichment
• *Escherichia coli*	• *Escherichia coli*
• *Streptococcus salivarius*	• *Enterococcus faecalis*
• *Anaerostipes hadrus*	• *Faecalibacterium pausnitzii*
• *Dorea longicatena*	• *Lactobacillus gasseri*
• *Enterocloster boltae*	• *Coprococcos catus*
• *Anaerobutyricum halli*	• *Anaerobutyricum halli*
• *Faecalibacterium pausnitzii*	• *Lactobacullus paracasei*
• [*Eubacterium*] *rectale*	• *Blautia sp. SC05B48*
• *Dialister pneumosintes*	• *Dorea longicatena*
• *Blautia sp. SC05B48*	• *Anaerostipes hadrus*

Figure 35: Relative species abundance of the microbiota in R1

Microbial community analysis based on full-length 16S rRNA gene sequencing throughout the operating period of 534 h. The figure was created by MMonitor and BioRender.com.

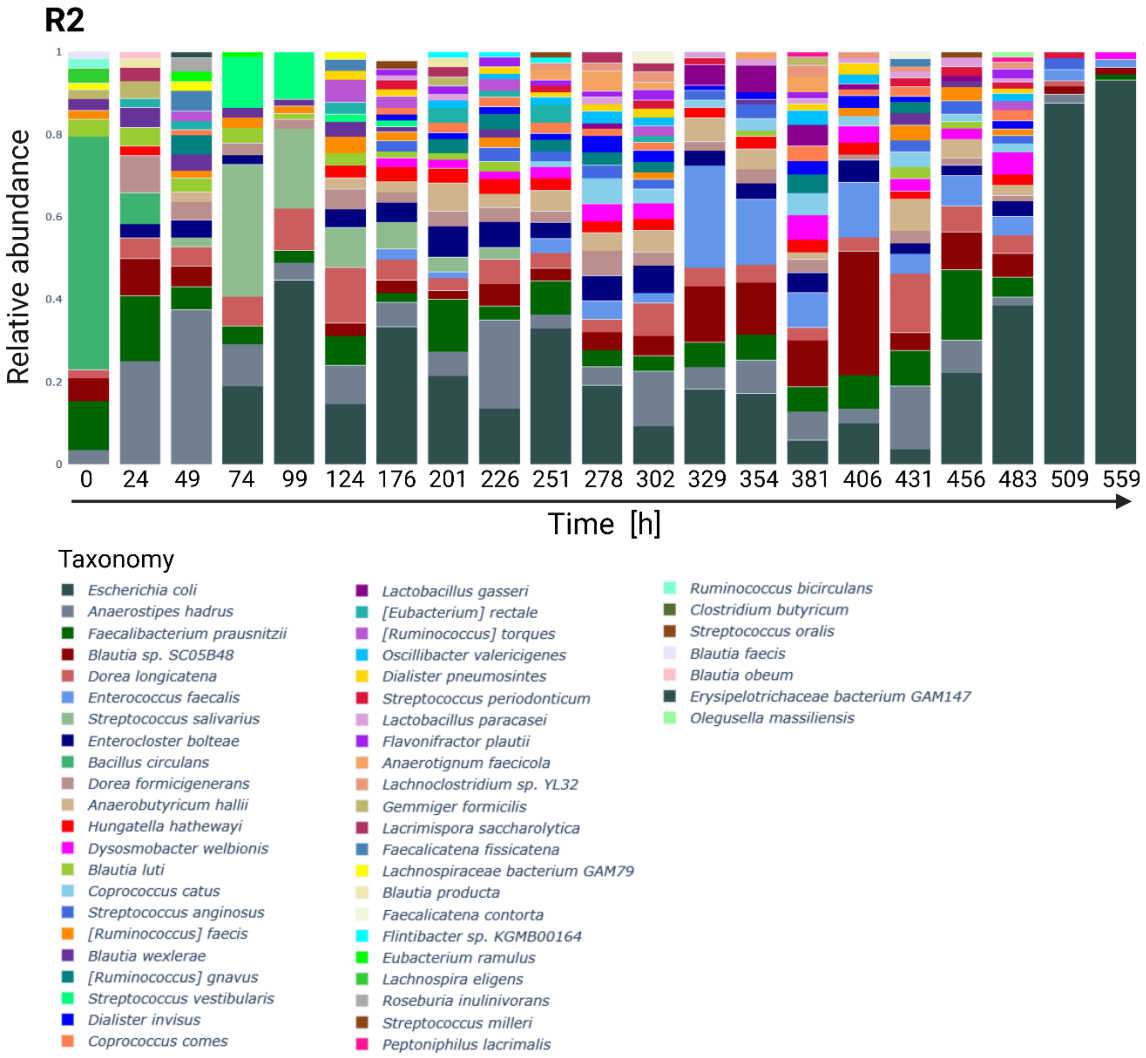

Figure 36: Relative species abundance of the microbiota in R2

Microbial community analysis based on full-length 16S rRNA gene sequencing throughout the operating period of 534 h. The figure was created by MMonitor and BioRender.com.

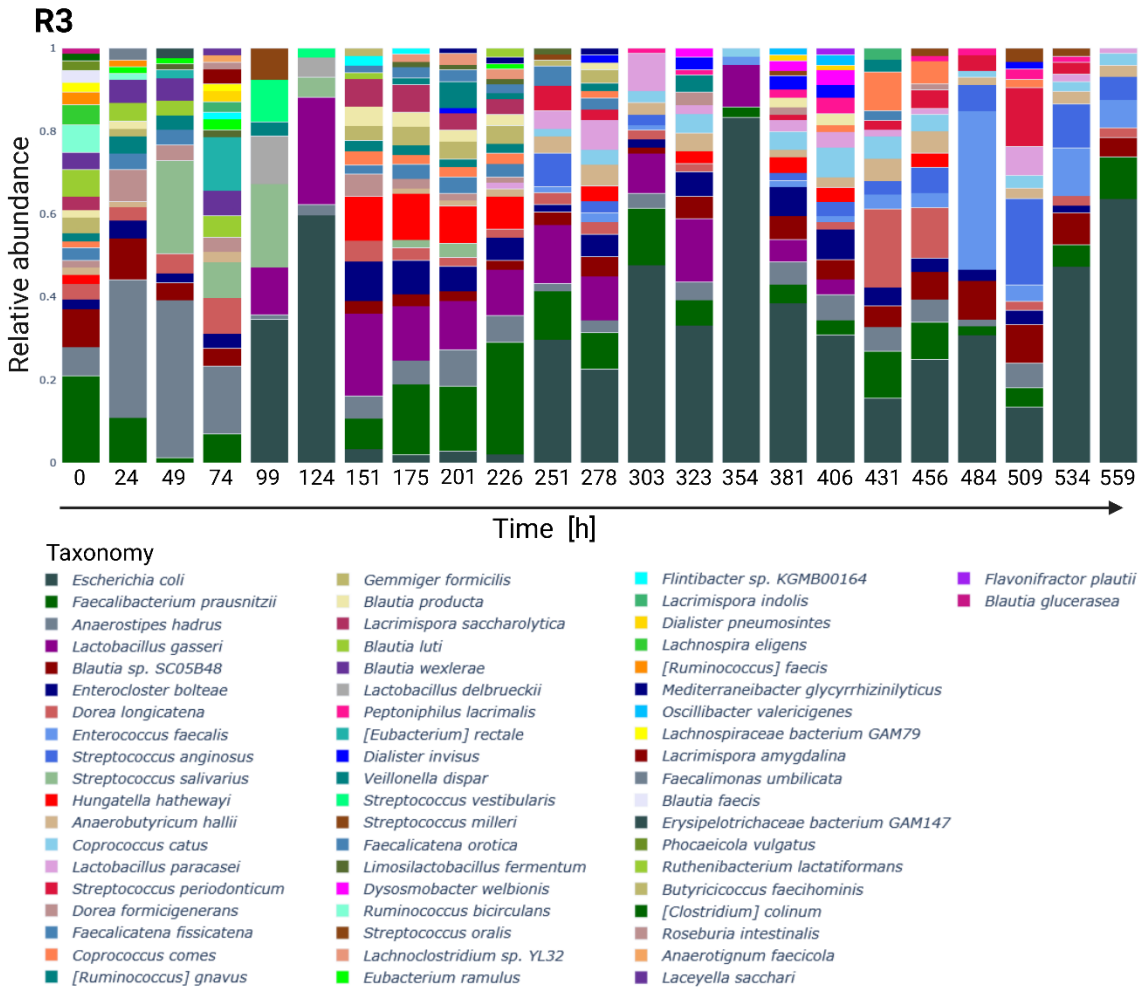

Figure 37: Relative species abundance of the microbiota in R3
Microbial community analysis based on full-length 16S rRNA gene sequencing throughout the operating period of 534 h. The figure was created by MMonitor and BioRender.com.

5.4.3. Alpha Diversity of R1, R2, and R3 throughout the enrichment

We investigated the microbial diversity for each BES with the Simpson and Shannon diversity index. The Shannon diversity index estimates both species richness and evenness, weighting on richness by inflating the number of rare taxa. The idea behind this metric is that the more species were observed, and the more even their abundances are, the higher the entropy or, the higher the uncertainty of predicting which species would be seen next if another read from this sample had been looked at [184]. The Simpson diversity index follows a similar idea but gives more weight to the abundance of common or dominant taxa inversely with species diversity. Therefore, a few rare species with only a few representatives will not affect the diversity of the sample [185].

In all BESs, Shannon diversity ranged from 1 to 4.3, the higher the value, the greater the sample diversity. The Shannon diversity index of the inoculum of R1 and R3 was lower than that of the other samples. In addition, low Shannon diversity indices were detected for R1 at 354 h, for R2 at 483 h, and for R3 at 323 h (**Figure 38A-C**). No outliers were detected for the measured metabolites at these specific time points (**Figure 32-34)**. Therefore, we strongly suggest that the decreases that were detected for R1, R2, and R3 are the result of insufficient sequencing depth, where fewer reads were generated than for the other samples.

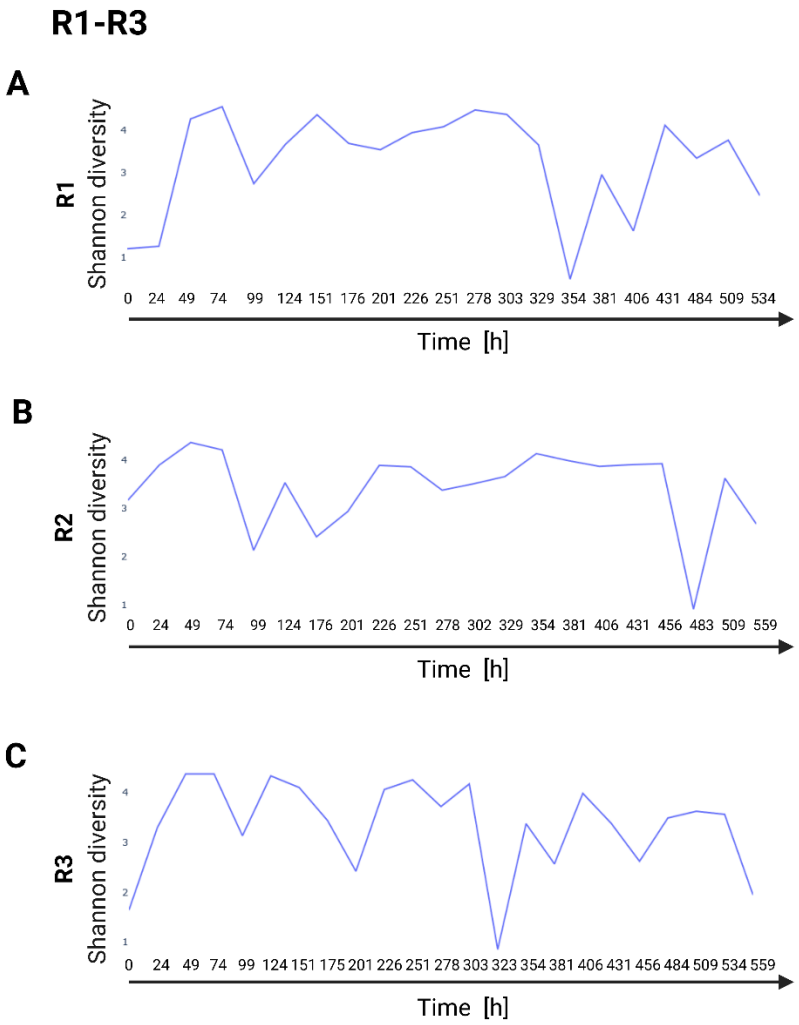

Figure 38: Alpha diversity of the community in R1-R3
The microbial species diversity based on Shannon Index analysis of species-level taxonomy from full-length 16S rRNA gene sequencing. (A) R1, (B) R2, (C) R3. The figure was created by MMonitor and BioRender.com.

The Shannon diversity index is biased toward measuring species richness. In all BESs, high species richness based on the Shannon diversity index was detected (**Figure 38** and **Figure 39B**).The Simpson diversity index is less sensitive to rare species than the Shannon diversity index and ranges between 0 and 1 – the greater the value, the greater the sample diversity and the less dominant are specific taxa. In our investigation the Simpson diversity index showed high species diversity and less dominating species but also some fluctuation of the index in all three BESs throughout the enrichment (**Figure 39A**).

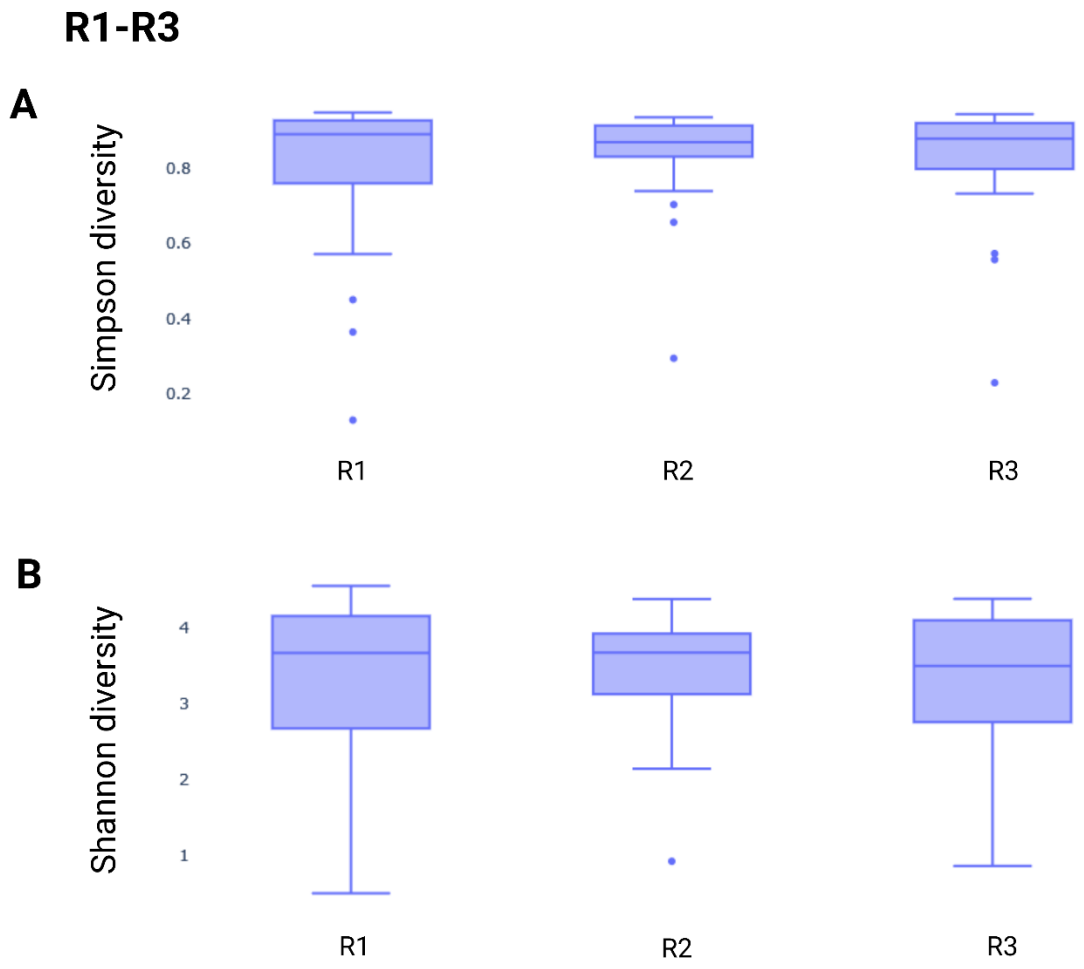

Figure 39: Microbial diversity analysis of R1-R3
The microbial diversity was analyzed based on (A) Simpson and (B) Shannon diversity index. Each box plot includes all 16S rRNA gene analyses from each BES. The figure was created by MMonitor and BioRender.com.

5.4.4. Microbial Community Analysis of R1-R3 on Phylum, Family and Species Level at 0 h, 201 h, 354 h, and 509 h

We found that the 10 most abundant species were the same in all three BESs. However, their individual relative abundances were different. Therefore, we examined the community at specific time points at 0 h, 201 h, 354 h, and 509 h where we found fluctuations in the profile of specific metabolites, such as acetate, propionate, and *n*-butyrate. It should be noted that MMonitor still uses the old International Code of Nomenclature of Prokaryotes (ICNP) from the time before the ICNP updated the nomenclature in 2022. For this reason, we adhered to the old nomenclature that was used by MMonitor.

An important result of this experiment was that we can use MMonitor to track the enrichment of microbes in a BES at different taxonomic levels. Here, the taxonomic profile found at the phylum, family and species levels are discussed. We found that Firmicutes (now Baccilota) dominated the community of the inoculum in all three BESs (time = 0 h). For R1, Firmicutes remain the dominant community, but Proteobacteria (now Pseudomonadota) were also found in small abundances (< 19.14%) throughout the entire operating period (**Figure 40**). For R2, only Firmicutes were detected in the inoculum, but also Proteobacteria got enriched at 201 h (21.39%) and 354 h (17.17%) and dominated the community at 509 h (87.54%) (**Figure 40**). In the inoculum for R3 (0 h), we found that the community was dominated by Firmicutes and less by Proteobacteria or Bacteriodetes (now Bacteroidota) at 0 h, 201 h, and 509 h (**Figure 40**). In between, at 354 h, it was reversed and Proteobacteria were the most abundant phyla over Firmicutes (**Figure 40**).

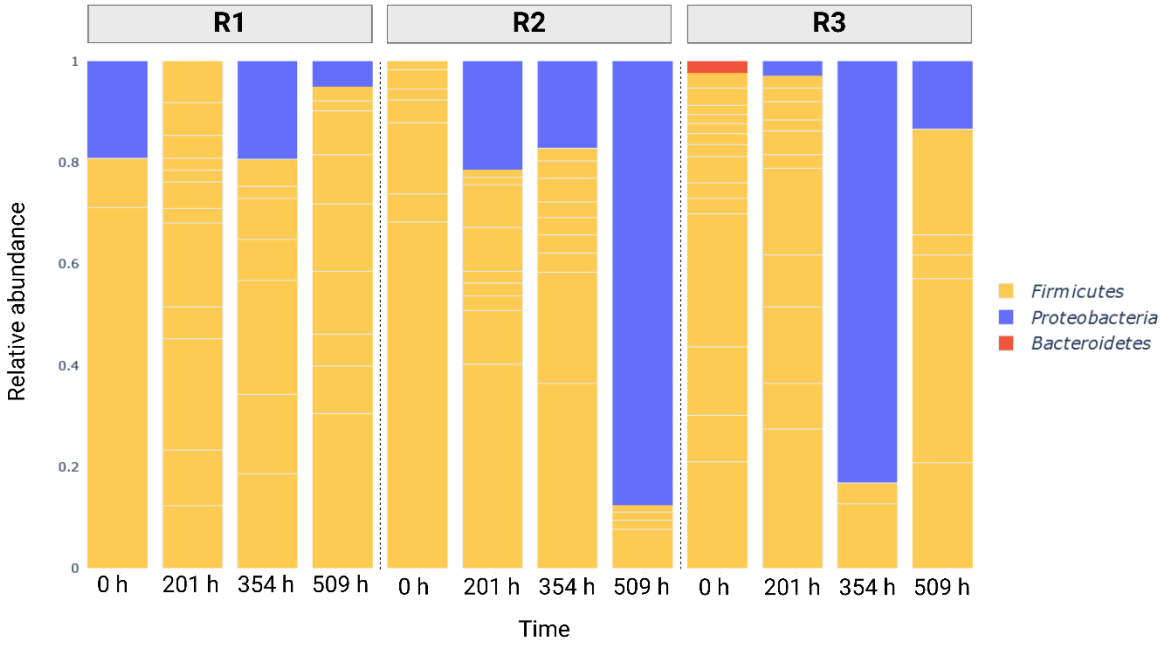

Figure 40: Phylum analysis of R1-R3
Th We analyzed the abundance of families in all the BESs for the time points: 0h (inoculum), 201 h, 354 h, and 509 h. The figure was created by MMonitor and BioRender.com.

On the family level, we found that the inoculum community is different for R1, R2, and R3, where *Lactobacillacea* and *Enterobacteriaceae* were only detected in R1 but not in R2 and R3 (**Figure 41**). Later in the operating period, both families were detected in R2 at 201 h and 354 h, and in R3 at 201 h, 354 h, and 509 h (**Figure 41**). This again indicates that the sequencing depth was insufficient to detect all families in the inocula of all BESs. At 201 h, the community was dominated by *Lachnospiraceae*, *Ruminococcaceae*, *Streptococcaceae*, *Veillonellaceae,* and *Clostridiaceae*, which were detected in R1, R2, and R3 (**Figure 41**). However, we also detected certain families that were not present in any of the other reactors. At 201 h, *Oscillospiraceae* were detected only in R1 and R2, but not in R3 (**Figure** 41).

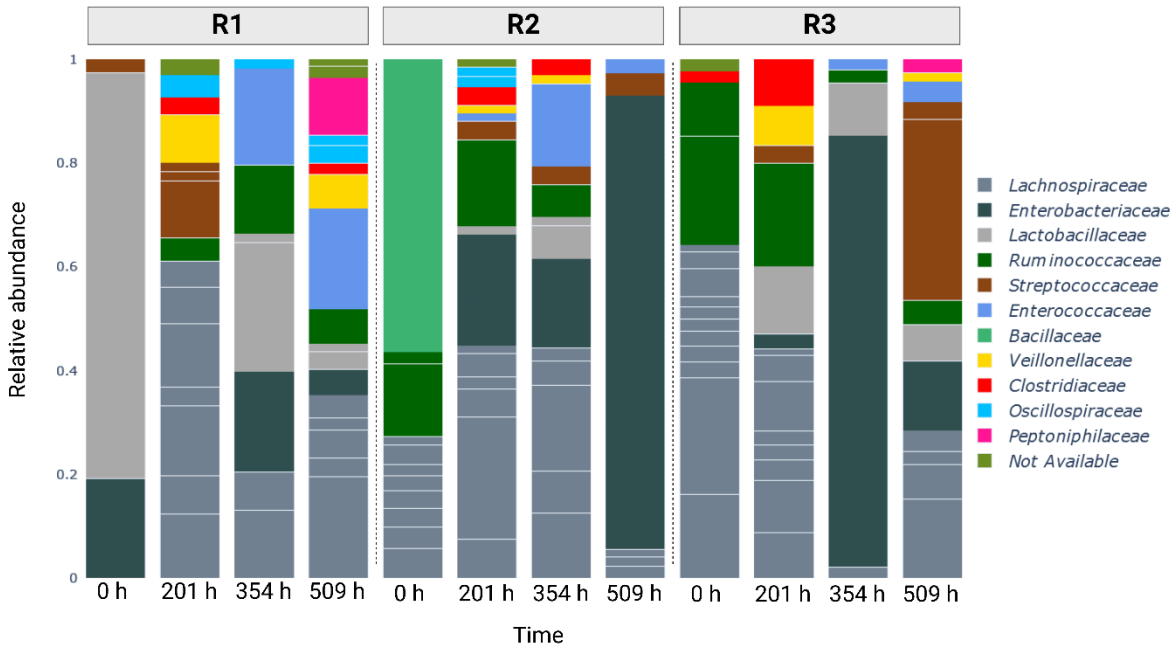

Figure 41: Family analysis of R1-R3
We analyzed the abundance of families in all the BESs for the time points: 0h (inoculum), 201 h, 354 h, and 509 h. The figure was created by MMonitor and BioRender.com.

We detected a common community of *Lachnospiraceae*, *Enterobacteriaceae*, *Lactobacillaceae*, *Ruminococcaceae* and *Enterococcaceae* in all three BESs in a later period at 354 h (**Figure** 41). While *Oscillospiraceae* was below detection in R2 and R3 and *Clostridiaceae* was not detected in R1 at 354 h (**Figure** 41). At 354 h, the community profile changed and was dominated only by *Lachnospiraceae*, *Enterobacteriaceae*, *Enterococcaceae* in R1, R2 and R3, while some families were not detected in all three BESs, such as *Lactobacillaceae*, *Ruminococcaceae* and *Peptoniphilaceae* (**Figure** 41).

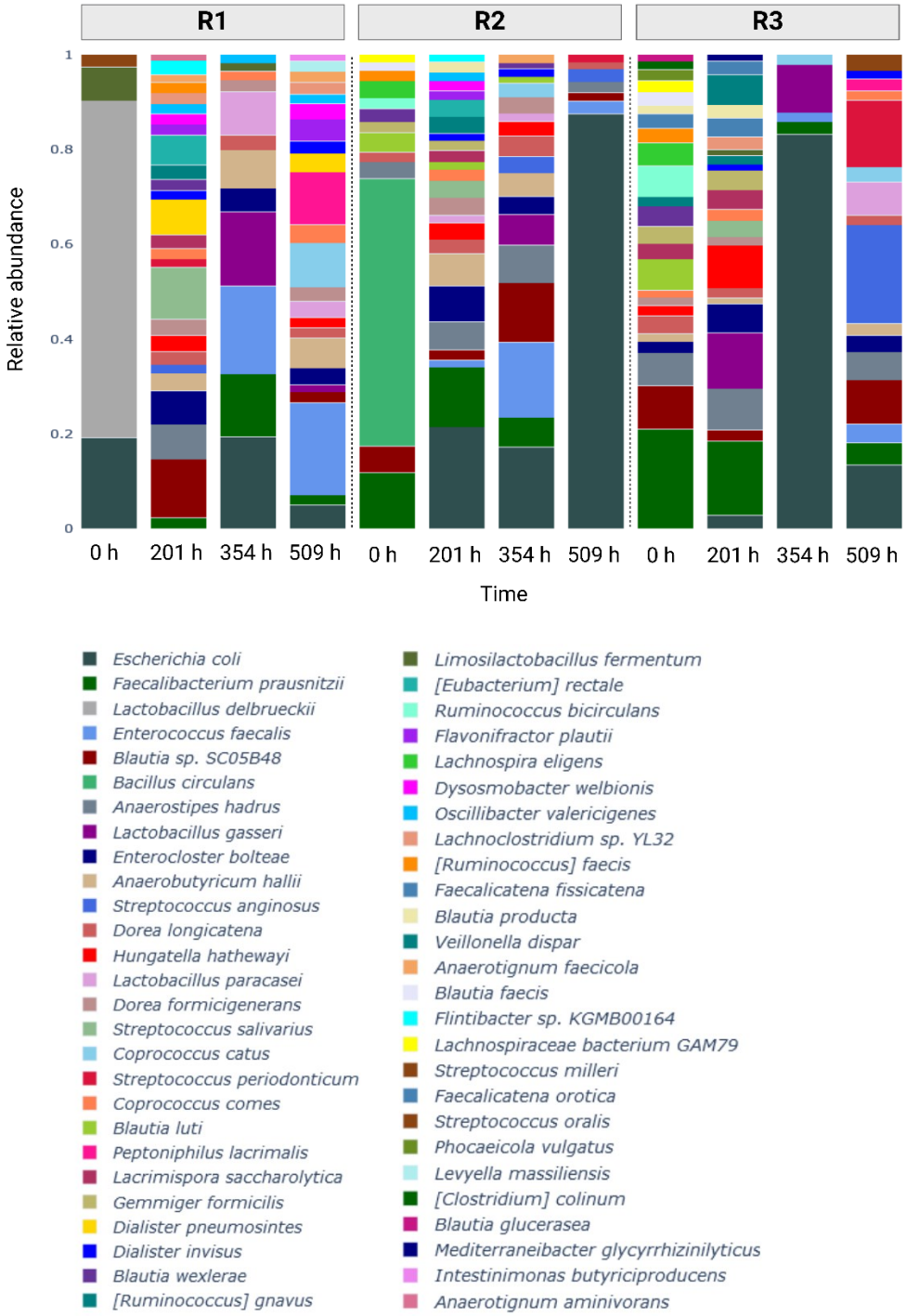

Figure 42: Microbial species composition of R1, R2, and R3
We analyzed the relative species abundance of the BESs for the time points: 0h (inoculum), 201 h, 354 h, and 509 h. The figure was created by MMonitor and BioRender.com.

On the species level, we detected high variations in the relative abundances of different species in the inoculum (0 h) of R1, R2, and R3 (**Figure 42**). Without going into detail, these variations were throughout all investgated time points of 201 h, 354 h and 509 h.

Besides the metabolic dynamics at 201 h, 354 h, and 509 h of BES cultivation, which were observed for acetate, propionate, *n*-valerate, and succinate, we also observed changes in the microbial composition (**Figure 42**). Besides the fluctuation of some metabolites, we also found a continuous production of *n*-butyrate and *n*-caproate starting from 201 h of BES operation.

At 201 h of BES operation, we detected higher concentrations of H_2, acetate, propionate, *n*-valerate and succinate, whereas the production of *n*-butyrate and *n*-caproate started to increase at this time point (**Figure 32-33**). The microbial community varied between the BESs at 210 h (**Figure 42**). In general, only a few different species with higher relative abundances were detected in the different reactors, whereas most species were found in all three BES reactors. At 354 h of BES cultivation, we detected a drop in the production of, *e.g.*, H_2, acetate, propionate, and *n*-valerate (**Figure 32-33**). No changes were found for the production of *n*-butyrate and *n*-caproate at 354 h (**Figure 32-33**). The detectable species count dropped at 354 h of BES cultivation compared to 201 h in R1 and R2. Therefore, it can be assumed that the major bacterial producers of acetate, propionate, and *n*-valerate were less abundant at 354 h than at 201 h (**Figure 42**). The differences in the microbial species community are assumed to be the driving factor for a changing fermentation profile of SCCs and MCCs rather than the abundance of the species present at both time points.

5.4.5. Biofilm Formation at the working electrode of R1-R3

We harvested a sample of the working electrode from R1, R2, and R3 at the end of the cultivation and investigated the surface by SEM regarding the attachment of microbes and biofilm formation at the Pt/C-doped electrode surface. An enormous biofilm formation was detected in the early stage of the enrichment (**Figure 43**). In all three of the BESs, the biofilm at the working electrode was composed of a highly diverse community of microbes embedded in the Pt/C coating of the working electrode (**Figure 44-46**). Furthermore, cellular structures (white arrows) such as extracellular polymeric substances (EPS) that support the adhesion of the microbes at working electrode and between the microbes were observed for R1, R2, and R3 (white arrows, **Figure 44-46)**

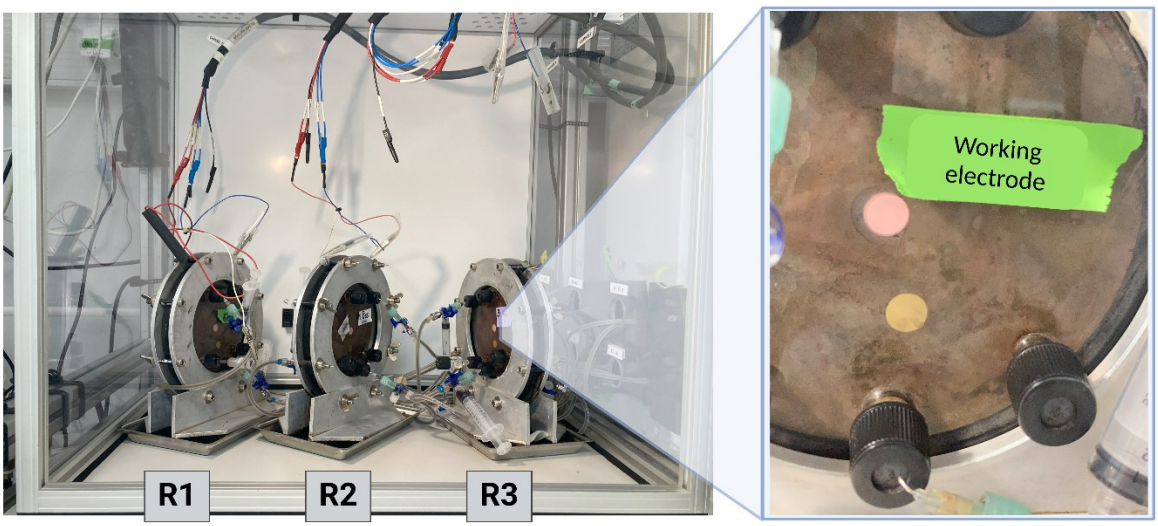

Figure 43: Biofilm at the working electrode in R1, R2, and R3
The growing biofilm was detected for all three BESs.

A

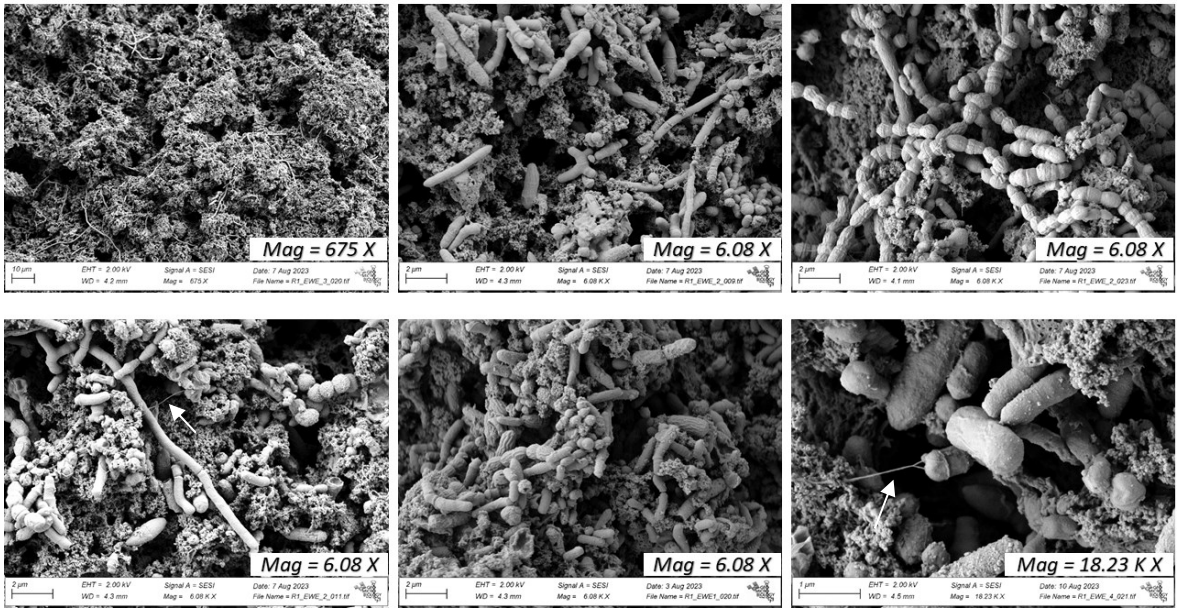

Figure 44: Biofilm formation at the working electrode of R1 at the end of the operating period
SEM micrographs show the biofilm formation of R1 at the magnifications 675 X, 6.08 X, and 18.23 X.

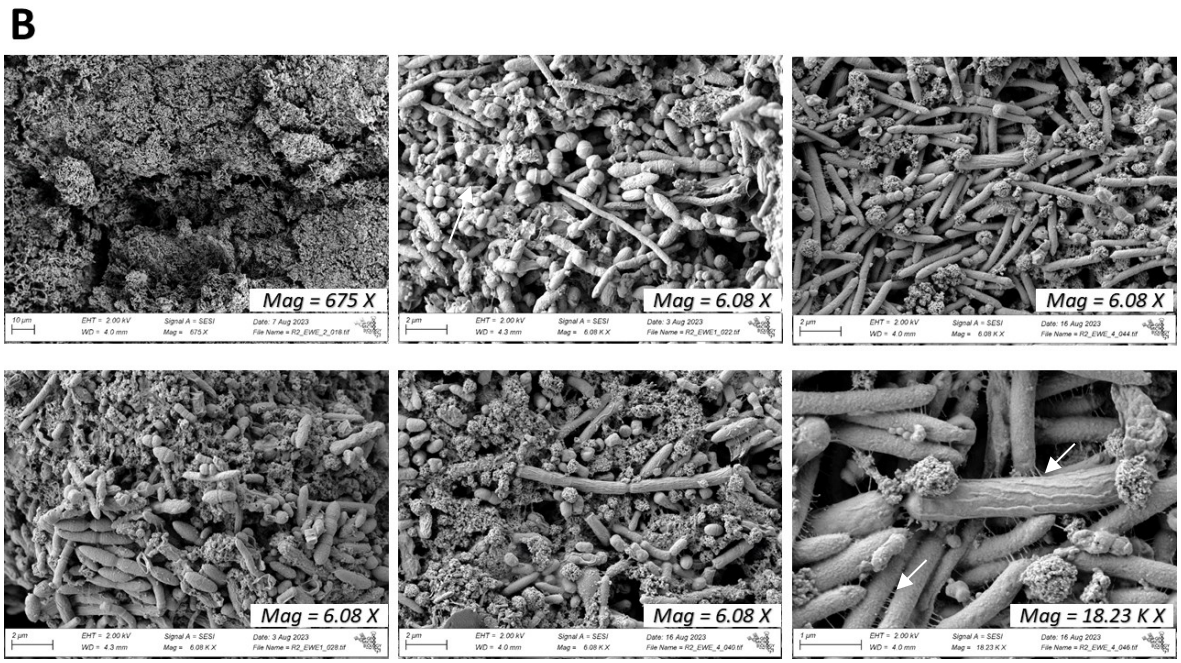

Figure 45: Biofilm formation at the working electrode of R2 at the end of the operating period

SEM micrographs show the biofilm formation of R2 the magnifications 675 X, 6.08 X, and 18.23 X.

Figure 46: Biofilm formation at the working electrode of R3 at the end of the operating period

SEM micrographs show the biofilm formation of R3 at the magnifications 675 X, 6.08 X, and 18.23 X.

5.5. Discussion

This experiment aimed to study microbial community dynamics from human feces under H_2 removal by oxidation at the working electrode. The results showed fluctuations in the concentration for some but not for all of the investigated metabolites but also in species relative abundances. Fluctuations in the metabolic profile along the BES cultivation were detected for acetate, propionate, *n*-valerate, and succinate, especially at 201 h and 354 of BES cultivation. The production of *n*-butyrate and *n*-caproate was unaffected at these two time points. Furthermore, we also detected fluctuations in the H_2 concentration. The performance of the BES, the biofilm formation at the working electrode, and further the microbial community composition influence the H_2 production and its removal by the working electrode. Due to the enormous growth of the biofilm at the working electrode, less H_2 was removed electrochemically, and thus the availability of H_2 in the system was increased. In BESs, the biofilm formation can have positive and negative effects on the system performance. Enhanced electron transfer and increased reactor stability are the positive effects [186-188]. Whereas biofoulding, competitive interactions and mass transfer limitations are the drawbacks of a biofilm [189-191].

Only for R1 and R3, the H_2 concentration was slightly higher at 354 h than at 201 h. In the case of R2, a lower H_2 concentration was found at 354 h, indicating that the species composition did not affect the H_2 availability in the BES reactors. Therefore, it becomes more apparent that the vast biofilm formation itself influenced the performance of the BES and can limit the H_2 transfer to the electrode. The biofilm formation is influenced by two physical factors: (1) the size of the electrode; and (2) the presence of shear forces by the medium flow across the electrode [192]. Higher shear forces can prevent biofilm formation but can also induce the production of EPSs, leading to more compact biofilms [193]. In the future, the biofilm formation must be balanced with the electrode performance to avoid microbial overgrowth, which might outcompete low-abundant species. In the field of microbial fuel cells, anode biofilm development is one of the most considerable constraints [194]. In the gut, the community of viruses, bacteria, fungi, and archaea live together as biofilms and adhere to the intestinal mucus surface. The biofilm is encased in their EPSs, extracellular DNA, proteins, and host and environmental factors and is highly resilient and shielded from variations in temperature and pH variations, and factors such as

antimicrobial substances, high pressure, high salinity, poor nutrient accessibility [195]. Furthermore, biofilms are protective and nutrient-rich environments that facilitate the survival of microbes [196]. In the human gut, biofilm promote homeostasis at various mucosal surfaces where its disruption is detrimental to health, and can cause pathophysiology. Dense microbial biofilms colonize the large intestinal mucosa, where the microbial colonization, density, and diversity vary along the length of the GI tract. As elsewhere in nature and in the gut, the biofilm mode of growth dominates over planktonic cells [197, 198]. The biofilm formation in the BES resulted in some H_2-producing microbes being closer to the electrode and others less. Therefore, it can take longer until the BES removed the produced H_2. The depth of the inner BES chamber is ~1 mm, whereas the microbes interact on µm-scale or even closer with the electrode. This architectural limitation and the BES electrode setup allowed the biofilm to grow thicker than we expected. The positive potential for H_2 removal at the working electrode caused a positive polarization of the electrode and attracted microbes that have a net negative surface charge. Thus, a non-chemical approach to reducing biofilm formation would be to apply negative polarization [199]. The biofilm formation at an electrode in BESs can take up to 9 weeks to establish stable cell performance and more than 17 weeks to obtain a mature electrode biofilm. However, even in identical systems, biofilm formation can vary in biofilm thickness, porosity, microbial composition, and viability, affecting the performance of the BES. [194, 200] These variations support what we found regarding the microbial composition, which was highly dynamic throughout the operating period.

Another important result of this experiment was that we were able to enrich for a very diverse and rich microbial community in the BES. However, we also detected time points that were less rich and diverse. We need to reconsider the composition of the rich media used for enrichment in the BES so that only those microbes that benefit from the H_2 removed by the electrode are able to grow. We suspect that the composition of the medium was too rich and therefore the microbes grew independently of the reactions occurring at the electrode. For this reason, the use of a minimal medium could be a different approach. Fluctuations in community composition may also be due to competition for nutrients and their conversion into microbial fermentation products, which may also be used as substrates by other microbes. In the example of acetate, which is the

most abundant SCC and is mostly a metabolic endproduct in bacteria, but can also be assimilated into biomass by *Enterobacteria*, *Pseudomonas*, *Neisseria* spp., and *Mycobacterium* spp., *via* the glyoxylate cycle and the TCA cycle. Nogal *et al.* (2021) showed that the gut microbiota composition and diversity might influence circulating acetate levels. The genera *Coprococcus*, *Barnesiella*, and *Ruminococcus*, were positively associated with acetate, whereas *Lachnoclostridium* and *Bacteroides* were negatively associated in the human gut of 948 female twins enrolled in the TwinsUK registry [201]. Theses genera, excluding of *Bacteroides* and *Barnesiella*, were also detected in our enrichment. Investigations on the GI tract of termites showed that acetogenesis constitutes a major H_2 sink and acetogens, methanogen, and sulfate reducers compete with one another for H_2 in the gut but can also co-exist at high abundances [202-208]. Furthermore, other main acetate-producing bacteria are *Provotella* spp. *Bifidobacterium* spp., *Streptococcus* spp., *Clostridium* spp., and *Akkermansia* [201, 209].

Apart from the primary fermentation products, we also detected lower amounts of SCCs and MCCs such as iso-butyrate, iso-valerate, and iso-caproate. The production of MCCs fluctuated wildly along the cultivation, which fits the fluctuations detected in the SCCs profile. MCCs are mainly produced by the genera *Bacteroides* and *Clostridium* during the fermentation of branched-chain amino acids (isoleucine, valine, and leucine) [210-212]. *In-vitro* studies showed that the pH and the carbon source influence the MCC production of protein-fermenting bacteria. There are only a few studies about the influence of MCCs on host health compared to SCCs. We speculated that the reduced availability of fermentable carbohydrates promotes a shift to more protein fermentation by the intestinal microbiota and consequently enhances MCC production. Furthermore, it was reported that host aging and an increased rate of apoptotic cells in the gut could lead to higher availability of fermentable amino acids, resulting in higher MCC production rates [212].

In our study, Firmicutes were the dominating phyla in R1, R2, and R3 throughout the operating period. Firmicutes (51%) and Bacteroides (41%) are the most prevalent H_2-producing bacterial species in the large intestine [213]. Both phyla have beneficial effects on human health. Bacteroides constantly produce H_2 when they bind to dimeric IgA antibodies to form colonies that anchor in the mucus layer near the epithelial cells [214]. In intestinal epithelial cells, H_2 eliminates hydroxyl radicals and protects the intestinal wall

from oxidative stress. H_2 can also penetrate the cell membrane by diffusion, enter the bloodstream, and circulate to the head, where it penetrates the blood-brain barrier and protects the brain cells from oxidative stress [213, 215, 216]. Firmicutes are the second phyla of H_2-producing bacteria, also known as *n*-butyrate-producing bacteria. High levels of Firmicutes were found in older people with long, healthy lives and suppressed colorectal cancer *via* the p21 gene. Furthermore, *n*-butyrate-producing bacteria are found in lower abundance in patients with ulcerative colitis and Crohn´s disease [217, 218]. It is speculated that the positive effects of *n*-butyrate production come along with H_2 production and the interactions between H_2-producing bacteria such as Firmicutes and Bacteroides contribute to the maintenance of human health [219, 220].

Besides the H_2 that is the end product of microbial carbohydrate fermentation, H_2 is also the result of the oxidation of reduced ferredoxin (Fd) and pyridine nucleotides by microbial hydrogenases. In this process, microbes can get rid of reducing equivalents and maintain their intracellular redox balance [24, 221]. Two-thirds of the sequences of human gut microbes listed in the Human Microbiome Project Gastrointestinal Tract reference genome database can metabolize H_2. 60% of them encoded [FeFe]-hydrogenases, 21% for [NiFe]-hydrogenases, and one organism (*M smithii*) encoded an [Fe]-hydrogenase. Hydrogenases are metalloenzymes that catalyze the redox reaction of H_2 ($H_2 \leftrightarrow 2H^+ + 2e^-$) and are found in anaerobic and aerobically-adapted microbes such as bacteria, archaea, and some Eukarya [24]. Since we mainly detected Firmicutes in the BESs, we had a closer look at whether those species play a role in the H_2 economy in the human gut. At 201 h, we found *E. rectale*, which is the most abundant bacterial species in human feces, and encodes [FeFe]-hydrogenases, and was found in two of three BES from this experiment. Different types of stains of *E. rectale* utilize acetate and produce H_2, *n*-butyrate, formate, and lactate when cultured in a YCFA medium [222]. Furthermore, *Ruminococcus* spp., *A. hadrus*, *Blautia spp.*, *C. comes*, *D. formicigenerans, D. longicatena, F. plautii* (not in R3), *Oscillibacter spp.* (not in R3)*, Veillonella* spp*.* (only in R3), *F. pausnitzii* also encodes for [FeFe]-hydrogenases and was detected at 201 . Microbes that encode for [NiFe]-hydrogenases and were observed at 201 h were *Dialister* spp., *E. coli*, and *Veillonella spp.* (encode also for [FeFe]-hydrogenase). Furthermore, mechanisms for H_2 sensing in anaerobic microorganisms are becoming more critical [91, 223].

Our study used the 16S Barcoding Kit of ONT, which is preferred compared to Illumina because the reads are less noisy and of higher accuracy, and a higher proportion of reads can be classified on the species level. Furthermore, the ONT sequencing platform is time- and cost-efficient, and the method of choice is when the focus is on species-level resolution, investigation of rare taxa, and accurate estimation of microbial richness [179]. The 16S Barcoding Kit comes with a conventional 27F primer, which reveals a significantly lower biodiversity of fecal microbiomes in comparison to the usage of a more degenerate primer set. This primer-associated sequencing bias led to errors in the taxonomic assignment of *Bifidobacterium*, which is one of the dominant genera in the human gut, due to mismatches with the 27F forward primer. Furthermore, by using the 16S Barcoding Kit, *Bacteroides* and *Phocaeicola* were detected in lower abundances on the genus level, whereas *Faecalibacterium* was detected in higher abundances [224, 225]. In our study, no *Bifidobacteria* species were detected in R1, R2, and R3 throughout the entire operating period. Therefore, using appropriate primer sets for 16S RNA gene amplification is crucial to avoid the risk of biasing microbial signature detection. The detected taxonomic diversity can be influenced substantially by the selection of the 16S region. n the field of human microbiome research, clinical applications or microbiome research from other environmental areas, the Nanopore sequencing platform is likely to play an essential role in the detection of microbiome signatures. The fast-developing kit chemistry and base-calling algorithms provide a higher taxonomic resolution from full-length 16S rRNA gene sequencing than short-read sequencing such as Illumina Miseq [225].

In the very end, we wanted to answer the question of whether we were able to enrich uncultured microbial species from human feces. We have explicitly investigated the microbial community at 201 h and 354 h because we detected changes in the metabolite profile and the microbial community. Unfortunately, all detected microbes whose relative abundance was more higher than 0.1% were already isolated from different sources, but most were from human feces. Therefore, lowering the relative abundance threshold may detect more species, some of which are uncultivated, but it may also lead to the detection of false positive species. In addition, the use of this BES must be viewed critically because the large biofilm formation and rapid growth minimize the chance of further enrichment of uncultured microbes.

5.6. Outlook

The main findings of this experiment were that the microbial community was highly diverse and changed throughout the operation period. Furthermore, the rapid growth and extensive biofilm formation did not result in the enrichment of uncultured microbes. Therefore, better control of the biofilm formation and the use of a less rich or even minimal medium would be a better starting point for the enrichment of syntrophic H_2 producers from the human GI tract. Furthermore, with more accurate real-time observation of the microbiota community combined with analysis of metabolic products, enrichment of uncultured H_2-producing microbes is still feasible in future studies. This may lead to enrichment of specific microbes rather than overgrowth of many.

Furthermore, one of the limitations of this study was that all samples were taken from the supernatant of the BESs and not directly from the working electrode surface. The similarity of the microbial compositions sampled from the supernatant to those growing on the working electrode can therefore only be speculated. In future studies, samples should be taken from the working electrode at defined time points and metagenomics should be performed in parallel. Metagenomic analysis represents an alternative approach to targeted amplicon sequencing in studying uncultured microbiomes. This approach can resolve the genetic content of all enriched microbial H_2 producers, represent the entire genetic makeup and offers insights into the presence of novel genes and biocatalysts. Metagenomic analysis link between the community function and the functionality of the BES to enrich certain microbes from their syntrophic partners.

Chapter 6
What is coming up afterward?

The basis for all the experiments was developing a BES to study the H_2 syntrophy of human gut microbes. We were able to design a BES setup that is suitable for long-term anaerobic, continuous cultivations. In the proof of concept experiment with *C. minuta*, we could prove that this BES can mimic microbial H_2 consumption and influence *C. minuta´*s metabolism. Besides removing H_2 at the working electrode, H_2 can also be made available to microbes that metabolise it, such as methanogens, sulphate-reducing bacteria or acetogens, through H_2 evolution by a BES. The findings of the co-cultivation experiment of *C. minuta* and *M. smithii* showed that we are on the right track. There, the H_2 produced by *C. minuta* is coupled to the H_2 consumption by *M. smithii* (to produce CH_4) and affects the metabolic output of *C. minuta*. We obtained these results only in two of three BESs. To thoroughly verify our hypothesis, we need to re-run the co-cultivation of *C. minuta* and *M. smithii* in the BES. To complete the story of unraveling the H_2 syntrophy of human gut microbes, we cultivated a human fecal sample under H_2 removal in the BES. A very dynamic change in the highly diverse microbial composition, along with fluctuations in the microbial metabolic profile and massive biofilm formation at the working electrode, was observed, showing the potential of this BES for the cultivation and investigation of an entire microbial gut community.

What is coming next? The detailed microbial analysis based on 16S rRNA gene sequencing at almost every 24 h showed that the microbial community is highly heterogeneous throughout the operating condition of with H_2 removal at the working electrode. Initially, we wanted to focus on the enrichment of H_2-producing microbes in the BES. We might need to change our goals and focus more on the enrichment of an H_2-producing community rather than on single or multiple species. Because many cell-cell interactions will occur in parallel with cell-electrode interactions driven by H_2 removal at the working electrode. Successful cultivation of the human gut microbiota depends on several factors, such as the optimal culture medium, appropriate environmental condition, biofilm formation, shear stress, cell-cell communication, and features of the cross-talk of microbes with epithelial

cells of the gut mucosa. Bacterial adhesion depends on the physical and mechanical but also on chemical properties of the physical substrate, such as fibronectin and mucins [146]. The primary static fermentation systems for *in-vitro* cultivation of the human gut microbiota are typical batch fermentation models (flask, closed vessel, beaker), which simulate one part of the digestive tract such as the mouth, stomach, colon, or small intestine. The major drawbacks of these cultivation approaches are the lack of absorption processes such as those performed by the intestinal mucosa and the challenge of standardization due to cell activity. Therefore, more dynamic systems should be considered where multiple reactors with individual compartment-specific properties such as pH, temperature, nutrient supply, and redox potential can be interconnected [226, 227]. The PolyFemS system and a cultivation approach by Li *et al.* (2022) maintained a stable microbial community profile and provided growth conditions for biofilm-associated microbes [228, 229].

Deciphering the link between the composition of the human gut microbiota and the eukaryotic cells of the host and consequent changes in the normal physiological state is currently one of the most pertinent research topics. To compare *in-vitro* cultivation with *in-vivo* communities, human gut microbiota cultivation approaches should target a constant community or minimize its fluctuation in future studies. When focussing on isolating uncultured microbes, fluctuation in the microbial composition can also be an advantage when less abundant microbes get enriched during the cultivation. Those microbes must be transferred to the next cultivation batch when they are highly abundant to keep them growing under the current BES operating conditions.

Regarding the isolation of uncultured microbes, metagenomic analysis with MMonitor can reveal the entire genetic makeup and offers insights into the presence of novel genes, biocatalysts, *etc*. The implementation of metagenomic tools can reveal the link between the community function and the functionality of the cultivation approach to enrich certain microbes from their syntrophic partners or microbial community. The term unculturable microbes does not suggest that these microbes can never be cultured in the laboratory. It indicates a gap of missing knowledge about the microbes´ habitat, interaction on the microbe-microbe level and with host cells, abiotic-biotic interactions, and the ecological role in the human gut. The biggest challenge of microbial replication in the laboratory is

maintaining and mimicking the natural growth conditions [230]. Uncultured microbes from the human gut store a hidden potential for new probiotic products and biotherapy.

In our experiments, we targeted the H_2 syntrophy of human gut microbes because H_2 is a common product of microbial fermentation, and its accumulation can modulate fermentation. Since the intestinal H_2 concentration varies between individuals, it indicates the importance of H_2 as an essential factor for shaping the microbial community and their metabolic output. The H_2 production in the human colon is mainly shaped by the diet, in particular by fermentable, microbiota-accessible carbohydrates that drive the colonic H_2 production [231-234]. The debate continues as to how H_2 levels in the colon regulate the fermentation of specific gut microbes and the effect of syntrophic associations. There could be two forms of microbial associations: obligate syntrophy, where H_2 accumulation can shut down fermentation, or facultative syntrophy, where reducing equivalents are not disposed of via, for example, acetate and *n*-butyrate, but via an alternative fermentation strategy to lactate in the human gut [144, 159, 235-238]. In the gut ecosystem's complexity, concrete information are still lacking to understand H_2 as a regulator of metabolic processes. With the BES, we could mimic the H_2 uptake as it is performed by hydrogenotrophs in the gut, which regulated the fermentation output of *C. minuta*. We have completed the engineering part of the BES design and provided a physical interaction site for the microbes at the electrode to dispose efficiently of H_2 to an H_2-removal electrode. Now we need to focus more on the second experiment of co-cultivation of *C. minuta* and *M. smithii*, and further on the enrichment of syntophic H_2 producers from the human gut.

References

1. Oh, Y.-K., M.S. Park, E.-H. Seol, S.-J. Lee, and S. Park, Isolation of hydrogen-producing bacteria from granular sludge of an upflow anaerobic sludge blanket reactor. Biotechnology and Bioprocess Engineering, 2003. **8**(1): p. 54-57 DOI: 10.1007/BF02932899.
2. Waters, J.L. and R.E. Ley, The human gut bacteria *Christensenellaceae* are widespread, heritable, and associated with health. BMC Biol, 2019. **17**(1): p. 83 DOI: 10.1186/s12915-019-0699-4.
3. Carbonero, F., A.C. Benefiel, and H.R. Gaskins, Contributions of the microbial hydrogen economy to colonic homeostasis. Nat Rev Gastroenterol Hepatol, 2012. **9**(9): p. 504-18 DOI: 10.1038/nrgastro.2012.85.
4. Ruaud, A., S. Esquivel-Elizondo, J. de la Cuesta-Zuluaga, J.L. Waters, L.T. Angenent, N.D. Youngblut, and R.E. Ley, Syntrophy via interspecies H_2 transfer between *Christensenella* and *Methanobrevibacter* underlies their global cooccurrence in the human gut. mBio, 2020. **11**(1) DOI: 10.1128/mBio.03235-19.
5. Zha, Y., H. Chong, P. Yang, and K. Ning, Microbial dark matter: from discovery to applications. Genomics, Proteomics & Bioinformatics, 2022. **20**(5): p. 867-881 DOI: https://doi.org/10.1016/j.gpb.2022.02.007.
6. Almeida, A., A.L. Mitchell, M. Boland, S.C. Forster, G.B. Gloor, A. Tarkowska, T.D. Lawley, and R.D. Finn, A new genomic blueprint of the human gut microbiota. Nature, 2019. **568**(7753): p. 499-504 DOI: 10.1038/s41586-019-0965-1.
7. Biagini, F., C. Daddi, M. Calvigioni, C. De Maria, Y.S. Zhang, E. Ghelardi, and G. Vozzi, Designs and methodologies to recreate in vitro human gut microbiota models. Bio-Design and Manufacturing, 2023. **6**(3): p. 298-318 DOI: 10.1007/s42242-022-00210-6.
8. Nakamura, N., H.C. Lin, C.S. McSweeney, R.I. Mackie, and H.R. Gaskins, Mechanisms of microbial hydrogen disposal in the human colon and implications for health and disease. Annu Rev Food Sci Technol, 2010. **1**: p. 363-95 DOI: 10.1146/annurev.food.102308.124101.
9. Feng, R., L. Chen, and K. Chen, Fermentation trip: amazing microbes, amazing metabolisms. Annals of Microbiology, 2018. **68**(11): p. 717-729 DOI: 10.1007/s13213-018-1384-5.
10. Huang, W.-C. and I.C. Tang, *Chapter 8 - Bacterial and yeast cultures – process characteristics, products, and applications*, in *Bioprocessing for Value-Added Products from Renewable Resources*, S.-T. Yang, Editor. 2007, Elsevier: Amsterdam. p. 185-223.
11. Bik, E.M., Composition and function of the human-associated microbiota. Nutr Rev, 2009. **67 Suppl 2**: p. S164-71 DOI: 10.1111/j.1753-4887.2009.00237.x.
12. Xu, J. and J.I. Gordon, Honor thy symbionts. Proc Natl Acad Sci U S A, 2003. **100**(18): p. 10452-9 DOI: 10.1073/pnas.1734063100.

13. Berg, R.D., The indigenous gastrointestinal microflora. Trends in Microbiology, 1996. **4**(11): p. 430-435 DOI: https://doi.org/10.1016/0966-842X(96)10057-3.

14. Luckey, T.D., Introduction to intestinal microecology. Am J Clin Nutr, 1972. **25**(12): p. 1292-4 DOI: 10.1093/ajcn/25.12.1292.

15. Flint, H.J., S.H. Duncan, K.P. Scott, and P. Louis, Interactions and competition within the microbial community of the human colon: links between diet and health. Environ Microbiol, 2007. **9**(5): p. 1101-11 DOI: 10.1111/j.1462-2920.2007.01281.x.

16. Sender, R. and R. Milo, The distribution of cellular turnover in the human body. Nature Medicine, 2021. **27**(1): p. 45-48 DOI: 10.1038/s41591-020-01182-9.

17. Husson, O., Redox potential (Eh) and pH as drivers of soil/plant/microorganism systems: a transdisciplinary overview pointing to integrative opportunities for agronomy. Plant and Soil, 2013. **362**(1): p. 389-417 DOI: 10.1007/s11104-012-1429-7.

18. Hillman, E.T., H. Lu, T. Yao, and C.H. Nakatsu, Microbial ecology along the gastrointestinal tract. Microbes Environ, 2017. **32**(4): p. 300-313 DOI: 10.1264/jsme2.ME17017.

19. Savage, D.C., Microbial ecology of the gastrointestinal tract. Annu Rev Microbiol, 1977. **31**: p. 107-33 DOI: 10.1146/annurev.mi.31.100177.000543.

20. Egert, M., A.A. de Graaf, H. Smidt, W.M. de Vos, and K. Venema, Beyond diversity: functional microbiomics of the human colon. Trends in Microbiology, 2006. **14**(2): p. 86-91 DOI: https://doi.org/10.1016/j.tim.2005.12.007.

21. Cummings, J.H. and H.N. Englyst, Fermentation in the human large intestine and the available substrates. Am J Clin Nutr, 1987. **45**(5 Suppl): p. 1243-55 DOI: 10.1093/ajcn/45.5.1243.

22. Cummings, J.H., E.W. Pomare, W.J. Branch, C.P. Naylor, and G.T. Macfarlane, Short chain fatty acids in human large intestine, portal, hepatic and venous blood. Gut, 1987. **28**(10): p. 1221-7 DOI: 10.1136/gut.28.10.1221.

23. Mortensen, P.B., H. Hove, M.R. Clausen, and K. Holtug, Fermentation to short-chain fatty acids and lactate in human faecal batch cultures intra- and inter-individual variations versus variations caused by changes in fermented saccharides. Scandinavian Journal of Gastroenterology, 1991. **26**(12): p. 1285-1294 DOI: 10.3109/00365529108998626.

24. Wolf, P.G., A. Biswas, S.E. Morales, C. Greening, and H.R. Gaskins, H_2 metabolism is widespread and diverse among human colonic microbes. Gut Microbes, 2016. **7**(3): p. 235-45 DOI: 10.1080/19490976.2016.1182288.

25. Duncan, S.H., P. Louis, J.M. Thomson, and H.J. Flint, The role of pH in determining the species composition of the human colonic microbiota. Environ Microbiol, 2009. **11**(8): p. 2112-22 DOI: 10.1111/j.1462-2920.2009.01931.x.

26. Walker, A.W., S.H. Duncan, E.C. McWilliam Leitch, M.W. Child, and H.J. Flint, pH and peptide supply can radically alter bacterial populations and short-chain fatty acid ratios within microbial communities from the human colon. Appl Environ Microbiol, 2005. **71**(7): p. 3692-700 DOI: 10.1128/AEM.71.7.3692-3700.2005.

27. Gibson, G.R., J.H. Cummings, G.T. Macfarlane, C. Allison, I. Segal, H.H. Vorster, and A.R. Walker, Alternative pathways for hydrogen disposal during fermentation in the human colon. Gut, 1990. **31**(6): p. 679-83 DOI: 10.1136/gut.31.6.679.

28. Macfarlane, G.T., G.R. Gibson, and J.H. Cummings, Comparison of fermentation reactions in different regions of the human colon. J Appl Bacteriol, 1992. **72**(1): p. 57-64 DOI: 10.1111/j.1365-2672.1992.tb04882.x.

29. Gibson, G.R., G.T. Macfarlane, and J.H. Cummings, Sulphate reducing bacteria and hydrogen metabolism in the human large intestine. Gut, 1993. **34**(4): p. 437-9 DOI: 10.1136/gut.34.4.437.

30. Cook, S.I. and J.H. Sellin, Review article: short chain fatty acids in health and disease. Aliment Pharmacol Ther, 1998. **12**(6): p. 499-507 DOI: 10.1046/j.1365-2036.1998.00337.x.

31. Hijova, E. and A. Chmelarova, Short chain fatty acids and colonic health. Bratisl Lek Listy, 2007. **108**(8): p. 354-8.

32. Binder, H.J., Role of colonic short-chain fatty acid transport in diarrhea. Annu Rev Physiol, 2010. **72**: p. 297-313 DOI: 10.1146/annurev-physiol-021909-135817.

33. Vernia, P., M.R. Ricciardi, C. Frandina, T. Bilotta, and G. Frieri, Lactose malabsorption and irritable bowel syndrome. Effect of a long-term lactose-free diet. Ital J Gastroenterol, 1995. **27**(3): p. 117-21.

34. Musso, G., R. Gambino, and M. Cassader, Interactions between gut microbiota and host metabolism predisposing to obesity and diabetes. Annu Rev Med, 2011. **62**: p. 361-80 DOI: 10.1146/annurev-med-012510-175505.

35. Bingham, S.A., N.E. Day, R. Luben, P. Ferrari, N. Slimani, T. Norat, F. Clavel-Chapelon, E. Kesse, A. Nieters, H. Boeing, A. Tjønneland, K. Overvad, C. Martinez, M. Dorronsoro, C.A. Gonzalez, T.J. Key, A. Trichopoulou, A. Naska, P. Vineis, R. Tumino, V. Krogh, H.B. Bueno-de-Mesquita, P.H. Peeters, G. Berglund, G. Hallmans, E. Lund, G. Skeie, R. Kaaks, and E. Riboli, Dietary fibre in food and protection against colorectal cancer in the European Prospective Investigation into Cancer and Nutrition (EPIC): an observational study. Lancet, 2003. **361**(9368): p. 1496-501 DOI: 10.1016/s0140-6736(03)13174-1.

36. Bergman, E.N., Energy contributions of volatile fatty acids from the gastrointestinal tract in various species. Physiol Rev, 1990. **70**(2): p. 567-90 DOI: 10.1152/physrev.1990.70.2.567.

37. Velázquez, M., C. Davies, R. Marett, J.L. Slavin, and J.M. Feirtag, Effect of Oligosaccharides and Fibre Substitutes on Short-chain Fatty Acid Production by Human Faecal Microflora. Anaerobe, 2000. **6**(2): p. 87-92 DOI: https://doi.org/10.1006/anae.1999.0318.

38. Bourquin, L.D., E.C. Titgemeyer, K.A. Garleb, and G.C. Fahey, Jr., Short-chain fatty acid production and fiber degradation by human colonic bacteria: effects of substrate and cell wall fractionation procedures. J Nutr, 1992. **122**(7): p. 1508-20 DOI: 10.1093/jn/122.7.1508.

39. Khan, K.M. and C.A. Edwards, Effect of Substrate Concentration on Short Chain Fatty Acid Production in In vitro Cultures of Human Faeces with Lactulose, a Rapidly

Fermented Carbohydrate. Microbial Ecology in Health and Disease, 2002. **14**(3): p. 160-164 DOI: 10.1080/089106002320644348.

40. Cho, I. and M.J. Blaser, The human microbiome: at the interface of health and disease. Nature Reviews Genetics, 2012. **13**(4): p. 260-270 DOI: 10.1038/nrg3182.

41. Erny, D., A.L. Hrabe de Angelis, D. Jaitin, P. Wieghofer, O. Staszewski, E. David, H. Keren-Shaul, T. Mahlakoiv, K. Jakobshagen, T. Buch, V. Schwierzeck, O. Utermohlen, E. Chun, W.S. Garrett, K.D. McCoy, A. Diefenbach, P. Staeheli, B. Stecher, I. Amit, and M. Prinz, Host microbiota constantly control maturation and function of microglia in the CNS. Nat Neurosci, 2015. **18**(7): p. 965-77 DOI: 10.1038/nn.4030.

42. Cryan, J.F. and T.G. Dinan, Mind-altering microorganisms: the impact of the gut microbiota on brain and behaviour. Nat Rev Neurosci, 2012. **13**(10): p. 701-12 DOI: 10.1038/nrn3346.

43. van de Wouw, M., M. Boehme, J.M. Lyte, N. Wiley, C. Strain, O. O'Sullivan, G. Clarke, C. Stanton, T.G. Dinan, and J.F. Cryan, Short-chain fatty acids: microbial metabolites that alleviate stress-induced brain-gut axis alterations. J Physiol, 2018. **596**(20): p. 4923-4944 DOI: 10.1113/jp276431.

44. Borre, Y.E., G.W. O'Keeffe, G. Clarke, C. Stanton, T.G. Dinan, and J.F. Cryan, Microbiota and neurodevelopmental windows: implications for brain disorders. Trends in Molecular Medicine, 2014. **20**(9): p. 509-518 DOI: https://doi.org/10.1016/j.molmed.2014.05.002.

45. Szentirmai, É., N.S. Millican, A.R. Massie, and L. Kapás, Butyrate, a metabolite of intestinal bacteria, enhances sleep. Scientific Reports, 2019. **9**(1): p. 7035 DOI: 10.1038/s41598-019-43502-1.

46. Wang, X., G. Sun, T. Feng, J. Zhang, X. Huang, T. Wang, Z. Xie, X. Chu, J. Yang, H. Wang, S. Chang, Y. Gong, L. Ruan, G. Zhang, S. Yan, W. Lian, C. Du, D. Yang, Q. Zhang, F. Lin, J. Liu, H. Zhang, C. Ge, S. Xiao, J. Ding, and M. Geng, Sodium oligomannate therapeutically remodels gut microbiota and suppresses gut bacterial amino acids-shaped neuroinflammation to inhibit Alzheimer's disease progression. Cell Research, 2019. **29**(10): p. 787-803 DOI: 10.1038/s41422-019-0216-x.

47. Vijay, N. and M.E. Morris, Role of monocarboxylate transporters in drug delivery to the brain. Curr Pharm Des, 2014. **20**(10): p. 1487-98 DOI: 10.2174/13816128113199990462.

48. Bolognini, D., A.B. Tobin, G. Milligan, and C.E. Moss, The pharmacology and function of receptors for short-chain fatty acids. Mol Pharmacol, 2016. **89**(3): p. 388-98 DOI: 10.1124/mol.115.102301.

49. Mohajeri, M.H., R.J.M. Brummer, R.A. Rastall, R.K. Weersma, H.J.M. Harmsen, M. Faas, and M. Eggersdorfer, The role of the microbiome for human health: from basic science to clinical applications. European Journal of Nutrition, 2018. **57**(1): p. 1-14 DOI: 10.1007/s00394-018-1703-4.

50. Sherwin, E., T.G. Dinan, and J.F. Cryan, Recent developments in understanding the role of the gut microbiota in brain health and disease. Ann N Y Acad Sci, 2018. **1420**(1): p. 5-25 DOI: 10.1111/nyas.13416.

51. Fung, T.C., C.A. Olson, and E.Y. Hsiao, Interactions between the microbiota, immune and nervous systems in health and disease. Nature Neuroscience, 2017. **20**(2): p. 145-155 DOI: 10.1038/nn.4476.

52. Calvani, R., A. Picca, M.R. Lo Monaco, F. Landi, R. Bernabei, and E. Marzetti, Of microbes and minds: a narrative review on the second brain aging. Front Med (Lausanne), 2018. **5**: p. 53 DOI: 10.3389/fmed.2018.00053.

53. Reigstad, C.S., C.E. Salmonson, J.F. Rainey, 3rd, J.H. Szurszewski, D.R. Linden, J.L. Sonnenburg, G. Farrugia, and P.C. Kashyap, Gut microbes promote colonic serotonin production through an effect of short-chain fatty acids on enterochromaffin cells. Faseb j, 2015. **29**(4): p. 1395-403 DOI: 10.1096/fj.14-259598.

54. Yano, Jessica M., K. Yu, Gregory P. Donaldson, Gauri G. Shastri, P. Ann, L. Ma, Cathryn R. Nagler, Rustem F. Ismagilov, Sarkis K. Mazmanian, and Elaine Y. Hsiao, Indigenous Bacteria from the Gut Microbiota Regulate Host Serotonin Biosynthesis. Cell, 2015. **161**(2): p. 264-276 DOI: https://doi.org/10.1016/j.cell.2015.02.047.

55. Puddu, A., R. Sanguineti, F. Montecucco, and G.L. Viviani, Evidence for the gut microbiota short-chain fatty acids as key pathophysiological molecules improving diabetes. Mediators Inflamm, 2014. **2014**: p. 162021 DOI: 10.1155/2014/162021.

56. Silva, Y.P., A. Bernardi, and R.L. Frozza, The role of short-chain fatty acids from gut microbiota in gut-brain communication. Front Endocrinol (Lausanne), 2020. **11**: p. 25 DOI: 10.3389/fendo.2020.00025.

57. Arpaia, N., C. Campbell, X. Fan, S. Dikiy, J. van der Veeken, P. deRoos, H. Liu, J.R. Cross, K. Pfeffer, P.J. Coffer, and A.Y. Rudensky, Metabolites produced by commensal bacteria promote peripheral regulatory T-cell generation. Nature, 2013. **504**(7480): p. 451-455 DOI: 10.1038/nature12726.

58. Smith, P.M., M.R. Howitt, N. Panikov, M. Michaud, C.A. Gallini, M. Bohlooly-Y, J.N. Glickman, and W.S. Garrett, The Microbial Metabolites, Short-Chain Fatty Acids, Regulate Colonic T_{reg} Cell Homeostasis. Science, 2013. **341**(6145): p. 569-573 DOI: doi:10.1126/science.1241165.

59. Haghikia, A., S. Jörg, A. Duscha, J. Berg, A. Manzel, A. Waschbisch, A. Hammer, D.-H. Lee, C. May, N. Wilck, A. Balogh, Annika I. Ostermann, N.H. Schebb, Denis A. Akkad, Diana A. Grohme, M. Kleinewietfeld, S. Kempa, J. Thöne, S. Demir, Dominik N. Müller, R. Gold, and Ralf A. Linker, Dietary fatty acids directly impact central nervous system autoimmunity via the small intestine. Immunity, 2015. **43**(4): p. 817-829 DOI: https://doi.org/10.1016/j.immuni.2015.09.007.

60. Braniste, V., M. Al-Asmakh, C. Kowal, F. Anuar, A. Abbaspour, M. Tóth, A. Korecka, N. Bakocevic, L.G. Ng, P. Kundu, B. Gulyás, C. Halldin, K. Hultenby, H. Nilsson, H. Hebert, B.T. Volpe, B. Diamond, and S. Pettersson, The gut microbiota influences blood-brain barrier permeability in mice. Science Translational Medicine, 2014. **6**(263): p. 263ra158-263ra158 DOI: doi:10.1126/scitranslmed.3009759.

61. Dalile, B., L. Van Oudenhove, B. Vervliet, and K. Verbeke, The role of short-chain fatty acids in microbiota–gut–brain communication. Nature Reviews Gastroenterology & Hepatology, 2019. **16**(8): p. 461-478 DOI: 10.1038/s41575-019-0157-3.

62. Nankova, B.B., R. Agarwal, D.F. MacFabe, and E.F. La Gamma, Enteric bacterial metabolites propionic and butyric acid modulate gene expression, including CREB-dependent catecholaminergic neurotransmission, in PC12 cells--possible relevance to autism spectrum disorders. PLoS One, 2014. **9**(8): p. e103740 DOI: 10.1371/journal.pone.0103740.

63. Clarke, G., R.M. Stilling, P.J. Kennedy, C. Stanton, J.F. Cryan, and T.G. Dinan, Minireview: gut microbiota: the neglected endocrine organ. Molecular Endocrinology, 2014. **28**(8): p. 1221-1238 DOI: 10.1210/me.2014-1108.

64. Cherrington, C.A., M. Hinton, G.R. Pearson, and I. Chopra, Short-chain organic acids at ph 5.0 kill Escherichia coli and Salmonella spp. without causing membrane perturbation. J Appl Bacteriol, 1991. **70**(2): p. 161-5 DOI: 10.1111/j.1365-2672.1991.tb04442.x.

65. Prohászka, L., B.M. Jayarao, A. Fábián, and S. Kovács, The role of intestinal volatile fatty acids in the Salmonella shedding of pigs. Zentralbl Veterinarmed B, 1990. **37**(8): p. 570-4 DOI: 10.1111/j.1439-0450.1990.tb01098.x.

66. Macfarlane, S. and G.T. Macfarlane, Regulation of short-chain fatty acid production. Proceedings of the Nutrition Society, 2003. **62**(1): p. 67-72 DOI: 10.1079/PNS2002207.

67. Topping, D.L. and P.M. Clifton, Short-chain fatty acids and human colonic function: roles of resistant starch and nonstarch polysaccharides. Physiol Rev, 2001. **81**(3): p. 1031-64 DOI: 10.1152/physrev.2001.81.3.1031.

68. Millet, S., M.J. Van Oeckel, M. Aluwé, E. Delezie, and D.L. De Brabander, Prediction of in vivo short-chain fatty acid production in hindgut fermenting mammals: problems and pitfalls. Crit Rev Food Sci Nutr, 2010. **50**(7): p. 605-19 DOI: 10.1080/10408390802565939.

69. Miller, T.L. and M.J. Wolin, Pathways of acetate, propionate, and butyrate formation by the human fecal microbial flora. Appl Environ Microbiol, 1996. **62**(5): p. 1589-92 DOI: 10.1128/aem.62.5.1589-1592.1996.

70. den Besten, G., K. van Eunen, A.K. Groen, K. Venema, D.-J. Reijngoud, and B.M. Bakker, The role of short-chain fatty acids in the interplay between diet, gut microbiota, and host energy metabolism. Journal of Lipid Research, 2013. **54**(9): p. 2325-2340 DOI: https://doi.org/10.1194/jlr.R036012.

71. Macy, J.M., L.G. Ljungdahl, and G. Gottschalk, Pathway of succinate and propionate formation in Bacteroides fragilis. J Bacteriol, 1978. **134**(1): p. 84-91 DOI: 10.1128/jb.134.1.84-91.1978.

72. Macy, J.M. and I. Probst, The biology of gastrointestinal bacteroides. Annu Rev Microbiol, 1979. **33**: p. 561-94 DOI: 10.1146/annurev.mi.33.100179.003021.

73. Pryde, S.E., S.H. Duncan, G.L. Hold, C.S. Stewart, and H.J. Flint, The microbiology of butyrate formation in the human colon. FEMS Microbiol Lett, 2002. **217**(2): p. 133-9 DOI: 10.1111/j.1574-6968.2002.tb11467.x.

74. Ragsdale, S.W. and E. Pierce, Acetogenesis and the Wood-Ljungdahl pathway of CO(2) fixation. Biochim Biophys Acta, 2008. **1784**(12): p. 1873-98 DOI: 10.1016/j.bbapap.2008.08.012.

75. Duncan, S.H., A. Barcenilla, C.S. Stewart, S.E. Pryde, and H.J. Flint, Acetate utilization and butyryl coenzyme A (CoA):acetate-CoA transferase in butyrate-producing bacteria from the human large intestine. Appl Environ Microbiol, 2002. **68**(10): p. 5186-90 DOI: 10.1128/aem.68.10.5186-5190.2002.

76. Dethlefsen, L. and D.A. Relman, Incomplete recovery and individualized responses of the human distal gut microbiota to repeated antibiotic perturbation. Proceedings of the National Academy of Sciences, 2011. **108**(supplement_1): p. 4554-4561 DOI: doi:10.1073/pnas.1000087107.

77. Culp, E.J. and A.L. Goodman, Cross-feeding in the gut microbiome: Ecology and mechanisms. Cell Host & Microbe, 2023. **31**(4): p. 485-499 DOI: https://doi.org/10.1016/j.chom.2023.03.016.

78. Palestrant, D., Z.E. Holzknecht, B.H. Collins, W. Parker, S.E. Miller, and R.R. Bollinger, Microbial biofilms in the gut: visualization by electron microscopy and by acridine orange staining. Ultrastruct Pathol, 2004. **28**(1): p. 23-7, https://www.ncbi.nlm.nih.gov/pubmed/14967595.

79. Swidsinski, A., J. Weber, V. Loening-Baucke, L.P. Hale, and H. Lochs, Spatial organization and composition of the mucosal flora in patients with inflammatory bowel disease. J Clin Microbiol, 2005. **43**(7): p. 3380-9 DOI: 10.1128/JCM.43.7.3380-3389.2005.

80. Tremaroli, V. and F. Backhed, Functional interactions between the gut microbiota and host metabolism. Nature, 2012. **489**(7415): p. 242-9 DOI: 10.1038/nature11552.

81. Clemente, J.C., L.K. Ursell, L.W. Parfrey, and R. Knight, The impact of the gut microbiota on human health: an integrative view. Cell, 2012. **148**(6): p. 1258-70 DOI: 10.1016/j.cell.2012.01.035.

82. Nozhevnikova, A.N., Y.I. Russkova, Y.V. Litti, S.N. Parshina, E.A. Zhuravleva, and A.A. Nikitina, Syntrophy and interspecies electron transfer in methanogenic microbial communities. Microbiology, 2020. **89**(2): p. 129-147 DOI: 10.1134/S0026261720020101.

83. Morris, B.E., R. Henneberger, H. Huber, and C. Moissl-Eichinger, Microbial syntrophy: interaction for the common good. FEMS Microbiol Rev, 2013. **37**(3): p. 384-406 DOI: 10.1111/1574-6976.12019.

84. Bryant, M.P., E.A. Wolin, M.J. Wolin, and R.S. Wolfe, *Methanobacillus omelianskii*, a symbiotic association of two species of bacteria. Arch Mikrobiol, 1967. **59**(1): p. 20-31 DOI: 10.1007/BF00406313.

85. Drake, H.L., Acetogenesis, acetogenic bacteria, and the acetyl-CoA "Wood/Ljungdahl" pathway: past and current perspectives. In: Drake H.L. (eds) Acetogenesis. Chapman & Hall Microbiology Series (Physiology / Ecology / Molecular Biology / Biotechnology). Springer, Boston, MA. . 1994 DOI: https://doi.org/10.1007/978-1-4615-1777-1_1.

86. Christl, S.U., P.R. Murgatroyd, G.R. Gibson, and J.H. Cummings, Production, metabolism, and excretion of hydrogen in the large intestine. Gastroenterology, 1992. **102**(4 Pt 1): p. 1269-77, https://www.ncbi.nlm.nih.gov/pubmed/1551534.

87. Cord-Ruwisch, R., H.-J. Seitz, and R. Conrad, The capacity of hydrogenotrophic anaerobic bacteria to compete for traces of hydrogen depends on the redox potential of the terminal electron acceptor. Archives of Microbiology, 1988. **149**(4): p. 350-357 DOI: 10.1007/BF00411655.

88. Thauer, R.K., K. Jungermann, and K. Decker, Energy conservation in chemotrophic anaerobic bacteria. Bacteriol Rev, 1977. **41**(1): p. 100-80, https://www.ncbi.nlm.nih.gov/pubmed/860983

89. Cook, G.M., C. Greening, K. Hards, and M. Berney, Energetics of pathogenic bacteria and opportunities for drug development. Adv Microb Physiol, 2014. **65**: p. 1-62 DOI: 10.1016/bs.ampbs.2014.08.001.

90. Schwartz, E., J. Fritsch, and B. Friedrich, *H_2-metabolizing prokaryotes*, in *The Prokaryotes: Prokaryotic Physiology and Biochemistry*, E. Rosenberg, et al., Editors. 2013, Springer Berlin Heidelberg: Berlin, Heidelberg. p. 119-199.

91. Greening, C., A. Biswas, C.R. Carere, C.J. Jackson, M.C. Taylor, M.B. Stott, G.M. Cook, and S.E. Morales, Genomic and metagenomic surveys of hydrogenase distribution indicate H_2 is a widely utilised energy source for microbial growth and survival. ISME J, 2016. **10**(3): p. 761-77 DOI: 10.1038/ismej.2015.153.

92. Choi, S., Microscale microbial fuel cells: advances and challenges. Biosens Bioelectron, 2015. **69**: p. 8-25 DOI: 10.1016/j.bios.2015.02.021.

93. Dutta, K. and P.P. Kundu, *Chapter 1 - Introduction to microbial fuel cells*, in *Progress and Recent Trends in Microbial Fuel Cells*, P.P. Kundu and K. Dutta, Editors. 2018, Elsevier. p. 1-6.

94. Rinaldi, A., B. Mecheri, V. Garavaglia, S. Licoccia, P. Di Nardo, and E. Traversa, Engineering materials and biology to boost performance of microbial fuel cells: a critical review. Energy & Environmental Science, 2008. **1**(4): p. 417-429 DOI: 10.1039/B806498A.

95. Guo, K., A. Prévoteau, S.A. Patil, and K. Rabaey, Engineering electrodes for microbial electrocatalysis. Current Opinion in Biotechnology, 2015. **33**: p. 149-156 DOI: https://doi.org/10.1016/j.copbio.2015.02.014.

96. Baudler, A., I. Schmidt, M. Langner, A. Greiner, and U. Schröder, Does it have to be carbon? Metal anodes in microbial fuel cells and related bioelectrochemical systems. Energy & Environmental Science, 2015. **8**(7): p. 2048-2055 DOI: 10.1039/C5EE00866B.

97. Zhou, X., X. Chen, H. Li, J. Xiong, X. Li, and W. Li, Surface oxygen-rich titanium as anode for high performance microbial fuel cell. Electrochimica Acta, 2016. **209**: p. 582-590 DOI: https://doi.org/10.1016/j.electacta.2016.05.103.

98. Santoro, C., C. Arbizzani, B. Erable, and I. Ieropoulos, Microbial fuel cells: from fundamentals to applications. A review. J Power Sources, 2017. **356**: p. 225-244 DOI: 10.1016/j.jpowsour.2017.03.109.

99. Logan, B.E., Exoelectrogenic bacteria that power microbial fuel cells. Nat Rev Microbiol, 2009. **7**(5): p. 375-81 DOI: 10.1038/nrmicro2113.

100. Borole, A.P., G. Reguera, B. Ringeisen, Z.-W. Wang, Y. Feng, and B.H. Kim, Electroactive biofilms: current status and future research needs. Energy & Environmental Science, 2011. **4**(12): p. 4813-4834 DOI: 10.1039/C1EE02511B.

101. Rosenbaum, M., U. Schröder, and F. Scholz, Investigation of the electrocatalytic oxidation of formate and ethanol at platinum black under microbial fuel cell conditions. Journal of Solid State Electrochemistry, 2006. **10**(10): p. 872-878 DOI: 10.1007/s10008-006-0167-2.

102. Hindatu, Y., M.S.M. Annuar, and A.M. Gumel, Mini-review: anode modification for improved performance of microbial fuel cell. Renewable and Sustainable Energy Reviews, 2017. **73**: p. 236-248 DOI: https://doi.org/10.1016/j.rser.2017.01.138.

103. Noori, M.T., P. Chatterjee, M.M. Ghangrekar, and C.K. Mukherjee, *Chapter 7 - Low-cost solutions for fabrication of microbial fuel cells: ceramic separator and electrode modifications*, in *Progress and Recent Trends in Microbial Fuel Cells*, P.P. Kundu and K. Dutta, Editors. 2018, Elsevier. p. 95-124.

104. Du, Z., H. Li, and T. Gu, A state of the art review on microbial fuel cells: a promising technology for wastewater treatment and bioenergy. Biotechnology Advances, 2007. **25**(5): p. 464-482 DOI: https://doi.org/10.1016/j.biotechadv.2007.05.004.

105. Niessen, J., F. Harnisch, M. Rosenbaum, U. Schröder, and F. Scholz, Heat treated soil as convenient and versatile source of bacterial communities for microbial electricity generation. Electrochemistry Communications, 2006. **8**(5): p. 869-873 DOI: https://doi.org/10.1016/j.elecom.2006.03.025.

106. Lovley, D.R., Bug juice: harvesting electricity with microorganisms. Nat Rev Microbiol, 2006. **4**(7): p. 497-508 DOI: 10.1038/nrmicro1442.

107. Torres, C.I., A.K. Marcus, H.-S. Lee, P. Parameswaran, R. Krajmalnik-Brown, and B.E. Rittmann, A kinetic perspective on extracellular electron transfer by anode-respiring bacteria. FEMS Microbiology Reviews, 2010. **34**(1): p. 3-17 DOI: https://doi.org/10.1111/j.1574-6976.2009.00191.x.

108. Lovley, D.R., Powering microbes with electricity: direct electron transfer from electrodes to microbes. Environ Microbiol Rep, 2011. **3**(1): p. 27-35 DOI: 10.1111/j.1758-2229.2010.00211.x.

109. Methe, B.A., K.E. Nelson, J.A. Eisen, I.T. Paulsen, W. Nelson, J.F. Heidelberg, D. Wu, M. Wu, N. Ward, M.J. Beanan, R.J. Dodson, R. Madupu, L.M. Brinkac, S.C. Daugherty, R.T. DeBoy, A.S. Durkin, M. Gwinn, J.F. Kolonay, S.A. Sullivan, D.H. Haft, J. Selengut, T.M. Davidsen, N. Zafar, O. White, B. Tran, C. Romero, H.A. Forberger, J. Weidman, H. Khouri, T.V. Feldblyum, T.R. Utterback, S.E. Van Aken, D.R. Lovley, and C.M. Fraser, Genome of *Geobacter sulfurreducens*: metal reduction in subsurface environments. Science, 2003. **302**(5652): p. 1967-9 DOI: 10.1126/science.1088727.

110. Reguera, G., K.D. McCarthy, T. Mehta, J.S. Nicoll, M.T. Tuominen, and D.R. Lovley, Extracellular electron transfer via microbial nanowires. Nature, 2005. **435**(7045): p. 1098-101 DOI: 10.1038/nature03661.

111. Ntagia, E., P. Rodenas, A. ter Heijne, C.J.N. Buisman, and T.H.J.A. Sleutels, Hydrogen as electron donor for copper removal in bioelectrochemical systems. International Journal of Hydrogen Energy, 2016. **41**(13): p. 5758-5764 DOI: https://doi.org/10.1016/j.ijhydene.2016.02.058.

112. Guzman, J.J.L., D.Z. Sousa, and L.T. Angenent, Development of a Bioelectrochemical System as a Tool to Enrich H2-Producing Syntrophic Bacteria. Front Microbiol, 2019. **10**: p. 110 DOI: 10.3389/fmicb.2019.00110.

113. Schröder, U., F. Harnisch, and L.T. Angenent, Microbial electrochemistry and technology: terminology and classification. Energy & Environmental Science, 2015. **8**(2): p. 513-519 DOI: 10.1039/C4EE03359K.

114. Lusk, B.G., I. Peraza, G. Albal, A.K. Marcus, S.C. Popat, and C.I. Torres, pH dependency in anode biofilms of *Thermincola ferriacetica* suggests a proton-dependent electrochemical response. Journal of the American Chemical Society, 2018. **140**(16): p. 5527-5534 DOI: 10.1021/jacs.8b01734.

115. Bond, D.R., S.M. Strycharz-Glaven, L.M. Tender, and C.I. Torres, On electron transport through Geobacter biofilms. ChemSusChem, 2012. **5**(6): p. 1099-105 DOI: 10.1002/cssc.201100748.

116. Strycharz-Glaven, S.M., R.M. Snider, A. Guiseppi-Elie, and L.M. Tender, On the electrical conductivity of microbial nanowires and biofilms. Energy & Environmental Science, 2011. **4**(11): p. 4366-4379 DOI: 10.1039/C1EE01753E.

117. Busalmen, J.P., A. Esteve-Nunez, A. Berna, and J.M. Feliu, C-type cytochromes wire electricity-producing bacteria to electrodes. Angew Chem Int Ed Engl, 2008. **47**(26): p. 4874-7 DOI: 10.1002/anie.200801310.

118. Gorby, Y.A., S. Yanina, J.S. McLean, K.M. Rosso, D. Moyles, A. Dohnalkova, T.J. Beveridge, I.S. Chang, B.H. Kim, K.S. Kim, D.E. Culley, S.B. Reed, M.F. Romine, D.A. Saffarini, E.A. Hill, L. Shi, D.A. Elias, D.W. Kennedy, G. Pinchuk, K. Watanabe, S. Ishii, B. Logan, K.H. Nealson, and J.K. Fredrickson, Electrically conductive bacterial nanowires produced by *Shewanella oneidensis* strain MR-1 and other microorganisms. Proc Natl Acad Sci U S A, 2006. **103**(30): p. 11358-63 DOI: 10.1073/pnas.0604517103.

119. Malvankar, N.S., M.T. Tuominen, and D.R. Lovley, Biofilm conductivity is a decisive variable for high-current-density *Geobacter sulfurreducens* microbial fuel cells. Energy & Environmental Science, 2012. **5**(2): p. 5790-5797 DOI: 10.1039/C2EE03388G.

120. Maxam, A.M. and W. Gilbert, A new method for sequencing DNA. Proceedings of the National Academy of Sciences, 1977. **74**(2): p. 560-564 DOI: 10.1073/pnas.74.2.560.

121. Sanger, F., G.G. Brownlee, and B.G. Barrell, A two-dimensional fractionation procedure for radioactive nucleotides. Journal of Molecular Biology, 1965. **13**(2): p. 373-IN4 DOI: https://doi.org/10.1016/S0022-2836(65)80104-8.

122. Nyrén, P. and A. Lundin, Enzymatic method for continuous monitoring of inorganic pyrophosphate synthesis. Analytical Biochemistry, 1985. **151**(2): p. 504-509 DOI: https://doi.org/10.1016/0003-2697(85)90211-8.

123. Heather, J.M. and B. Chain, The sequence of sequencers: The history of sequencing DNA. Genomics, 2016. **107**(1): p. 1-8 DOI: 10.1016/j.ygeno.2015.11.003.

124. Woese, C.R., Bacterial evolution. Microbiol Rev, 1987. **51**(2): p. 221-71, https://www.ncbi.nlm.nih.gov/pubmed/2439888.

125. Olsen, G.J., C.R. Woese, and R. Overbeek, The winds of (evolutionary) change: breathing new life into microbiology. J Bacteriol, 1994. **176**(1): p. 1-6 DOI: 10.1128/jb.176.1.1-6.1994.

126. Haque, F., J. Li, H.C. Wu, X.J. Liang, and P. Guo, Solid-state and biological nanopore for real-time sensing of single chemical and sequencing of DNA. Nano Today, 2013. **8**(1): p. 56-74 DOI: 10.1016/j.nantod.2012.12.008.

127. Kasianowicz, J.J., E. Brandin, D. Branton, and D.W. Deamer, Characterization of individual polynucleotide molecules using a membrane channel. Proc Natl Acad Sci U S A, 1996. **93**(24): p. 13770-3 DOI: 10.1073/pnas.93.24.13770.

128. Li, J., D. Stein, C. McMullan, D. Branton, M.J. Aziz, and J.A. Golovchenko, Ion-beam sculpting at nanometre length scales. Nature, 2001. **412**(6843): p. 166-9 DOI: 10.1038/35084037.

129. Dekker, C., Solid-state nanopores. Nat Nanotechnol, 2007. **2**(4): p. 209-15 DOI: 10.1038/nnano.2007.27.

130. Clarke, J., H.C. Wu, L. Jayasinghe, A. Patel, S. Reid, and H. Bayley, Continuous base identification for single-molecule nanopore DNA sequencing. Nat Nanotechnol, 2009. **4**(4): p. 265-70 DOI: 10.1038/nnano.2009.12.

131. Eisenstein, M., Oxford Nanopore announcement sets sequencing sector abuzz. Nat Biotechnol, 2012. **30**(4): p. 295-6 DOI: 10.1038/nbt0412-295.

132. Loman, N.J. and A.R. Quinlan, Poretools: a toolkit for analyzing nanopore sequence data. Bioinformatics, 2014. **30**(23): p. 3399-401 DOI: 10.1093/bioinformatics/btu555.

133. Lu, H.Y., F. Giordano, and Z.M. Ning, Oxford Nanopore MinION sequencing and genome sssembly. Genomics Proteomics & Bioinformatics, 2016. **14**(5): p. 265-279 DOI: 10.1016/j.gpb.2016.05.004.

134. Smith, N.W., P.R. Shorten, E. Altermann, N.C. Roy, and W.C. McNabb, Examination of hydrogen cross-feeders using a colonic microbiota model. BMC Bioinformatics, 2021. **22**(1): p. 3 DOI: 10.1186/s12859-020-03923-6.

135. Smith, N.W., P.R. Shorten, E.H. Altermann, N.C. Roy, and W.C. McNabb, Hydrogen cross-feeders of the human gastrointestinal tract. Gut Microbes, 2019. **10**(3): p. 270-288 DOI: 10.1080/19490976.2018.1546522.

136. Samuel, B.S. and J.I. Gordon, A humanized gnotobiotic mouse model of host-archaeal-bacterial mutualism. Proc Natl Acad Sci U S A, 2006. **103**(26): p. 10011-6 DOI: 10.1073/pnas.0602187103.

137. James, S.C., K. Fraser, W. Young, W.C. McNabb, and N.C. Roy, Gut microbial metabolites and biochemical pathways involved in irritable bowel syndrome: effects of diet and nutrition on the microbiome. J Nutr, 2020. **150**(5): p. 1012-1021 DOI: 10.1093/jn/nxz302.

138. Song, M. and A.T. Chan, Diet, gut microbiota, and colorectal cancer prevention: a review of potential mechanisms and promising targets for future research. Curr Colorectal Cancer Rep, 2017. **13**(6): p. 429-439 DOI: 10.1007/s11888-017-0389-y.

139. Duarte, M.E., J. Tyus, and S.W. Kim, Synbiotic effects of enzyme and probiotics on intestinal health and growth of newly weaned pigs challenged with enterotoxigenic F18^{+} *Escherichia coli*. Front Vet Sci, 2020. **7**: p. 573 DOI: 10.3389/fvets.2020.00573.

140. Markowiak, P. and K. Śliżewska, The role of probiotics, prebiotics and synbiotics in animal nutrition. Gut Pathog, 2018. **10**: p. 21 DOI: 10.1186/s13099-018-0250-0.

141. Duarte, M.E. and S.W. Kim, Intestinal microbiota and its interaction to intestinal health in nursery pigs. Animal Nutrition, 2022. **8**: p. 169-184 DOI: https://doi.org/10.1016/j.aninu.2021.05.001.

142. Buckel, W. and R.K. Thauer, Flavin-based electron bifurcation, ferredoxin, flavodoxin, and anaerobic respiration with protons (Ech) or NAD^+ (Rnf) as electron acceptors: a historical review. Front Microbiol, 2018. **9**: p. 401 DOI: 10.3389/fmicb.2018.00401.

143. Li, F., J. Hinderberger, H. Seedorf, J. Zhang, W. Buckel, and R.K. Thauer, Coupled ferredoxin and crotonyl coenzyme A (CoA) reduction with NADH catalyzed by the butyryl-CoA dehydrogenase/Etf complex from Clostridium kluyveri. J Bacteriol, 2008. **190**(3): p. 843-50 DOI: 10.1128/jb.01417-07.

144. Louis, P. and H.J. Flint, Formation of propionate and butyrate by the human colonic microbiota. Environ Microbiol, 2017. **19**(1): p. 29-41 DOI: 10.1111/1462-2920.13589.

145. Chen, J.S. and L.E. Mortenson, Purification and properties of hydrogenase from Clostridium pasteurianum W5. Biochim Biophys Acta, 1974. **371**(2): p. 283-98 DOI: 10.1016/0005-2795(74)90025-7.

146. An, Y.H. and R.J. Friedman, Concise review of mechanisms of bacterial adhesion to biomaterial surfaces. Journal of Biomedical Materials Research, 1998. **43**(3): p. 338-348 DOI: https://doi.org/10.1002/(SICI)1097-4636(199823)43:3<338::AID-JBM16>3.0.CO;2-B.

147. Hori, K. and S. Matsumoto, Bacterial adhesion: from mechanism to control. Biochemical Engineering Journal, 2010. **48**(3): p. 424-434 DOI: https://doi.org/10.1016/j.bej.2009.11.014.

148. Daniel, C., N. Paris, O. Pierre, N. Griffon, S. Breant, N. Orlova, P. Serre, D. Leprovost, S. Denglos, A. Mouchet, J. Dubiel, R. Gozlan, G. Chatellier, R. Bey, M. Frank, C. Hassen-Khodja, M.F. Mamzer, M. Hilka, and A.-H.C.C. Initiative, AP-HP Health Data Space (AHDS) to the test of the Covid-19 pandemic. Stud Health Technol Inform, 2022. **294**: p. 28-32 DOI: 10.3233/SHTI220390.

149. Sharma, S. and J.C. Conrad, Attachment from flow of *Escherichia coli* bacteria onto silanized glass substrates. Langmuir, 2014. **30**(37): p. 11147-11155 DOI: 10.1021/la502313y.

150. Oh, J.K., Y. Yegin, F. Yang, M. Zhang, J. Li, S. Huang, S.V. Verkhoturov, E.A. Schweikert, K. Perez-Lewis, E.A. Scholar, T.M. Taylor, A. Castillo, L. Cisneros-Zevallos, Y. Min, and M. Akbulut, The influence of surface chemistry on the kinetics and thermodynamics of bacterial adhesion. Scientific Reports, 2018. **8**(1): p. 17247 DOI: 10.1038/s41598-018-35343-1.

151. Kankainen, M., L. Paulin, S. Tynkkynen, I. von Ossowski, J. Reunanen, P. Partanen, R. Satokari, S. Vesterlund, A.P. Hendrickx, S. Lebeer, S.C. De Keersmaecker, J. Vanderleyden, T. Hämäläinen, S. Laukkanen, N. Salovuori, J. Ritari, E. Alatalo, R. Korpela, T. Mattila-Sandholm, A. Lassig, K. Hatakka, K.T. Kinnunen, H. Karjalainen, M. Saxelin, K. Laakso, A. Surakka, A. Palva, T. Salusjärvi, P. Auvinen, and W.M. de Vos, Comparative genomic analysis of *Lactobacillus rhamnosus* GG reveals pili containing a human- mucus binding protein. Proc Natl Acad Sci U S A, 2009. **106**(40): p. 17193-8 DOI: 10.1073/pnas.0908876106.

152. Sicard, J.-F., G. Le Bihan, P. Vogeleer, M. Jacques, and J. Harel, Interactions of intestinal bacteria with components of the intestinal mucus. Frontiers in Cellular and Infection Microbiology, 2017. **7** DOI: 10.3389/fcimb.2017.00387.

153. Zheng, S., M. Bawazir, A. Dhall, H.E. Kim, L. He, J. Heo, and G. Hwang, Implication of surface properties, bacterial motility, and hydrodynamic conditions on bacterial surface sensing and their initial adhesion. Front Bioeng Biotechnol, 2021. **9**: p. 643722 DOI: 10.3389/fbioe.2021.643722.

154. Goodrich, J.K., J.L. Waters, A.C. Poole, J.L. Sutter, O. Koren, R. Blekhman, M. Beaumont, W. Van Treuren, R. Knight, J.T. Bell, T.D. Spector, A.G. Clark, and R.E. Ley, Human genetics shape the gut microbiome. Cell, 2014. **159**(4): p. 789-799 DOI: 10.1016/j.cell.2014.09.053.

155. Goodrich, J.K., J.L. Waters, A.C. Poole, J.L. Sutter, O. Koren, R. Blekhman, M. Beaumont, W. Van Treuren, R. Knight, J.T. Bell, T.D. Spector, A.G. Clark, and R.E. Ley, Human genetics shape the gut microbiome. Cell, 2014. **159**(4): p. 789-99 DOI: 10.1016/j.cell.2014.09.053.

156. Hansen, E.E., C.A. Lozupone, F.E. Rey, M. Wu, J.L. Guruge, A. Narra, J. Goodfellow, J.R. Zaneveld, D.T. McDonald, J.A. Goodrich, A.C. Heath, R. Knight, and J.I. Gordon, Pan-genome of the dominant human gut-associated archaeon, *Methanobrevibacter smithii*, studied in twins. Proc Natl Acad Sci U S A, 2011. **108 Suppl 1**(Suppl 1): p. 4599-606 DOI: 10.1073/pnas.1000071108.

157. Upadhyaya, B., L. McCormack, A.R. Fardin-Kia, R. Juenemann, S. Nichenametla, J. Clapper, B. Specker, and M. Dey, Impact of dietary resistant starch type 4 on human gut microbiota and immunometabolic functions. Scientific Reports, 2016. **6**(1): p. 28797 DOI: 10.1038/srep28797.

158. Klimenko, N.S., A.V. Tyakht, A.S. Popenko, A.S. Vasiliev, I.A. Altukhov, D.S. Ischenko, T.I. Shashkova, D.A. Efimova, D.A. Nikogosov, D.A. Osipenko, S.V. Musienko, K.S. Selezneva, A. Baranova, A.M. Kurilshikov, S.M. Toshchakov, A.A. Korzhenkov, N.I. Samarov, M.A. Shevchenko, A.V. Tepliuk, and D.G. Alexeev, Microbiome responses to an uncontrolled short-term diet intervention in the frame of the citizen science project. Nutrients, 2018. **10**(5): p. 576, https://www.mdpi.com/2072-6643/10/5/576

159. Angenent, L.T., K. Karim, M.H. Al-Dahhan, B.A. Wrenn, and R. Domíguez-Espinosa, Production of bioenergy and biochemicals from industrial and agricultural wastewater. Trends Biotechnol, 2004. **22**(9): p. 477-85 DOI: 10.1016/j.tibtech.2004.07.001.

160. Liu, Y. and W.B. Whitman, Metabolic, phylogenetic, and ecological diversity of the methanogenic archaea. Ann N Y Acad Sci, 2008. **1125**: p. 171-89 DOI: 10.1196/annals.1419.019.

161. Barredo, M.S. and L.M. Evison, Effect of propionate toxicity on methanogen-enriched sludge, Methanobrevibacter smithii, and Methanospirillum hungatii at different pH values. Appl Environ Microbiol, 1991. **57**(6): p. 1764-9 DOI: 10.1128/aem.57.6.1764-1769.1991.

162. Morotomi, M., F. Nagai, and Y. Watanabe, Description of Christensenella minuta gen. nov., sp. nov., isolated from human faeces, which forms a distinct branch in

the order Clostridiales, and proposal of Christensenellaceae fam. nov. Int J Syst Evol Microbiol, 2012. **62**(Pt 1): p. 144-149 DOI: 10.1099/ijs.0.026989-0.

163. Sonnenburg, J.L., L.T. Angenent, and J.I. Gordon, Getting a grip on things: how do communities of bacterial symbionts become established in our intestine? Nat Immunol, 2004. **5**(6): p. 569-73 DOI: 10.1038/ni1079.

164. de Vos, W.M., Microbial biofilms and the human intestinal microbiome. npj Biofilms and Microbiomes, 2015. **1**(1): p. 15005 DOI: 10.1038/npjbiofilms.2015.5.

165. TerAvest, M.A., Z. He, M.A. Rosenbaum, E.C. Martens, M.A. Cotta, J.I. Gordon, and L.T. Angenent, Regulated expression of polysaccharide utilization and capsular biosynthesis loci in biofilm and planktonic *Bacteroides thetaiotaomicron* during growth in chemostats. Biotechnol Bioeng, 2014. **111**(1): p. 165-73 DOI: 10.1002/bit.24994.

166. Macfarlane, S. and G.T. Macfarlane, Composition and metabolic activities of bacterial biofilms colonizing food residues in the human gut. Appl Environ Microbiol, 2006. **72**(9): p. 6204-11 DOI: 10.1128/AEM.00754-06.

167. Lagier, J.C., F. Armougom, M. Million, P. Hugon, I. Pagnier, C. Robert, F. Bittar, G. Fournous, G. Gimenez, M. Maraninchi, J.F. Trape, E.V. Koonin, B. La Scola, and D. Raoult, Microbial culturomics: paradigm shift in the human gut microbiome study. Clinical Microbiology and Infection, 2012. **18**(12): p. 1185-1193 DOI: https://doi.org/10.1111/1469-0691.12023.

168. Lagier, J.C., P. Hugon, S. Khelaifia, P.E. Fournier, B. La Scola, and D. Raoult, The rebirth of culture in microbiology through the example of culturomics to study human gut microbiota. Clin Microbiol Rev, 2015. **28**(1): p. 237-64 DOI: 10.1128/CMR.00014-14.

169. Lagier, J.-C., G. Dubourg, M. Million, F. Cadoret, M. Bilen, F. Fenollar, A. Levasseur, J.-M. Rolain, P.-E. Fournier, and D. Raoult, Culturing the human microbiota and culturomics. Nature Reviews Microbiology, 2018. **16**(9): p. 540-550 DOI: 10.1038/s41579-018-0041-0.

170. Matar, G. and M. Bilen, Culturomics, a potential approach paving the way toward bacteriotherapy. Current Opinion in Microbiology, 2022. **69**: p. 102194 DOI: https://doi.org/10.1016/j.mib.2022.102194.

171. Lagier, J.-C., S. Khelaifia, M.T. Alou, S. Ndongo, N. Dione, P. Hugon, A. Caputo, F. Cadoret, S.I. Traore, E.H. Seck, G. Dubourg, G. Durand, G. Mourembou, E. Guilhot, A. Togo, S. Bellali, D. Bachar, N. Cassir, F. Bittar, J. Delerce, M. Mailhe, D. Ricaboni, M. Bilen, N.P.M. Dangui Nieko, N.M. Dia Badiane, C. Valles, D. Mouelhi, K. Diop, M. Million, D. Musso, J. Abrahão, E.I. Azhar, F. Bibi, M. Yasir, A. Diallo, C. Sokhna, F. Djossou, V. Vitton, C. Robert, J.M. Rolain, B. La Scola, P.-E. Fournier, A. Levasseur, and D. Raoult, Culture of previously uncultured members of the human gut microbiota by culturomics. Nature Microbiology, 2016. **1**(12): p. 16203 DOI: 10.1038/nmicrobiol.2016.203.

172. Jin, Z., A. Ng, C.F. Maurice, and D. Juncker, The mini colon model: a benchtop multi-bioreactor system to investigate the gut microbiome. Gut Microbes, 2022. **14**(1): p. 2096993 DOI: 10.1080/19490976.2022.2096993.

173. Gianetto-Hill, C.M., S.J. Vancuren, B. Daisley, S. Renwick, J. Wilde, K. Schroeter, M.C. Daigneault, and E. Allen-Vercoe, The robogut: a bioreactor model of the human colon for evaluation of gut microbial community ecology and function. Curr Protoc, 2023. **3**(4): p. e737 DOI: 10.1002/cpz1.737.

174. García-Villalba, R., H. Vissenaekens, J. Pitart, M. Romo-Vaquero, J.C. Espín, C. Grootaert, M.V. Selma, K. Raes, G. Smagghe, S. Possemiers, J. Van Camp, and F.A. Tomas-Barberan, Gastrointestinal simulation model TWIN-SHIME shows differences between human urolithin-metabotypes in gut microbiota composition, pomegranate polyphenol metabolism, and transport along the intestinal tract. Journal of Agricultural and Food Chemistry, 2017. **65**(27): p. 5480-5493 DOI: 10.1021/acs.jafc.7b02049.

175. Chiu, C.Y. and S.A. Miller, Clinical metagenomics. Nat Rev Genet, 2019. **20**(6): p. 341-355 DOI: 10.1038/s41576-019-0113-7.

176. Martínez-Porchas, M., E. Villalpando-Canchola, and F. Vargas-Albores, Significant loss of sensitivity and specificity in the taxonomic classification occurs when short 16S rRNA gene sequences are used. Heliyon, 2016. **2**(9): p. e00170 DOI: https://doi.org/10.1016/j.heliyon.2016.e00170.

177. Workman, R.E., A.D. Tang, P.S. Tang, M. Jain, J.R. Tyson, R. Razaghi, P.C. Zuzarte, T. Gilpatrick, A. Payne, J. Quick, N. Sadowski, N. Holmes, J.G. de Jesus, K.L. Jones, C.M. Soulette, T.P. Snutch, N. Loman, B. Paten, M. Loose, J.T. Simpson, H.E. Olsen, A.N. Brooks, M. Akeson, and W. Timp, Nanopore native RNA sequencing of a human poly(A) transcriptome. Nature Methods, 2019. **16**(12): p. 1297-1305 DOI: 10.1038/s41592-019-0617-2.

178. Curry, K.D., Q. Wang, M.G. Nute, A. Tyshaieva, E. Reeves, S. Soriano, Q. Wu, E. Graeber, P. Finzer, W. Mendling, T. Savidge, S. Villapol, A. Dilthey, and T.J. Treangen, Emu: species-level microbial community profiling of full-length 16S rRNA Oxford Nanopore sequencing data. Nature Methods, 2022. **19**(7): p. 845-853 DOI: 10.1038/s41592-022-01520-4.

179. Szoboszlay, M., L. Schramm, D. Pinzauti, J. Scerri, A. Sandionigi, and M. Biazzo, Nanopore is preferable over Illumina for 16S amplicon sequencing of the gut microbiota when species-level taxonomic classification, accurate estimation of richness, or focus on rare taxa is required. Microorganisms, 2023. **11**(3): p. 804, https://www.mdpi.com/2076-2607/11/3/804

180. Kim, D., L. Song, F.P. Breitwieser, and S.L. Salzberg, Centrifuge: rapid and sensitive classification of metagenomic sequences. Genome Res, 2016. **26**(12): p. 1721-1729 DOI: 10.1101/gr.210641.116.

181. Li, H., Minimap2: pairwise alignment for nucleotide sequences. Bioinformatics, 2018. **34**(18): p. 3094-3100 DOI: 10.1093/bioinformatics/bty191.

182. Moon, T.K., The expectation-maximization algorithm. IEEE Signal Processing Magazine, 1996. **13**(6): p. 47-60 DOI: 10.1109/79.543975.

183. Cock, P.J., T. Antao, J.T. Chang, B.A. Chapman, C.J. Cox, A. Dalke, I. Friedberg, T. Hamelryck, F. Kauff, B. Wilczynski, and M.J. de Hoon, Biopython: freely available Python tools for computational molecular biology and bioinformatics. Bioinformatics, 2009. **25**(11): p. 1422-3 DOI: 10.1093/bioinformatics/btp163.

184. Shannon, C.E., A mathematical theory of communication. The Bell System Technical Journal, 1948. **27**(3): p. 379-423 DOI: 10.1002/j.1538-7305.1948.tb01338.x.

185. Simpson, E.H., Measurement of diversity. Nature, 1949. **163**(4148): p. 688-688 DOI: 10.1038/163688a0.

186. Yasri, N., E.P.L. Roberts, and S. Gunasekaran, The electrochemical perspective of bioelectrocatalytic activities in microbial electrolysis and microbial fuel cells. Energy Reports, 2019. **5**: p. 1116-1136 DOI: https://doi.org/10.1016/j.egyr.2019.08.007.

187. Angelaalincy, M.J., R. Navanietha Krishnaraj, G. Shakambari, B. Ashokkumar, S. Kathiresan, and P. Varalakshmi, Biofilm engineering approaches for improving the performance of microbial fuel cells and bioelectrochemical systems. Frontiers in Energy Research, 2018. **6** DOI: 10.3389/fenrg.2018.00063.

188. Islam, M.A., A. Karim, B. Ethiraj, T. Raihan, M.M.R. Khan, A. Kadier, S. Al Nadhari, A.A. Al-Masri, and F. Ameen, Interspecies microbial interactions in bioelectrochemical system and biodegradation: a state of the art review. Science of The Total Environment, 2023. **891**: p. 164623 DOI: https://doi.org/10.1016/j.scitotenv.2023.164623.

189. Pasternak, G., A. de Rosset, N. Tyszkiewicz, B. Widera, J. Greenman, and I. Ieropoulos, Prevention and removal of membrane and separator biofouling in bioelectrochemical systems: a comprehensive review. iScience, 2022. **25**(7): p. 104510 DOI: https://doi.org/10.1016/j.isci.2022.104510.

190. Yang, W., J. Li, Q. Fu, L. Zhang, Z. Wei, Q. Liao, and X. Zhu, Minimizing mass transfer losses in microbial fuel cells: theories, progresses and prospectives. Renewable and Sustainable Energy Reviews, 2021. **136**: p. 110460 DOI: https://doi.org/10.1016/j.rser.2020.110460.

191. Thakur, P. and S. Sugumar, Chapter 8 - Mechanisms of competition in biofilm communities, in Application of Biofilms in Applied Microbiology, M.P. Shah, Editor. 2022, Academic Press. p. 135-152.

192. Moß, C., A. Behrens, and U. Schröder, The Llmits of three-dimensionality: systematic assessment of effective anode macrostructure dimensions for mixed-culture electroactive biofilms. ChemSusChem, 2020. **13**(3): p. 582-589 DOI: 10.1002/cssc.201902923.

193. Liu, Y. and J.H. Tay, The essential role of hydrodynamic shear force in the formation of biofilm and granular sludge. Water Res, 2002. **36**(7): p. 1653-65 DOI: 10.1016/s0043-1354(01)00379-7.

194. Naaz, T., A. Kumar, A. Vempaty, N. Singhal, S. Pandit, P. Gautam, and S.P. Jung, Recent advances in biological approaches towards anode biofilm engineering for improvement of extracellular electron transfer in microbial fuel cells. Environmental Engineering Research, 2023. **28**(5): p. 220666-0 DOI: 10.4491/eer.2022.666.

195. Buret, A.G. and T. Allain, Gut microbiota biofilms: from regulatory mechanisms to therapeutic targets. J Exp Med, 2023. **220**(3) DOI: 10.1084/jem.20221743.

196. Poma, N., F. Vivaldi, A. Bonini, P. Salvo, A. Kirchhain, Z. Ates, B. Melai, D. Bottai, A. Tavanti, and F. Di Francesco, Microbial biofilm monitoring by electrochemical

transduction methods. TrAC Trends in Analytical Chemistry, 2021. **134**: p. 116134 DOI: https://doi.org/10.1016/j.trac.2020.116134.

197. Motta, J.-P., J.L. Wallace, A.G. Buret, C. Deraison, and N. Vergnolle, Gastrointestinal biofilms in health and disease. Nature Reviews Gastroenterology & Hepatology, 2021. **18**(5): p. 314-334 DOI: 10.1038/s41575-020-00397-y.

198. Flemming, H.C. and S. Wuertz, Bacteria and archaea on earth and their abundance in biofilms. Nat Rev Microbiol, 2019. **17**(4): p. 247-260 DOI: 10.1038/s41579-019-0158-9.

199. Sultana, S.T., J.T. Babauta, and H. Beyenal, Electrochemical biofilm control: a review. Biofouling, 2015. **31**(9-10): p. 745-58 DOI: 10.1080/08927014.2015.1105222.

200. V. H. Tran, H., E. Kim, and S.P. Jung, Anode biofilm maturation time, stable cell performance time, and time-course electrochemistry in a single-chamber microbial fuel cell with a brush-anode. Journal of Industrial and Engineering Chemistry, 2022. **106**: p. 269-278 DOI: https://doi.org/10.1016/j.jiec.2021.11.001.

201. Nogal, A., P. Louca, X. Zhang, P.M. Wells, C.J. Steves, T.D. Spector, M. Falchi, A.M. Valdes, and C. Menni, Circulating levels of the short-chain fatty acid acetate mediate the effect of the gut microbiome on visceral fat. Front Microbiol, 2021. **12**: p. 711359 DOI: 10.3389/fmicb.2021.711359.

202. Gibson, G.R., J.H. Cummings, and G.T. Macfarlane, Competition for hydrogen between sulphate-reducing bacteria and methanogenic bacteria from the human large intestine. J Appl Bacteriol, 1988. **65**(3): p. 241-7 DOI: 10.1111/j.1365-2672.1988.tb01891.x.

203. Christl, S.U., G.R. Gibson, and J.H. Cummings, Role of dietary sulphate in the regulation of methanogenesis in the human large intestine. Gut, 1992. **33**(9): p. 1234-8 DOI: 10.1136/gut.33.9.1234.

204. Breznak, J.A. and J.M. Switzer, Acetate synthesis from H_2 plus CO_2 by termite gut microbes. Appl Environ Microbiol, 1986. **52**(4): p. 623-30 DOI: 10.1128/aem.52.4.623-630.1986.

205. Breznak, J.A., *Acetogenesis from carbon dioxide in termite guts*, in *Acetogenesis*, H.L. Drake, Editor. 1994, Springer US: Boston, MA. p. 303-330.

206. Odelson, D.A. and J.A. Breznak, Volatile fatty acid production by the hindgut microbiota of xylophagous termites. Appl. Environ. Microbiol., 1983. **45**.

207. Gibson, G.R., G.T. Macfarlane, and J.H. Cummings, Occurrence of sulphate-reducing bacteria in human faeces and the relationship of dissimilatory sulphate reduction to methanogenesis in the large gut. J Appl Bacteriol, 1988. **65**(2): p. 103-11 DOI: 10.1111/j.1365-2672.1988.tb01498.x.

208. Stewart, J.A., V.S. Chadwick, and A. Murray, Carriage, quantification, and predominance of methanogens and sulfate-reducing bacteria in faecal samples. Lett Appl Microbiol, 2006. **43**(1): p. 58-63 DOI: 10.1111/j.1472-765X.2006.01906.x.

209. Leclerc, M., A. Bernalier, G. Donadille, and M. Lelait, H_2/CO_2 metabolism in acetogenic bacteria isolated from the human colon. Anaerobe, 1997. **3**(5): p. 307-315 DOI: https://doi.org/10.1006/anae.1997.0117.

210. Smith, E.A. and G.T. Macfarlane, Enumeration of amino acid fermenting bacteria in the human large intestine: effects of pH and starch on peptide metabolism and dissimilation of amino acids. FEMS Microbiology Ecology, 1998. **25**(4): p. 355-368 DOI: 10.1111/j.1574-6941.1998.tb00487.x.

211. Aguirre, M., A. Eck, M.E. Koenen, P.H.M. Savelkoul, A.E. Budding, and K. Venema, Diet drives quick changes in the metabolic activity and composition of human gut microbiota in a validated in vitro gut model. Research in Microbiology, 2016. **167**(2): p. 114-125 DOI: https://doi.org/10.1016/j.resmic.2015.09.006.

212. Rios-Covian, D., S. Gonzalez, A.M. Nogacka, S. Arboleya, N. Salazar, M. Gueimonde, and C.G. de Los Reyes-Gavilan, An overview on fecal branched short-chain fatty acids along human life and as related with body mass index: associated dietary and anthropometric factors. Front Microbiol, 2020. **11**: p. 973 DOI: 10.3389/fmicb.2020.00973.

213. Ichikawa, Y., H. Yamamoto, S.I. Hirano, B. Sato, Y. Takefuji, and F. Satoh, The overlooked benefits of hydrogen-producing bacteria. Med Gas Res, 2023. **13**(3): p. 108-111 DOI: 10.4103/2045-9912.344977.

214. Donaldson, G.P., M.S. Ladinsky, K.B. Yu, J.G. Sanders, B.B. Yoo, W.C. Chou, M.E. Conner, A.M. Earl, R. Knight, P.J. Bjorkman, and S.K. Mazmanian, Gut microbiota utilize immunoglobulin A for mucosal colonization. Science, 2018. **360**(6390): p. 795-800 DOI: 10.1126/science.aaq0926.

215. Liu, C., R. Kurokawa, M. Fujino, S. Hirano, B. Sato, and X.-K. Li, Estimation of the hydrogen concentration in rat tissue using an airtight tube following the administration of hydrogen via various routes. Scientific Reports, 2014. **4**(1): p. 5485 DOI: 10.1038/srep05485.

216. Russell, G., A. Nenov, H. Kisher, and J.T. Hancock, Molecular hydrogen as medicine: an assessment of administration methods. Hydrogen, 2021. **2**(4): p. 444-460, https://www.mdpi.com/2673-4141/2/4/25.

217. Naito, Y., T. Takagi, R. Inoue, S. Kashiwagi, K. Mizushima, S. Tsuchiya, Y. Itoh, K. Okuda, Y. Tsujimoto, A. Adachi, N. Maruyama, Y. Oda, and S. Matoba, Gut microbiota differences in elderly subjects between rural city Kyotango and urban city Kyoto: an age-gender-matched study. J Clin Biochem Nutr, 2019. **65**(2): p. 125-131 DOI: 10.3164/jcbn.19-26.

218. Archer, S.Y., S. Meng, A. Shei, and R.A. Hodin, p21(WAF1) is required for butyrate-mediated growth inhibition of human colon cancer cells. Proc Natl Acad Sci U S A, 1998. **95**(12): p. 6791-6 DOI: 10.1073/pnas.95.12.6791.

219. Frank, D.N., A.L. St Amand, R.A. Feldman, E.C. Boedeker, N. Harpaz, and N.R. Pace, Molecular-phylogenetic characterization of microbial community imbalances in human inflammatory bowel diseases. Proc Natl Acad Sci U S A, 2007. **104**(34): p. 13780-5 DOI: 10.1073/pnas.0706625104.

220. Ostojic, S.M., Hydrogen-rich water as a modulator of gut microbiota? Journal of Functional Foods, 2021. **78**: p. 104360 DOI: https://doi.org/10.1016/j.jff.2021.104360.

221. Hylemon, P.B., S.C. Harris, and J.M. Ridlon, Metabolism of hydrogen gases and bile acids in the gut microbiome. FEBS Lett, 2018. **592**(12): p. 2070-2082 DOI: 10.1002/1873-3468.13064.

222. Duncan, S.H. and H.J. Flint, Proposal of a neotype strain (A1-86) for *Eubacterium rectale*. Request for an opinion. International Journal of Systematic and Evolutionary Microbiology, 2008. **58**(7): p. 1735-1736 DOI: https://doi.org/10.1099/ijs.0.2008/004580-0.

223. Zheng, Y., J. Kahnt, I.H. Kwon, R.I. Mackie, and R.K. Thauer, Hydrogen formation and its regulation in *Ruminococcus albus*: involvement of an electron-bifurcating [FeFe]-hydrogenase, of a non-electron-bifurcating [FeFe]-hydrogenase, and of a putative hydrogen-sensing [FeFe]-hydrogenase. J Bacteriol, 2014. **196**(22): p. 3840-52 DOI: 10.1128/jb.02070-14.

224. Matsuo, Y., S. Komiya, Y. Yasumizu, Y. Yasuoka, K. Mizushima, T. Takagi, K. Kryukov, A. Fukuda, Y. Morimoto, Y. Naito, H. Okada, H. Bono, S. Nakagawa, and K. Hirota, Full-length 16S rRNA gene amplicon analysis of human gut microbiota using MinION™ nanopore sequencing confers species-level resolution. bioRxiv, 2020: p. 2020.05.06.078147 DOI: 10.1101/2020.05.06.078147.

225. Waechter, C., L. Fehse, M. Welzel, D. Heider, L. Babalija, J. Cheko, J. Mueller, J. Pöling, T. Braun, S. Pankuweit, E. Weihe, R. Kinscherf, B. Schieffer, U. Luesebrink, M. Soufi, and V. Ruppert, Comparative analysis of full-length 16s ribosomal RNA genome sequencing in human fecal samples using primer sets with different degrees of degeneracy. Front Genet, 2023. **14**: p. 1213829 DOI: 10.3389/fgene.2023.1213829.

226. Ji, H., J. Hu, S. Zuo, S. Zhang, M. Li, and S. Nie, In vitro gastrointestinal digestion and fermentation models and their applications in food carbohydrates. Critical Reviews in Food Science and Nutrition, 2022. **62**(19): p. 5349-5371 DOI: 10.1080/10408398.2021.1884841.

227. Dupont, D., M. Alric, S. Blanquet-Diot, G. Bornhorst, C. Cueva, A. Deglaire, S. Denis, M. Ferrua, R. Havenaar, J. Lelieveld, A.R. Mackie, M. Marzorati, O. Menard, M. Minekus, B. Miralles, I. Recio, and P. Van den Abbeele, Can dynamic in vitro digestion systems mimic the physiological reality? Critical Reviews in Food Science and Nutrition, 2019. **59**(10): p. 1546-1562 DOI: 10.1080/10408398.2017.1421900.

228. Li, S., N. Abdulkadir, F. Schattenberg, U. Nunes da Rocha, V. Grimm, S. Müller, and Z. Liu, Stabilizing microbial communities by looped mass transfer. Proc Natl Acad Sci U S A, 2022. **119**(17): p. e2117814119 DOI: 10.1073/pnas.2117814119.

229. Zihler, A., M. Gagnon, C. Chassard, and C. Lacroix, Protective effect of probiotics on *Salmonella* infectivity assessed with combined in vitro gut fermentation-cellular models. BMC Microbiology, 2011. **11**(1): p. 264 DOI: 10.1186/1471-2180-11-264.

230. Chaudhary, D.K., A. Khulan, and J. Kim, Development of a novel cultivation technique for uncultured soil bacteria. Scientific Reports, 2019. **9**(1): p. 6666 DOI: 10.1038/s41598-019-43182-x.

231. Sonnenburg, E.D. and J.L. Sonnenburg, Starving our microbial self: the deleterious consequences of a diet deficient in microbiota-accessible carbohydrates. Cell Metab, 2014. **20**(5): p. 779-786 DOI: 10.1016/j.cmet.2014.07.003.

232. Muir, J.G., Z.X. Lu, G.P. Young, D. Cameron-Smith, G.R. Collier, and K. O'Dea, Resistant starch in the diet increases breath hydrogen and serum acetate in human subjects. Am J Clin Nutr, 1995. **61**(4): p. 792-9 DOI: 10.1093/ajcn/61.4.792.

233. Oku, T. and S. Nakamura, Comparison of digestibility and breath hydrogen gas excretion of fructo-oligosaccharide, galactosyl-sucrose, and isomalto-oligosaccharide in healthy human subjects. Eur J Clin Nutr, 2003. **57**(9): p. 1150-6 DOI: 10.1038/sj.ejcn.1601666.

234. Campbell, A., K. Gdanetz, A.W. Schmidt, and T.M. Schmidt, H_2 generated by fermentation in the human gut microbiome influences metabolism and competitive fitness of gut butyrate producers. Microbiome, 2023. **11**(1): p. 133 DOI: 10.1186/s40168-023-01565-3.

235. Stams, A.J., Metabolic interactions between anaerobic bacteria in methanogenic environments. Antonie Van Leeuwenhoek, 1994. **66**(1-3): p. 271-94 DOI: 10.1007/bf00871644.

236. Duncan, S.H., A. Belenguer, G. Holtrop, A.M. Johnstone, H.J. Flint, and G.E. Lobley, Reduced dietary intake of carbohydrates by obese subjects results in decreased concentrations of butyrate and butyrate-producing bacteria in feces. Appl Environ Microbiol, 2007. **73**(4): p. 1073-8 DOI: 10.1128/AEM.02340-06.

237. Louis, P. and H.J. Flint, Diversity, metabolism and microbial ecology of butyrate-producing bacteria from the human large intestine. FEMS Microbiol Lett, 2009. **294**(1): p. 1-8 DOI: 10.1111/j.1574-6968.2009.01514.x.

238. Stams, A.J. and C.M. Plugge, Electron transfer in syntrophic communities of anaerobic bacteria and archaea. Nat Rev Microbiol, 2009. **7**(8): p. 568-77 DOI: 10.1038/nrmicro2166.